A NEW MEASURE FOR EVALUATING SHIELDING PERFORMANCE OF AN EQUIPMENT ENCLOSURE AT FREQUENCIES ABOVE 1 GHZ

Yong Cui

This thesis is submitted to the University of York for the degree of Doctor of Philosophy.

University of York
Department of Electronics

November 2007

Contents

Abstract

The measure of shielding effectiveness (SE) and the related measurement techniques proposed by the current IEEE Standard 299 are only applicable for large screened enclosures having dimensions more than 2 m. To propose reasonable measures to assess the shielding performance of an equipment enclosure, together with the relevant measurement techniques, is the subject of this thesis. This work is informing the new developments in IEEE Standard 299.

To coincide with the practical applications of most equipment enclosures, two measurement approaches distinguished by the location of the radiation source are considered in this thesis, and the measurement is performed in the radiating near-field with test frequencies above 1 GHz. The contents inside the enclosure are stressed and involved in all the measurements.

In the first measurement approach, to measure the enclosure's ability to prevent the electromagnetic waves of internal contents from radiating outside to cause interference with nearby equipments, an emission source is placed inside the enclosure and a receive antenna is placed outside. A new measure shielding of radiating power (*SRP*) is proposed here, which consists of two parameters: the average shielding of radiating power (*ASRP*) and the enhancement factor $E.F._{95th}$. Two measurement environments: anechoic chamber and reverberation chamber are considered and compared. To avoid the huge measurement work in an anechoic chamber, the reverberation chamber is proposed as an ideal test environment to determine the *ASRP*, and the estimation of the enhancement factor $E.F._{95th}$ can be given directly based on statistic analyses on both measurement and simulation results.

In the second measurement approach, to measure the enclosure's ability to shield the internal contents against external interference, the enclosure is placed in a small reverberation chamber and illuminated by external electromagnetic field. Another new measure shielding of absorption cross section (*SACS*) is proposed here. However, measurement results indicate this measure has distinct advantages and disadvantages, so it is suggested prudently. Finally the first measure is proposed and reverberation chamber is suggested as the ideal test environment.

List of Figures

6.5 The measurement results of $\langle \sigma_{ci,out} \rangle$ and $\langle \sigma_{ci,in} \rangle$ of the RC and those of the truncated pyramid foam block. The front panel shown in Fig. 6.3(a) is employed.

6.6 Measurement results of *SACS* and *ASRP* of the enclosure with the front panel shown in Fig. 6.3(a)

6.7 The measurement results of $\langle \sigma_{ci,out} \rangle$ and $\langle \sigma_{ci,in} \rangle$ of the truncated pyramid foam block. The front panel shown in Fig. 6.3(b) is employed.

List of Tables

Abbreviations and Symbols

Abbreviations

ASRP	Average Shielding of Radiating Power
ASTM	American Society for Testing and Materials
CCF	Chamber Calibration Factor
CD	Compact Disk
CGE	Comb Generator Emitter
CISPR	Comtié International Spécial des Perturbations Radioélectriques
	(International Special Committee on Radio Interference)
CPD	Cumulative Distribution Function
E.F.	Enhancement Factor
EM	Electromagnetic
EMC	Electromagnetic Compatibility
EMI	Electromagnetic Interference
EUT	Equipment Under Test
IEC	International Electrotechni al Commission
IEEE	Institution of Electrical and Electronics Engineers
LCD	Liquid Crystal Display
LED	Light-emission Diode
LUF	Lowest Usable Frequency
OATS	Open Area Test Site
PCB	Printed Circuit board
RC	Representative Content

RF	Radio Frequency
SACS	Shielding of Average Cross Section
SDCom	Society Standards Development Committee
SE	Shielding Effectiveness
SRF	Shielding of Radiating Fields
SRFP	Shielding of Radiating Fields in Positions
SRFO	Shielding of Radiating Fields in Order
SRP	Shielding of Radiating Power
TLM	Transmission Line Modelling
WA	Width of Autocorrelation

Symbols

a	length of a reverberation chamber
A	correction factor representing the effect of the possible consequence of the second reflection of an infinite material sheet on the transmitted field
b	width of a reverberation chamber
c_0	speed of light in free space
d	height of a reverberation chamber
D	the largest dimension of the EUT
D_{max}	the maximum directivity of a radiation source in the far-field
E	electric field strength
E_{att}	electric field strength obtained during the attenuation measurement step
$E_{att}(i, j)$	the E_{att} at the $(i,\ j)th$ test point on the cylindrical scan surface
$\boldsymbol{E_{att}}$	a matrix with entries $E_{att}(i,\ j)$

$E_{att,\ desc}$	an array in which all the E_{att} are arranged in descending order
E_h	electric field strength measured by the receive antenna oriented at the 'h' (vertical) direction
E_{ref}	electric field strength obtained during the reference measurement step
$E_{ref}(i, j)$	the E_{ref} at the $(i,\ j)th$ test point on the cylindrical scan surface
$\boldsymbol{E_{ref}}$	a matrix with entries $E_{ref}(i,\ j)$
$E_{ref,\ desc}$	an array in which all the E_{ref} are arranged in descending order
E_θ	electric field strength measured by the receive antenna oriented at the 'θ' (azimuth) direction
$E_\perp$	magnitude of the electric field component which are vertical to the propagation direction of the wave
f_{mnp}	resonant frequency of mode mnp
h	scan height of the measurement antenna during the cylindrical scan
$H_\perp$	magnitude of the magnetic field component which are vertical to the propagation direction of the wave
i	row index
j	column index
k	wave number
L	loss
L_R	reflection loss
L_A	absorption loss
m	the number of antenna positions on each azimuth cut during the cylindrical scan

n	the number of antenna positions on the vertical direction (height) during the cylindrical scan
N_m	the number of resonant modes inside a reverberation chamber
p	power density
p_{ave}	average power density on a whole spherical or cylindrical surface around the EUT
$p_{inc,ns}$	power density incident onto an aperture without a sample
$p_{inc,s}$	power density incident onto an aperture with a sample
p_{95th}	the upper 95^{th} percentile of the power densities on a whole spherical or cylindrical surface around the EUT
P	power
P_{att}	power measured in the attenuation measurement step
P_d	dissipated power inside a reverberation chamber
P_{d1}	power dissipated in the walls of a reverberation chamber
P_{d2}	power absorbed in loading objects within a reverberation chamber
P_{d3}	power lost through the aperture leakage of a reverberation chamber
P_{d4}	power dissipated in the loads of receive antennas inside a reverberation chamber
P_{EUT}	radiated power of EUT
P_{out}	output power of a network analyzer
P_r	received power by a receive antenna in a reverberation chamber
P_{ref}	power measured in the reference measurement step
P_{RXEUT}	radiated power of an EUT received by a receive antenna in a reverberation chamber
P_t	transmitted power from a transmit antenna in a reverberation chamber

$P_{t,ns}$	power transmitted through an aperture without a material sample
$P_{t,s}$	power transmitted through an aperture with a material sample
Q	quality factor
r	radius of a circle
S_{11}	reflection coefficient
S_{21}	transmission coefficient
$SE(i, j)$	the SE at the $(i, j)th$ test point on the cylindrical scan surface
V	chamber volume
z	thickness of a barrier
Z	wave impedance
Z_0	characteristic impedance of a transmission line
Δx	scan step on the azimuth direction during the cylindrical scan
Δy	scan step on the vertical direction during the cylindrical scan
α	attenuation constant of a barrier material
ε	permittivity
η	intrinsic impedance of a material
η_0	intrinsic impedance of free space
η_{TX}	antenna efficiency factor of a transmit antenna
λ	wavelength
μ	permeability
θ	rotation angle of the dummy EUT or the RC during the cylindrical scan
ρ	radial distance
σ	absorption cross section

$\langle \sigma_{c,in} \rangle$	average value of $\langle \sigma_{ci,in} \rangle$ over a certain frequency range
$\langle \sigma_{c,out} \rangle$	average value of $\langle \sigma_{ci,out} \rangle$ over a certain frequency range
$\langle \sigma_{ci,in} \rangle$	at each frequency the absorption cross section of the equipment content as the enclosure is present.
$\langle \sigma_{ci,out} \rangle$	at each frequency the absorption cross section of the equipment content as the enclosure is absent
τ_{ab}	transmission coefficient from medium a to medium b
ω	angular frequency

Acknowledgements

Firstly, I would like to express my gratitude to my supervisor Prof. Andy Marvin for his invaluable suggestions, advice and encouragement.

I feel grateful to York EMC Services Ltd. Without the studentship provided by them, I cannot further my study in such an attractive and significant work in the EMC field.

I also wish to thank Dr. Tad Konefal and Dr. Janet Clegg for discussions in the associated numerical modelling techniques for electromagnetics. Especially I want to thank Dr. John Dawson for his scrupulous and patient review on this thesis. With his help, I have got considerable improvement on my thesis.

Thanks also go to my wife Dingding Wang for her moral support and encouragement over the most difficult period of this project.

Most of all, I want to express my gratitude to my mother. I cannot thank her enough for being so understanding and supportive in many ways throughout my research period. I dedicate this thesis to my mother as a small gift.

Declaration

Parts of the work reported in this thesis have previously been reported as follows:

- Andrew Marvin and Yong Cui, "Shielding measurements of equipment enclosures in the radiating near field," *IEEE Trans. Electromagn. Compat.*, vol. 49, No. 4, pp. 860-867, Nov. 2007.
- Andrew Marvin and Yong Cui, "Radiated interference measurements in the radiating near-field," presented at the workshop on 'EMC/EME in wireless communications systems' EMC Europe 2006, Barcelona, 4 - 8 Sept. 2006.
- Andrew Marvin and Yong Cui, "Finding the representative contents for the measurement of shielding effectiveness," presented at the workshop on 'Characterization of small shielding enclosures' EMC Europe 2006, Barcelona, 4 - 8 Sept. 2006.
- M P Robinson, A C Marvin and Yong Cui, "Techniques for determination of Q factors for EMC applications," EMC Europe 2006, Barcelona, Vol. 2, pp 999 - 1004, 4 - 8 Sept, 2006. ISBN: 84-689-9440-5.
- Andrew Marvin and Yong Cui, "Anechoic and reverberation chamber shielding measurement at frequencies above 1 GHz," *in Proc. of IEEE Int. Symp. On EMC*, PORTLAND, pp 410-415, 14 - 18 Aug. 2006.
- Andrew Marvin and Yong Cui, "On determining the maximum emissions of enclosures at frequencies above 1 GHz," Invited paper, XXVIIth URSI General Assembly 2005, New Delhi, India, 22 - 30 Oct. 2005. Paper No. EO1.7. [Online]. Available: http://www.ursi.org/Proceedings/ProcGA05/pdf/E01.7(0227).pdf
- Andrew Marvin and Yong Cui, "Measurements of interference from modern IT systems to microwave radio systems," Workshop on 'Future Challenging Research Domains within EMC in Dynamic Wireless Communication Applications'. Invited paper in EMC Europe Workshop 2005 - EMC of Wireless Systems, Rome, 19 - 21 Sept. 2005.

- Andrew Marvin and Yong Cui, "Toward evaluating the Shielding of enclosures with contents at frequencies above 1GHz," *in Proc. Of IEEE Int. Symp. On EMC*, CHICAGO, Vol. 1, pp200-205, 8 –12 Aug. 2005. ISBN: 0-7803-9380-5.
- Andrew Marvin and Yong Cui, "Suggested definitions of shielding for enclosures at microwave frequencies," presented at the workshop on 'Shielding effectiveness of enclosures: theory and measurement techniques' 2005 IEEE Int. Symp. on EMC, Chicago, 8 - 12 Aug. 2005. ISBN: 0-7803-9380-5.

Chapter 1

Introduction

1.1 Background

1.1.1 Shielding Effectiveness of Materials and Measurement Techniques

1.1.1.1 Shielding Materials and Definition of Shielding Effectiveness

As an electromagnetic field impinges on a barrier of infinite extent, the incident field is reduced as it passes through the barrier. This phenomenon is named as shielding. Based on this characteristic, shielding materials are used to cover an electronic product or a portion of that product to prevent the external electromagnetic field from coupling inside to cause interference with the internal contents or prevent the emission from the internal contents from radiating outside to cause interference with other equipments. That is, the application of shielding materials is one way to achieve electromagnetic compatibility (EMC) or prevent electromagnetic interference (EMI).

In practice, various shielding materials such as metals, plastics, carbon fibres etc are considered to fabricate equipment enclosures, connectors, gaskets or cable cloth, which can provide shielding protection and satisfy the mechanical requirement as well. The shielding performance of the product of a shielding material depends on both the product structure and the material realizing it. So before study the shielding performances of the products of shielding materials, it is necessary to understand the shielding performances of materials.

Traditionally, the measure shielding effectiveness (SE) is used to specify the effectiveness of a material or an enclosure to attenuate the electromagnetic fields, which is defined as the ratio of the signal received (from a transmit antenna) without the barrier to the signal received when the barrier is placed between the transmitter

and receiver. During the SE measurement of a material, the material tested is generally fabricated as a flat sample acting as the barrier. The signal tested may be the electric field strength E, the magnetic field strength H or the power P. Then the SE of materials is defined as [1], [2], [3], [4]:

$$SE = \frac{E_{ref}}{E_{att}}, \quad (1.1)$$

$$SE = \frac{H_{ref}}{H_{att}} \quad (1.2)$$

or

$$SE = \frac{P_{ref}}{P_{att}}. \quad (1.3)$$

Here E_{ref}, H_{ref} and P_{ref} are, respectively, the magnitude of the electric field, the magnitude of the magnetic field and the power measured when the sample is absent. Similarly, E_{att}, H_{att} and P_{att} are, respectively, the magnitude of the electric field, the magnitude of the magnetic field and the power measured when the sample is present. The three definitions represent respectively, the shielding effectiveness against electric field, magnetic field and power. In general, the SE value is expressed in decibels. Consequently, the above three equations should be changed respectively to

$$SE = 20\log_{10}\left(\frac{E_{ref}}{E_{att}}\right) \text{dB}, \quad (1.4)$$

$$SE = 20\log_{10}\left(\frac{H_{ref}}{H_{att}}\right) \text{dB} \quad (1.5)$$

and

$$SE = 10\log_{10}\left(\frac{P_{ref}}{P_{att}}\right) \text{dB}. \quad (1.6)$$

These definitions also imply that the SE measurement generally consists of two major steps: the reference measurement during which the item under test is absent and the attenuation measurement during which the item under test is present. These two steps have been expressed in most of the SE measurement techniques for materials or enclosures [5], [6], [7].

1.1.1.2 The Shielding Mechanism of Materials

The shielding performances of an infinite sheet material may be analysed using the widely accepted Schelkunoff model [8], that is, as an electromagnetic wave impinges on and passes through a barrier, two main phenomena take place to reduce the incident field: one is the reflection at the left and right interfaces of the barrier and the other is the absorption caused by the barrier medium. See Fig. 1.1 for the illustration of the field reflection and absorption in an infinite barrier.

In Fig. 1.1, medium 2 represents the infinite barrier; medium 1 and medium 3 represent respectively the medium on either side of the barrier. E_i is the incident field strength and E_r is the reflected field strength results from the first reflection between medium 1 and medium 2. τ_{12} is the transmission coefficient from medium 1 to medium 2 and τ_{23} is the transmission coefficient from medium 2 to medium 3, then the reflection loss, L_R, caused by reflection at the left and right interfaces can be determined by

$$L_R = \tau_{12}\tau_{23}. \quad (1.7)$$

As the wave crosses the left interface and proceeds through the barrier, its amplitude is attenuated according to the factor $e^{-\alpha z}$, where α is the attenuation constant of the barrier material and z is the thickness of the barrier. Consequently, the absorption loss of the barrier, L_A, is determined by

$$L_A = e^{-\alpha z}. \quad (1.8)$$

In most cases where the $e^{-\alpha z}$ of the barrier material is less than 0.1, the consequence of the second reflection is negligible, since the wave will suffer substantial attenuation as it travels back and forth through the barrier, so the transmitted field

strength is $E_i\tau_{12}\tau_{23}e^{-\alpha z}$. However, in the case where a thin barrier is tested or the test frequency is low, the absorption loss is small and the effect of the consequence of the second reflection cannot be neglected, which will, in general, increase the transmitted field strength and so reduce the SE of the barrier [9]. In this case, the transmitted field strength may be determined by $AE_i\tau_{12}\tau_{23}e^{-\alpha z}$, where A is the correction factor representing the effect of the possible consequence of the second reflection on the transmitted field. Thus, the shielding effectiveness of the barrier can be estimated as:

$$SE = \frac{1}{A\tau_{12}\tau_{23}e^{-\alpha z}}. \quad (1.9)$$

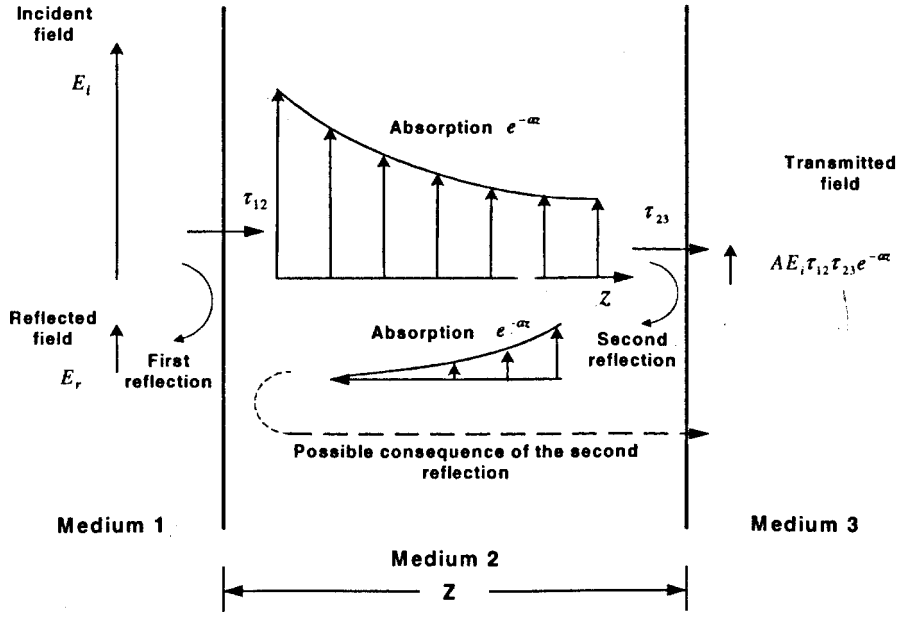

Fig. 1.1 Illustration of the reflection and absorption in an infinite barrier.

1.1.1.3 Shielding Effectiveness: Far-Field versus Near-Field

As discussed above, the SE of an infinite flat barrier results from both the reflection and absorption of the barrier. The absorption loss $e^{-\alpha z}$ depends on the barrier thickness and its attenuation constant, so it is only determined by the barrier. If the barrier is at the position sufficiently distant from the radiating source, i.e. in its far-field, the reflection loss L_R is also only determined by the barrier. However if the barrier is in the vicinity of the radiating source, i.e. in its near-field, the reflection

loss of the barrier not only depends on the material realizing the barrier, but also depends on the source type and the distance between the barrier and the source. The reflection loss of the barrier against the radiation from different types of sources in the near-field and far-field can be analysed quantitatively as follows.

The reflection loss of a barrier results from the difference between the wave impedance, Z, and the barrier intrinsic impedance, η. The concept of the impedance for an electromagnetic wave was firstly proposed by Schelkunoff [8], which is generally defined as

$$Z = \frac{E_\perp}{H_\perp} \quad (1.10)$$

where $E_\perp$ and $H_\perp$ are respectively, the magnitude of the electric field component and the magnitude of the magnetic field component, both of which are mutually orthogonal and normal to the propagation direction of the wave.

The wave impedance, Z, depends on the type of wave. Consider an electromagnetic wave propagating in free space. The radiation from a radiating source in its far-field is approximate a plane wave, of which the impedance is a constant in that both $E_\perp$ and $H_\perp$ are proportional to $1/\rho$, where ρ is the radial distance from the source. This constant equal to 120π ohms is called the 'intrinsic impedance' of free space [8] and usually symbolized by η_0. However, in the near-field, the radiation of a low current, high voltage radiator (such as a dipole) has $E_\perp$ approximately proportional to $1/\rho^3$ and $H_\perp$ approximately proportional to $1/\rho^2$, thus Z is roughly proportional to $1/\rho$ and usually much larger than η_0. The near-field radiation of a high current, low voltage radiator (such as a loop) is the dual to that of a low current, high voltage radiator. Such radiation has $E_\perp$ approximately proportional to $1/\rho^2$ and $H_\perp$ approximately proportional to $1/\rho^3$, and so the impedance is roughly proportional to ρ, which is usually less than η_0. The plot of the wave impedances of different radiation sources vs. test distance in free space is given in Fig. 1.2. In terms of an electrically small source, the distance $\rho = \lambda/2\pi$ is defined as the boundary between

the near-field and far-field, where λ is the wavelength. This criterion is only suitable for an electrically small source. A more realistic space division to categorize the radiated fields of an electrically large antenna or radiating equipments will be given in Chapter 3.

It should be mentioned that the transition of the field structure between the near-field and the far-field is quite gradual and it is more precise to consider another region around $\lambda/2\pi$ as a transition one.

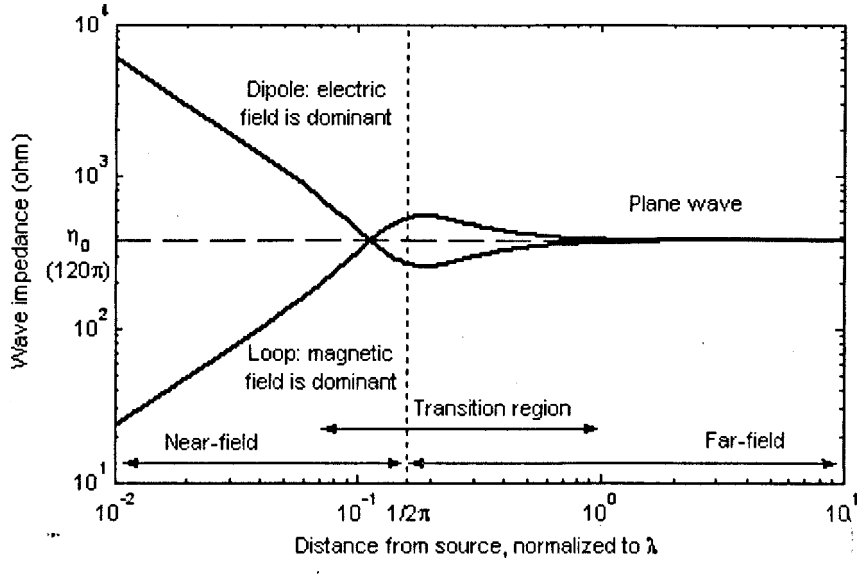

Fig. 1.2 Wave impedance vs. test distance for different radiation sources.

The exact solutions of the wave impedance of different wave types are given by Paul in [9]. If the wave impedance, Z, and the barrier intrinsic impedance, η, are known, the reflection loss of the barrier, L_R, can also be determined as described by Paul [9]:

$$L_R = \frac{(Z+\eta)^2}{4Z\eta}. \quad (1.11)$$

As shown in Fig. 1.2, at low frequencies, where the tested barrier is generally located in the near-field, the wave impedance Z of the radiation from a magnetic source is much less than the Z of the radiation from an electric source. Thus, according to Equation (1.11), the reflection loss L_R of the barrier against a magnetic source is small and much less than that against an electric source. At low frequencies, the absorption loss L_A of a barrier is also limited due to the large skin depth. Thus, the

SE of a barrier against a magnetic source is generally small and less than that against an electric source. However, at the higher frequencies, where the tested barrier is generally located in the far-field, a larger SE value can be expected, being mainly due to a higher absorption loss.

From the above discussion, the SE of a barrier in the near-field of an electric source is different from that in the near-field of a magnetic source, both of which are also different from the SE of the barrier measured in the far-field, i.e., the SE of the barrier against a plane wave. Thus, the SE measurement generally includes far-field and near-field measurements. During the far-field measurement, usually the electric field is measured and Equation (1.1) is used to determine SE because the results of Equation (1.1), (1.2) and (1.3) are identical for a planar material. However, during the near-field measurement, the SE of a planar material against electric field and magnetic field should be considered separately.

1.1.1.4 Shielding Effectiveness Measurement Techniques for Materials

In the past, various techniques have been developed and some standardised for the SE measurement of materials. These techniques are introduced as follows.

- **Modified MIL STD 285**

The MIL STD 285 [5], developed in the USA for military purposes and published in 1956, was the only "old" standard for measuring the SE of large enclosures. Although this standard was used widely in both industry and military, it was only suitable for the SE measurement up to about several hundred MHz and so has been cancelled and replaced with IEEE STD 299 [6]. These two standards will be introduced in the next subsection 1.1.2.

The MIL STD 285 method is also modified and used widely for evaluating the shielding performance of large sheet materials. A shielded room with an open window is required during the measurement, as shown in Fig. 1.3. The transmit antenna is located inside the room and the receive antenna is outside. Both antennas are directed towards the widow and at a fixed distance from each other. The SE is determined by the ratio between the signals measured with and without the test

object mounted in the window. By employing different measurement antennas, such as dipoles, loops and horns, the electric field and magnetic field in the near-field and the radiating power in the far-field can be measured. Consequently, the SE of the material against electric field, magnetic field or power may be determined. Although this method is applicable for relatively broad frequency range, it requires large sheet samples and does not consider the effects of the reflections inside the screened room on the measurement.

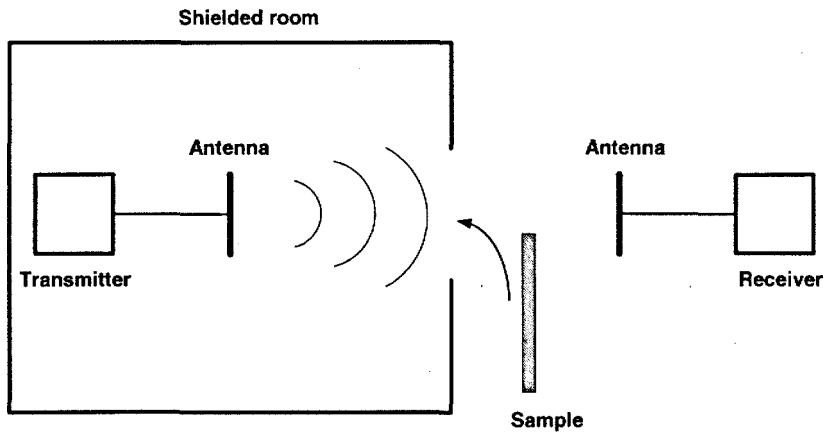

Fig. 1.3 Measurement setup of modified MIL STD 285 for a large flat material sample.

The measurement setup shown in Fig. 1.3 may also be used to determine the SE of gaskets. During the measurement, the outside of the window is enclosed by the gasket tested, and covered by a metal plate. The gasket should be clamped tightly between the metal plate and the wall of the screened room. Such measurement technique has been standardized and described in MIL-G-83528 [10], being also a modified version of MIL STD 285.

- **ASTM D4935**

The ASTM D4935 [3] was developed by the American Society for Testing and Materials (ASTM) for the SE measurement of thin, flat material samples. The measurement technique used is based on the transmission line method. During the measurement, a coaxial TEM cell consists of an interrupted inner conductor and a flanged outer conductor is used to contain the flat material samples. See Fig. 1.4.

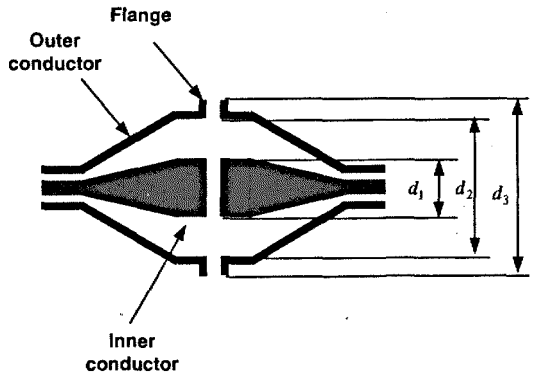

Fig. 1.4 Sketch of the cross section of a coaxial TEM cell.

The diameter of the inner conductor d_1 and the diameter of the outer conductor d_2 should satisfy two constraints. Firstly, the characteristic impedance Z_0 of the coaxial TEM cell should be equal to that of the standard coaxial cable connected, which is determined by

$$Z_0 = \frac{\eta_0}{2\pi} \ln\left(\frac{d_2}{d_1}\right). \quad (1.12)$$

Secondly, to avoid the higher order modes which may results in the field inside the TEM cell is no longer a TEM wave, the maximum operation frequency, f_{max}, should be less than the cutoff frequency of the TE_{11} mode, f_c, given by

$$f_c = \frac{c_0}{\pi(d_1 + d_2)} \quad (1.13)$$

where c_0 is the speed of light in vacuum.

During the SE measurement, the two ports of the coaxial TEM cell may be connected respectively with the two ports of a network analyser. A constant power is derived from the output port of the network analyser. A reference sample and a load sample, being made of the same material, are employed respectively in the reference measurement step and the attenuation step. See Fig. 1.5 for the measurement setup.

In the reference measurement step, the reference sample is placed between the flanges and P_{ref} is measured, while in the attenuation measurement step, the reference sample is replaced with the load sample and P_{att} is measured. Then the SE of the load sample is determined by Equation (1.3). Because only TEM wave is present in the

TEM cell, only plane wave (far-field measurement) can be provided during the measurement.

The d_1, d_2 and d_3 of the coaxial TEM cell defined in ASTM D4935 are, respectively, 33 mm, 76 mm and 128 mm. According to Equation (1.13), the test frequencies of such cell should not exceed 1.7 GHz, which is actually limited in range from 30 MHz to 1.5 GHz in ASTM D4935. The main disadvantage of the fixture used in ASTM D4935 is the narrow frequency band of operation. However, this limitation may be overcome by the smaller coaxial TEM cells proposed in [11] or [12] which may allow the measurement frequencies ranging up to around 10 GHz.

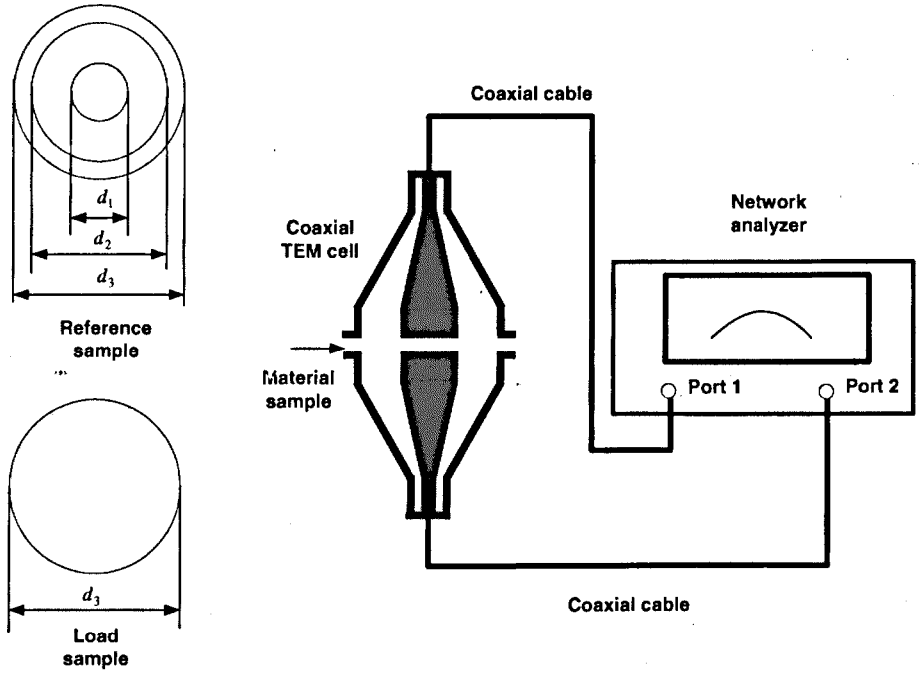

Fig. 1.5 Measurement set-up of ASTM D4935 for a flat material sample.

- **IEC61000-4-21: Annex G**

Due to the fast development of reverberation chamber techniques, reverberation chambers are widely used in the measurements concerning EMI and EMC problems. The document IEC61000-4-21 [4] issued by the International Electrotechnical Commission (IEC) involves a series of reverberation chamber test methods for radiated immunity, radiated emissions and screening effectiveness testing, where

Annex G is specified for the SE measurement of gaskets and materials and Annex H is specified for enclosures, in both of which, a "nested chamber" approach (e.g., a small reverberation chamber within a large reverberation chamber) is used to determine the SE. The lowest usable frequency (LUF) of the nested chambers is determined by the smaller one, being generally around 1 GHz. Thus, only radiated phenomena (far-field) are considered. In other words, the nested chamber method is specified to determine the SE against a plane wave, i.e. the radiating power.

In IEC61000-4-21: Annex G, to test the SE of material, the material flat sample should be mounted over the aperture of the cover plate of the test fixture. The test fixture acts as a small reverberation chamber and a receive antenna and a paddle wheel tuner/stirrer are installed inside to detect any radio frequency energy that "leaks" into the fixture. See Fig. 1.6 for the typical measurement set-up of SE of gaskets/materials in a reverberation chamber. The SE of the material sample is determined by the ratio of the power coupled to the reference antenna to that coupled to the test fixture.

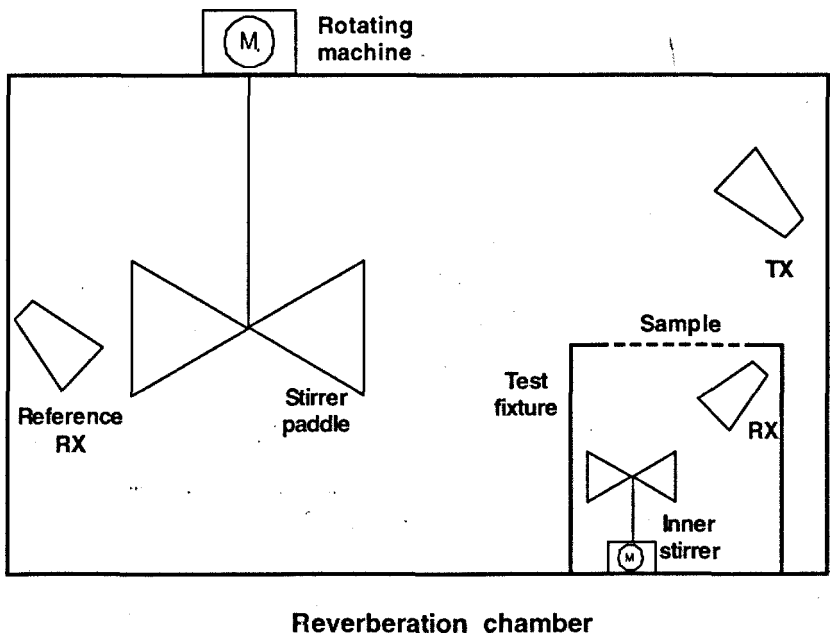

Fig. 1.6 Measurement set-up (IEC61000-4-21: Annex G) for SE of gaskets/materials in a reverberation chamber.

The main limitation of this method is that it does not account for the effects of the Q-factors of the chambers, which may result in different SE values if there is any

change in Q-factors of the chambers. It should be notified that this problem has been solved by a modified method proposed in [7], where the SE of a material is determined as following:

$$SE = \frac{P_{t,s} / p_{inc,s}}{P_{t,ns} / p_{inc,ns}} \quad (1.14)$$

where $P_{t,s}$ is the power transmitted through the aperture with the material sample, $P_{t,ns}$ is the power transmitted through the same aperture without the sample, $p_{inc,s}$ and $p_{inc,ns}$ are respectively the power densities incident onto the aperture with and without the sample. Based on this definition, all the environmental effects can be removed or normalized out and the measurement results only account for the effects of the material sample in the aperture. The SE defined by Equation (1.14) is actually the ratio of the absorption cross section (σ) of the aperture with and without a sample in the aperture, being only dependent on the sample during the reverberation chamber measurement. The measurement procedure to obtain the SE defined by Equation (1.14) is complicated, being detailed in [7].

- **Other Technique**

As discussed above, to avoid the higher order modes inside the TEM cell, the coaxial TEM cell method [3] is typically restricted up to the frequency of around 1 GHz. Although the modified MIL STD 285 method and the reverberation chamber approach [4] allow measurements above 1 GHz, both require a large flat sample during the measurement. To characterize the shielding effectiveness of small flat samples at frequencies above 1 GHz, a new measurement technique based on a simple measuring cell has been proposed by Catrysse in [13].

The measuring cell consists of two broadband horns and a copper plate. There is an embedded hole in the copper plate, where the small sample tested can be placed. During the measurement, the two horns are clamped tightly against the copper plate. The measuring equipment is a generator and a receiver or spectrum analyzer. The SE of the sample tested is determined by the ratio of the signal measured in the absence

of the sample to that in the presence of the sample. To minimize the leakage over the measuring structure, a metal frame is used to clamp the sample in the embedded hole of the copper plate, and conductive foam gaskets are introduced between the horns and the copper plate. The actual measurement setup is shown in the picture of Fig. 1.7.

Such measurement technique allows a quick testing of small flat samples at frequencies from 1 GHz to several GHz. However, at higher frequencies, the contact between the horns and the copper plate is very critical, so that reliable measurement results are not expected.

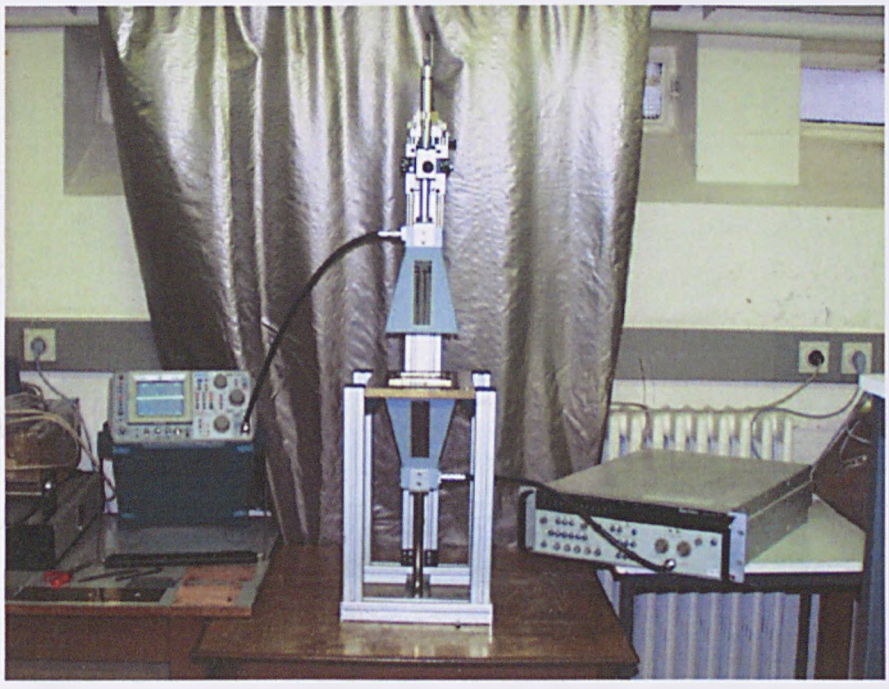

Fig. 1.7 A simple measuring cell for the SE measurement of small samples at frequencies above 1 GHz. Picture courtesy of Johan Catrysse.

1.1.2 Shielding Effectiveness of Enclosures and Measurement Techniques

1.1.2.1 Shielding Effectiveness of Enclosures

The concept of SE can be applied to enclosures as well as materials. Unlike a flat material sheet, of which the SE is determined only by the material and the sheet thickness, the shielding performances of enclosures are generally determined by [14]:

- The material realizing the enclosure
- The geometry and dimensions of the enclosure
- The presence of apertures
- The characteristics of the incident electromagnetic field
- Orientation and polarization of the source outside the enclosure
- Position and orientation of the contents inside the enclosure

It is also emphasized here that the field within an enclosure varies with orientation within the enclosure and if the enclosure is electrically large, the field is also position dependent due to resonance. That is, the SE of an enclosure also depends on the position and polarization of the measurement antenna inside the enclosure.

1.1.2.2 Shielding Effectiveness Measurement Techniques for Large Screened Enclosures

Although SE is the currently acceptable measure for assessing the effectiveness of either a material or enclosure to attenuate electromagnetic (EM) fields, the measurement techniques for an enclosure are different from those for materials mainly because the enclosure structure is different from that of a planar material sample.

Traditionally, during the SE measurement of an enclosure, the enclosure is illuminated by an EM wave from an external antenna and the attenuated signal is measured by a receive antenna at a certain point inside the enclosure. As the enclosure is absent, the reference signal is obtained by the receive antenna at the

same point. The SE of the tested enclosure is the ratio of the reference signal to the attenuated signal. Various techniques based on this two antennas method were developed to measure the SE of large screened enclosures. The relevant standards are MIL STD 285 [5], IEEE STD 299 [6] and IEC61000-4-21: Annex H [4].

- **MIL STD 285**

This standard was specifically developed for the SE assessment of large enclosures. The measurement method described in the MIL STD 285 for enclosures is similar to the modified one for large flat materials, except that the shielded room is replaced with the enclosure tested and the enclosure is illuminated by a wave from an external transmit antenna.

Three frequency regions are involved in this standard, in each of which, only one or several spot frequency measurements are suggested:

- Magnetic field (low wave impedance) measured at one frequency in the 150 to 200 kHz range
- Electric field (high wave impedance) measured at 200 kHz, 1 MHz and 18 MHz
- Plane wave measured at 400 MHz

Both near-field measurement and far-field measurement are included in this standard. During the near-field measurement, loop antennas are employed for the measurement of magnetic field and Equation (1.2) is used to determine the SE against magnetic field; rod antennas are used for the measurement of electric field and Equation (1.1) is used to determine the SE against electric field. In terms of the far-field measurement, tuned dipoles are specified as the measurement antenna and the SE may be determined by Equation (1.1) or (1.3).

- **IEEE STD 299**

The IEEE STD 299 was developed by the Institute of Electrical and Electronics Engineers (IEEE) for determining the SE of screened enclosures having no dimension less than 2.0 m. Three frequency ranges are involved in this standard:

1. Low-frequency range for the measurement of magnetic component *H*: 9 kHz ~ 20 MHz
2. Resonance range for the measurement of electrical component *E*: 20 MHz ~ 300 MHz
3. High-frequency range for the measurement of plane wave power *P*: 300 MHz ~ 18 GHz

Loops are specified as the measurement antennas in the low-frequency range. Biconical antennas and dipoles are respectively the measurement antennas at the lower frequency band (20 ~ 100 MHz) and the upper frequency band (100 ~ 300 MHz) of the resonance range, while dipoles and horns are employed respectively in the lower frequency band (0.3 ~ 1.0 GHz) and the upper frequency band (1.0 ~ 18 GHz) of the high-frequency range. Consequently, Equation (1.2), (1.1) and (1.3) are used respectively, to determine the SE in the low-frequency range, resonance range and high-frequency range.

This standard suggests a frequency-swept measurement rather than the fixed-frequency measurement specified in MIL STD 285.

- **IEC61000-4-21: Annex H**

IEC61000-4-21: Annex H describes the measurement technique for determining the SE of enclosures in reverberation chamber. The measurement set-up in IEC61000-4-21: Annex H is similar to that for materials in IEC61000-4-21: Annex G, except that during the SE measurement of enclosures, the test fixture is replaced with the enclosure tested.

One main advantage of reverberation chambers is that the field structure inside a working reverberation chamber is complex and detailed, which means the fields are incident on the item under test with various polarizations and angles of incidence [15]. That is, in terms of SE measurement, the reverberation chamber can provide a more realistic environment than other techniques. However, as the discussion in the above introduction of IEC61000-4-21: Annex G, only the far-field measurement, i.e. the measurement of the SE against radiating power, can be performed in the

reverberation chamber. Another shortcoming of this measurement technique is because both a receive antenna and a paddle wheel tuner/stirrer are required to install inside the tested enclosure during the measurement, such measurement technique is not easily applied for small enclosures. The basic knowledge of reverberation chamber measurement will be introduced in Chapter 5.

1.1.2.3 Demand of New Techniques and Measures for Equipment Enclosures

Because of the fast development of the communication technologies and information technologies in the last two decades, issues related to the EMI and EMC problems of inter-system with these technologies at large arose. Thus the assessment of the shielding performance of an equipment enclosure, of which the dimensions are usually between 0.1 m and 2 m, is of great importance.

However, the measurement techniques described in the above standards are not suitable to measure the shielding performance of an equipment enclosure. The main reasons are as follows:

- The largest dimension of equipment enclosures is usually less than 2 m. Thus, the standard EMC measurement antennas, such as biconical, log-periodic and horn antennas, are physically too large to place inside such enclosures.
- The equipment enclosure generally has a number of slots for ventilation, disc insertion and cable penetration etc. Different incidence angles and polarizations of the external fields mean various excitations on the apertures, resulting in different attenuated fields inside the enclosure and so different shielding performance of the enclosure. Thus the coplanar antennas method used in IEEE STD 299 and MIT STD 285 is not applicable for the shielding measurement of equipment enclosure with apertures, and a 'scan method' used for the measurement of field structure/pattern may be more suitable.
- At frequencies above 1 GHz, an equipment enclosure may be electrically large and the field structure inside may be complex due to resonance. This means the measurement result strongly depends on the antenna position

inside the enclosure and the field variation inside the enclosure should be accounted during the derivation of the shielding effectiveness [16].

- Considering an equipment enclosure usually has a high fraction of their internal volume occupied by the enclosure contents, such as printed circuit boards (PCBs), these contents may absorb a considerable fraction of the internal EM energy or greatly disturb the internal field distribution and so affect the shielding performance of the enclosure [17], [18], [19]. Thus during the shielding measurement of an equipment enclosure, the contents inside should be considered This is in direct contrast to the traditional SE measurement of a larger shielded room during which the contents inside the enclosure are just ignored.

In a word, there are no standard test procedures presently available for determining the shielding performance of equipment enclosures at frequencies above 1 GHz. Although other measurement techniques have also been developed for equipment enclosures, such as the application of small measurement antennas [20], the consideration of the field variation inside the enclosure [16] and the effect of contents [17], [18], [21], [22] during the measurement, none of them can deal with all the issues discussed above.

Considering the SE of an enclosure may be dependent on the position and polarization of the measurement antenna, a single figure for SE is not able to express the shielding performance of the enclosure and so in fact has no real use. This implies a new definition for the effectiveness of a shielding enclosure may be required.

1.2 Aim and Scope

As discussed above, the testing of small enclosures should be very different from the testing of large screened rooms. Currently, a new working group WG 299.1, organized and sponsored by IEEE EMC Society Standards Development Committee (SDCom), is developing measurement techniques for determining the shielding effectiveness of small enclosures and boxes having minimum linear dimensions

between 0.1 m and 2 m, only. This is a sub-class of the enclosures not covered by the existing IEEE Std. 299.

The aim of this thesis is to propose suitable measurement techniques and associated measures to assess the effectiveness of electromagnetic shielding of equipment enclosures at frequencies above 1 GHz. So this thesis is directly informing the new developments in IEEE STD 299.

It is suggested that the new measure and the relevant measurement techniques proposed should incorporate the practical applications of the equipment. Based on this idea, many efforts have been made in this thesis, which are described as follows.

Firstly, although many studies have been performed on the measurement or numerical analysis for the SE of an equipment enclosure [18], [20], [23], [24], [25], frequencies below 1 GHz were generally concerned, say, only up to the fundamental cavity mode resonance. However, considering that the base clock frequency and its harmonics of current consumer electronic equipment are frequently in excess of 1 GHz, it is time to consider the shielding measurement of equipment enclosures at frequencies above 1 GHz. The frequency range of the shielding measurements in this thesis is from 1GHz to 6GHz.

Secondly, the measurement standards [4], [5], [6] and the associated measurement practices only focus on the near field or/and the far field measurement. Considering the scenario where the equipment are usually located, such as several IT systems in a medium sized room, the possible interference is likely caused by radiated emissions of the equipment in their radiating near-field (the concept of radiating near-field will be introduced in Chapter 3). Thus, in this thesis, the measurements in the near-field or the far-field are not considered, but the measurements in the radiating near-field are.

Thirdly, in practice, an equipment enclosure has ability to inhibit the emission of the internal contents from radiating outside to cause interference with the nearby equipment or to shield the internal contents against the external interference. In this thesis, these two shielding abilities are termed radiating shielding and immunity shielding respectively. Both of these shielding abilities are considered and measured

by two different measurement approaches. For each of these shielding abilities, a new measure is proposed.

In the first measurement approach, to measure the ability of the enclosure to prevent the electromagnetic waves from the internal contents radiating outside, an emission source is placed inside the enclosure and a receive antenna is placed outside. Two measurement environments: an anechoic chamber and a reverberation chamber are considered. In each environment, a new measurement technique is developed to measure the radiated power from the equipment content with the enclosure and without the enclosure. Based on the measurement results, a new measure shielding of radiating power (*SRP*) is proposed, which consists of two parameters: the first one is average shielding of radiating power (*ASRP*) used to indicate the average radiating shielding performance of the enclosure. The second one is enhancement factor $E.F._{95th}$ (the ratio of the upper 95^{th} percentile of the power density to the average measured when the enclosure is present), and the worst radiating shielding performance is determined by the ratio of *ASRP* to $E.F._{95th}$.

In the second measurement approach, to measure the enclosure's ability to shield the internal contents against external interference, the enclosure is placed in a small reverberation chamber and illuminated by external electromagnetic field. The proposed measurement technique is used to determine the average absorption cross section of the equipment content with and without the enclosure. Based on the measurement results, another new measure shielding of absorption cross section (*SACS*) is proposed.

1.3 Structure of the Thesis

To make the thesis is readable and accessible to readers with different backgrounds, the layout of the thesis coincides with the progress sequence of this project. The division of the materials presented in this thesis is as follows:

- **Chapter 2** A dummy equipment under test (EUT) with similar structure and comparable electromagnetic properties to a typical electronic equipment is established. This EUT is employed in the subsequent shielding measurements.

- **Chapter 3** Chapter 3 considers the radiating shielding measurements of an equipment enclosure in anechoic chambers. A scan method to measure the radiation pattern of the dummy EUT or the content of the dummy EUT in an anechoic chamber is proposed.

- **Chapter 4** Based on the radiation patterns measured in the anechoic chamber, several new definitions for the radiating shielding performance of an equipment enclosure are considered. The measurement results based on these definitions are presented and compared. By evaluating the advantages and disadvantages of these definitions, the definition shielding of radiating power, *SRP*, is finally proposed as a suitable one for the radiating shielding. The relevant measurement work in anechoic chambers is time consuming, so to determine this measure swiftly, another method is developed and introduced in Chapter 5.

- **Chapter 5** In this chapter, a reverberation chamber measurement technique is proposed to determine swiftly the average shielding of radiating power, *ASRP*, and a modelling technique is employed to simulate the equipment's emission patterns from which the enhancement factor $E.F._{95th}$ can be derived. Then, the *SRP* can be obtained from the combination of the measurement and simulation results.

- **Chapter 6** To evaluate the immunity shielding performance of an equipment enclosure, a new definition shielding of average cross section, *SACS*, is proposed and the relevant measurement technique in a small reverberation chamber is illustrated. Advantages and disadvantages of this measurement method are discussed.

- **Chapter 7** Conclusions drawn from the thesis are presented in this chapter. Directions for future research are discussed here.

Chapter 2

Setup of the Dummy EUT

2.1 Introduction

The goal of this chapter is to establish a dummy EUT having the similar structure and comparable electromagnetic properties to a typical electronic equipment. This dummy EUT will be employed for the following shielding measurements. The application of the dummy EUT has the advantage that the following measurement techniques proposed would be appropriate to practical equipments but the detailed specifications of these equipments are avoided. The application of a single dummy EUT also enables the comparisons between the measurement results from different measurement techniques.

A typical electronic equipment usually consists of an enclosure made from a conductive material and a printed circuit board (PCB) mounted inside. The enclosure generally has a number of apertures for the ventilation, display and insertion. The structure of the PCB is complex, both sides of which are generally populated with a number of components connected with numerous conducting tracks.

It is well known that the apertures have effect on the shielding performance of the enclosure. According to Babinet's principle [26], the apertures on an infinite screen act as antennas whose conductor dimensions are those of the apertures. Thus it can be expected that fields inside or outside the enclosure will radiate through the apertures, reducing the effectiveness of the enclosure. The radiation from the apertures on an enclosure may also be analyzed as those derived from a waveguide section short-circuited at one end and open at the other or diffractions from small apertures on a wall [27].

The theoretical analysis and the measurement results shown in [22] have indicated that any lossy objects introduced in an enclosure will reduce the Q factor of the enclosure and thus have effects on its shielding performance. Because the PCB inside

an equipment enclosure usually occupies a high fraction of the internal volume, disturbing the internal field distribution and absorbing the internal electromagnetic (EM) energy, the shielding performance of the enclosure also partially depends on the PCB. This has been verified by the measurement results given in [17], [18], [19]. Thus it is suggested here during the shielding measurement of an equipment enclosure, the contents inside should be considered. This is in direct contrast to the traditional SE measurement of a larger shielded room during which the contents inside the enclosure are not considered due to the contents usually having a small volume fill. For example, an Agilent spectrum analyser E4404B with dimensions of 0.4 m × 0.35 m × 0.2 m only occupies 0.35% internal volume of a screened enclosure with dimensions of 2 m × 2 m × 2 m, the smallest possible dimensions meeting the applicability of IEEE STD 299. However, in terms of a desktop computer chassis, generally 20% ~ 40% of its internal volume is filled by the equipment contents.

Because both the apertures and the PCB may have great effects on the shielding performance of an equipment enclosure, both of them will be concerned in the configuration of the dummy EUT. Considering the component populations and dimensions of the PCBs are varied, the idea using a representative conte : (RC) [18] to represent a typical PCB has also been used here. The reason for using a single RC is the same principle as vehicle crash testing, during which a crash dummy with comparable mechanical properties to a real human is employed, but standardised and repeatable.

The organization of this chapter is as follows. In section 2.2 the configurations of the dummy EUT are detailed. In section 2.3 a new measure called "width of autocorrelation" (*WA*) is proposed, which can be used to compare approximately, the absorption ability of different PCBs or RCs in an equipment enclosure over a specified frequency range. The associated measurement technique is described and the measurement results are presented. Based on the calculation results of *WA*, a new method to find a suitable RC at frequencies above 1 GHz is illustrated. In section 2.4 the main contents in this chapter are summarized.

2.2 Configuration of the Dummy EUT

2.2.1 Configuration of the Enclosure

The dummy EUT used in this work has dimensions of 480 mm × 480 mm × 120 mm, representing a 19-inch rack unit. The enclosure of this dummy EUT is made of brass sheet with thickness of 2 mm. It is mentioned here that other enclosures with comparable dimensions may be also considered in the configuration of the dummy EUT, which should not affect the feasibility of following measurement techniques proposed.

The front panel of the dummy EUT was perforated with a large 160 mm × 40 mm slot at the centre of the panel, and a number of smaller slots with dimensions of 35 mm × 5 mm and 30 mm × 5 mm. To obtain different slot configurations, the number and dimensions of these slots were changed by copper tapes. A 180 mm × 60 mm brass plate perforated with a 100 mm × 5 mm slot was also used to cover the large 160 mm × 40 mm slot. Three different slot configurations in the front panel were employed during our measurements. See Fig. 2.1.

In each slot configuration, the apertures are comparable to those in the practical equipment enclosures. The two 30 mm × 40 mm apertures shown in Fig. 2.1(a) have the comparable dimensions to those of small displays, such as the light-emission diode (LED) display and the liquid crystal display (LCD), while the 100 mm × 5 mm slot in Fig. 2.1(b) can represent a compact disc (CD) sized opening and in Fig. 2.1(c) the slots of 35 mm × 5 mm or 30 mm × 5 mm may be appropriate to represent the apertures for ventilation. For the future computational electromagnetic simulation, the minimum width of the slots is restricted to 5 mm, 1/10 of the wavelength of 6 GHz (the highest frequency considered in our measurements), satisfying the $\lambda/10$ criterion of the transmission line modelling (TLM) technique.

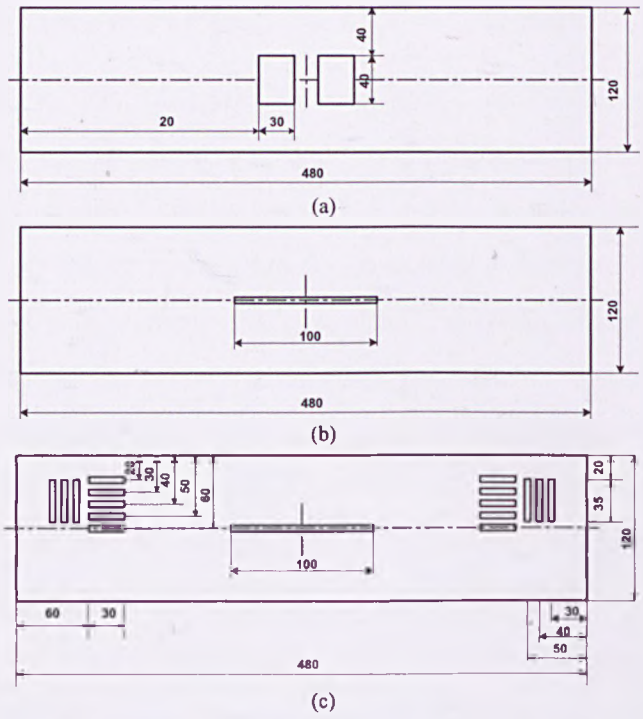

Fig. 2.1 Geometry of the front panel with different slot arrangements. All dimensions in millimeters. Configurations of slots in the front panel: (a) two rectangular slots, (b) one CD slot with width of 5 mm and (c) one CD slot, 6 vertical slots and 10 horizontal slots, all of which are 5 mm wide.

The picture of the dummy EUT with one 100 mm × 5 mm CD slot in the front panel is given in Fig. 2.2.

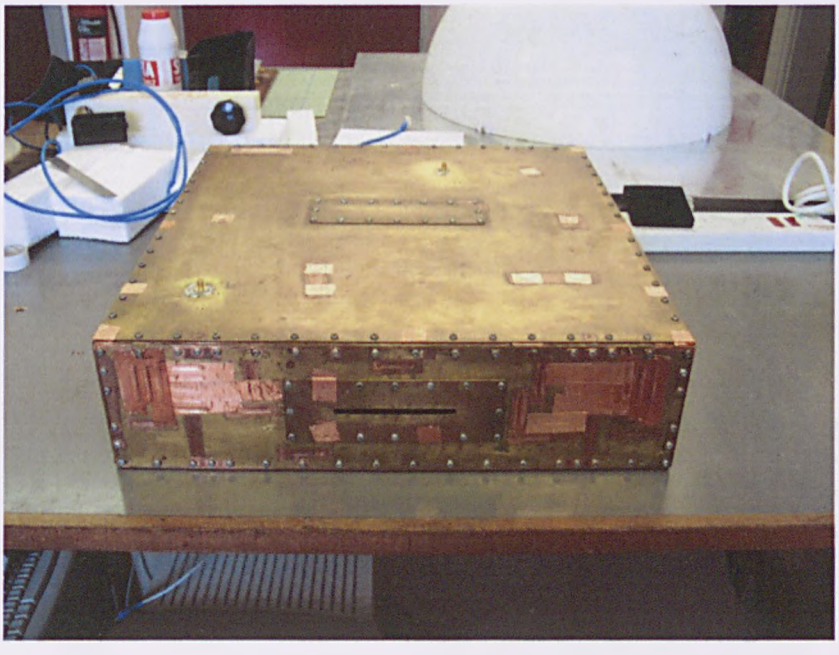

Fig. 2.2 The dummy EUT with one CD slot in the front panel.

2.2.2 Configuration of the Representative Content

It has been shown in [21], [28] that for computation modelling purposes, a typical circuit board which has complex structure can be represented as a thin homogeneous sheet. The idea of using a homogeneous sheet representing a circuit card has been extended in the shielding measurement work demonstrated in [18], where the combination of a PCB laminate and a layer of carbon-loaded foam was considered as representative content, i.e. RC. The laminate provides the ground plane and the carbon-loaded foam layer represents the absorbing properties of the components populated on the circuit card. The RC is also involved for the shielding measurement work presented here, which consists of a PCB laminate, a layer of carbon-loaded foam and a comb generator (YES CGE02), as shown in Fig. 2.3. The area of the RC is 300 mm × 240 mm, representing a reasonable fill of the 480 mm × 480 mm × 120 mm enclosure. The CGE02, which is mounted on the same side as the carbon loaded foam, has emissions with a harmonic spacing of 250 MHz from 250 MHz to 26 GHz [29].

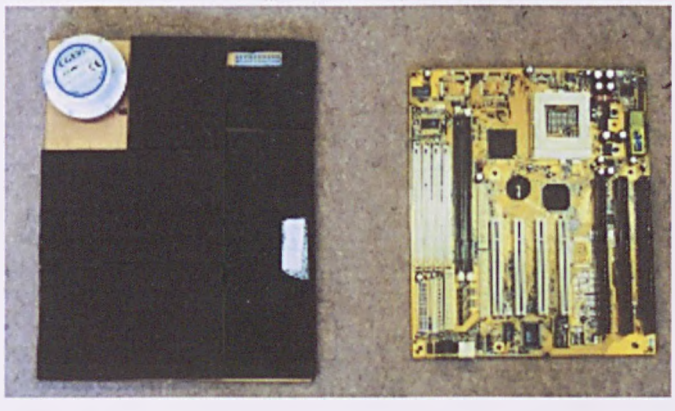

Fig. 2.3 The RC consists of a PCB laminate and a carbon-loaded foam layer with a CGE02 (left) used to represent a typical circuit board (right).

Previously, radiation frequencies considered in EMC problems were generally from 30 MHz to 1 GHz. However, considering the clock speed of the modern IT systems is frequently in excess of 1 GHz, it is time to concern the EMC problems at frequencies beyond 1 GHz. In terms of the shielding measurements presented in this thesis, the radiations from the CGE02 at six spot frequencies from 1GHz to 6 GHz with 1 GHz interval are tested. Due to the limited number of the spot frequencies, it

is likely that the resonance frequencies of a tested enclosure, at which the SE of the enclosure is usually small, may be missed during the measurements. However, the measurement techniques, rather than the measurement results, are concerned in this thesis. The missing of the resonance frequencies would not affect the validity of the measurement techniques proposed here.

Consider the radiation from an aperture excited by an incident wave from the other side. The radiated field strength depends on the incidence angle and the polarization of the incident wave. As a radiation source is placed inside an electrically large enclosure with apertures, the field distribution inside the enclosure is complex mainly due to resonance. It may be predicted that the phase, amplitude and polarization of the arrival on the inner side of the aperture are dependent on the source position, that is, different internal source positions mean various excitations on the aperture, which may result in different radiations and so different shielding performances of the enclosure. In a real system, the emission source may be located at any position on the PCB. To test the possible effect of the source position on the shielding performance, six different source positions on the PCB laminate of the RC (see Fig. 2.4) are considered, on each of which the CGE02 can be mounted and tested respectively during the shielding measurement.

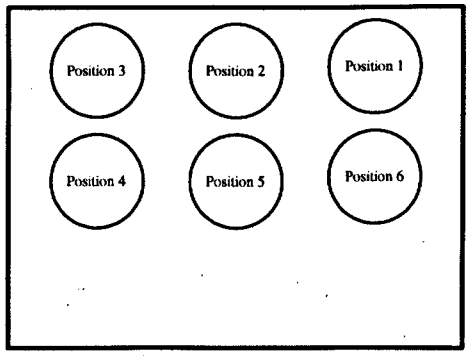

Fig. 2.4 Different CGE02 positions on the RC.

The consideration of three different slot configurations in the front panel of the dummy EUT, six different source positions on the RC and six different measurement frequencies can promise a statistically significant population of EUT configurations has been used in this work.

2.3 Determination of the Representative Content

2.3.1 Previous Method

A method to determine a suitable RC has been proposed in [18], where the determined RC was employed in the shielding measurements at frequencies below 1 GHz. This method also is illustrated as follows.

A suitable RC should have the similar absorbing properties to those of a typical circuit board. These are mainly determined by the type and thickness of the carbon-loaded foam layer of the RC. To determine a suitable RC, at first, either the circuit board or the tested RC should be placed respectively at the same position in a sealed cavity with comparable dimensions to an equipment enclosure. Two monopoles are placed inside the cavity and connected with the two ports of a network analyser via coaxial cables. Then the S_{21}, i.e. the transmission coefficient, between the two monopoles is measured. To avoid direct coupling, the two monopoles should be placed respectively in two adjacent sides of the enclosure and oriented in orthogonal directions. A sketch of the measurement setup for the S_{21} of the loaded cavity is given in Fig. 2.5.

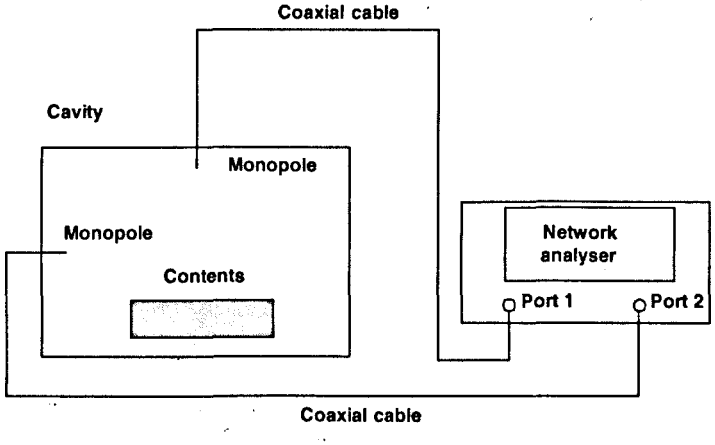

Fig. 2.5 The measurement setup for the determination of an appropriate RC.

The dimensions of the cavity used in [18] for the determination of a RC were 400 mm × 400 mm × 125 mm. However, the cavity used here has dimensions of 480 mm × 480 mm × 120 mm, being same as those of the dummy EUT. Fig. 2.6 shows the cavity used here and the positions of the connectors on this cavity.

Fig. 2.6 The 480 mm × 480 mm × 120 mm cavity used for the determination of a suitable RC.

Considering the cavity used is electrically small at frequencies below 1 GHz, the frequency response of the S_{21} of the cavity should be relative simple at these frequencies. Thus, the properties of the RC (foam thickness and type), may be determined by the closest agreement between the frequency response of the cavity loaded with the circuit board and that of the cavity loaded with the tested RC. Fig. 2.7 gives the examples of S_{21} between two monopoles in a cavity containing a PCB and a RC of the same size respectively, both of which are simple and can be compared directly. These two frequency responses are almost identical at frequencies below 1 GHz, meaning at these frequencies the RC has similar absorbing properties to the PCB and so can be used to represent the PCB during the shielding measurement.

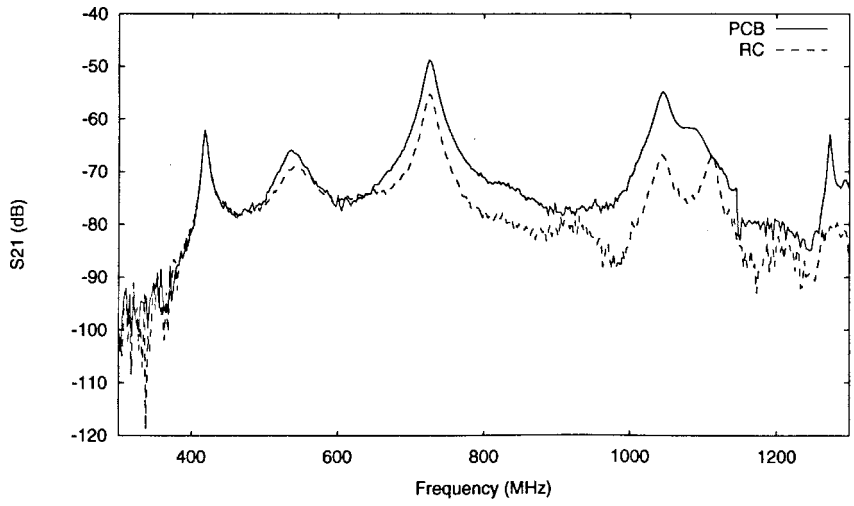

Fig. 2.7 Comparison between the S_{21} of a cavity loaded with a PCB and that loaded with a RC of the same size at frequencies from 400 MHz to 1 GHz. The PCB dimensions are 240 mm × 90 mm. The cavity dimensions are 400 mm × 400 mm × 125 mm. Figure courtesy of Andy Marvin.

2.3.2 A Proposed New Measure for Width of Autocorrelation

At frequencies much higher than 1 GHz, a cavity with dimensions close to a typical equipment enclosure becomes electrically large, a large number of modes may exist inside and the frequency response of S_{21} is complex. For such a case, the RC cannot be determined by the direct shape comparison between the frequency responses of S_{21}, as the examples shown in Fig. 2.8. That is, the curve-matching method demonstrated in the above subsection is limited and a new one should be considered.

It is likely this difficulty may be coped with by using a statistical approach. Here the autocorrelation of the frequency response of S_{21} is considered. By taking autocorrelation, the complicated frequency response of an overmoded structure is changed to 'one peak' shape, which makes it possible to compare the gross electromagnetic properties of different contents and avoids the inevitable differences between the fine structure of the frequency responses at the same time [30].

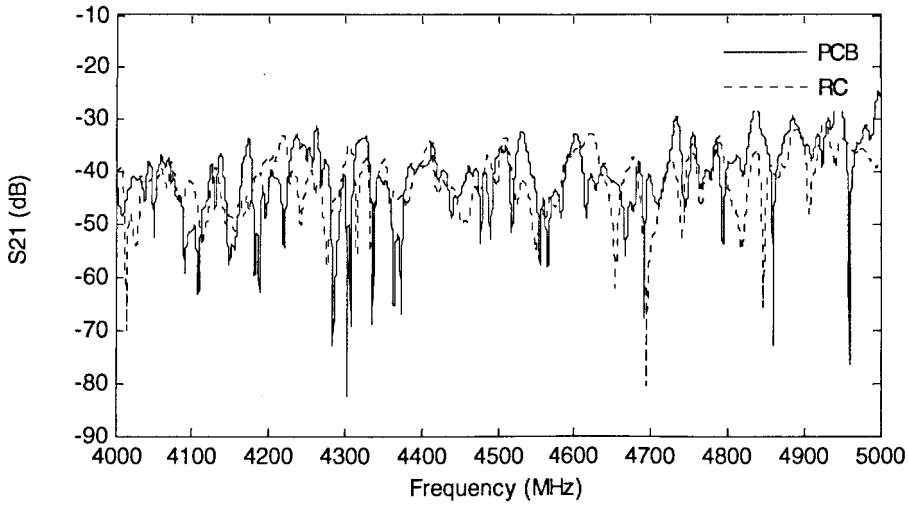

Fig. 2.8 Comparison between the S_{21} of a cavity loaded with a PCB and that loaded with a RC at frequencies from 4 GHz to 5 GHz. The PCB dimensions are 240 mm × 300 mm. The cavity dimensions are 480 mm × 480 mm × 120 mm.

The application of the autocorrelation on the frequency response is illustrated as follows. During the measurement, the frequency response is generally measured at N discrete spot frequencies with the same interval. The autocorrelation of the sequence of N measured values x_n is defined as:

$$C[n] = \sum_{m=0}^{N-n-1} x_{m+n} x_m \qquad (2.1)$$

The range of the lag n is [-N+1 N-1], so the length of the autocorrelation results is 2N-1. The autocorrelation results are symmetrical about n=0. Here the Matlab command 'xcorr' is employed to perform the autocorrelation calculation, which produces a normalized value 1 at n=0.

The S_{21} of an empty cavity and that of this cavity loaded with a circuit card measured at different frequency ranges are shown in Fig. 2.9. Their autocorrelation results are plotted respectively in Fig. 2.10. Obviously, the plot of the autocorrelation of S_{21} is mush simpler than the plot of the S_{21}.

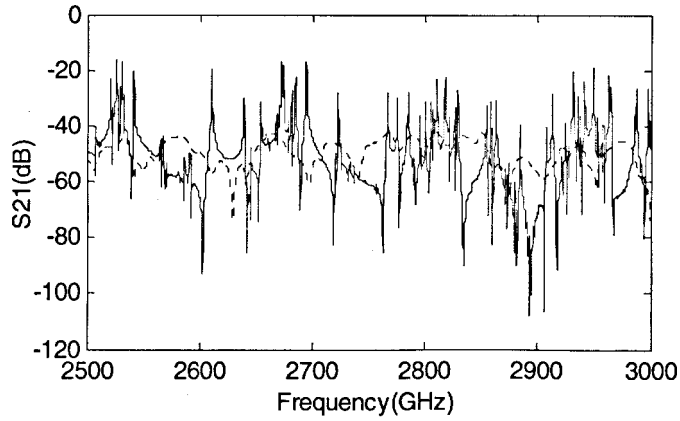

(a)

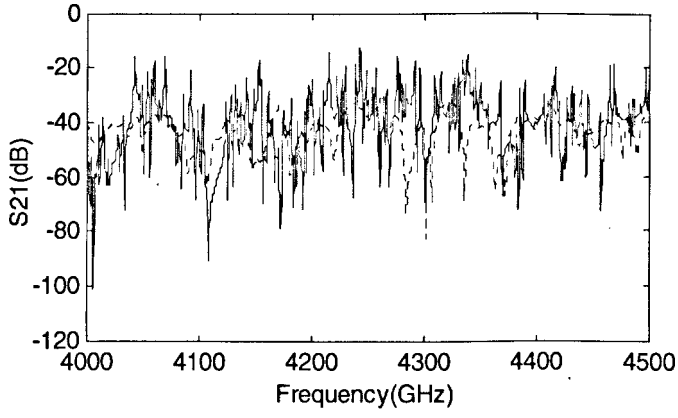

(b)

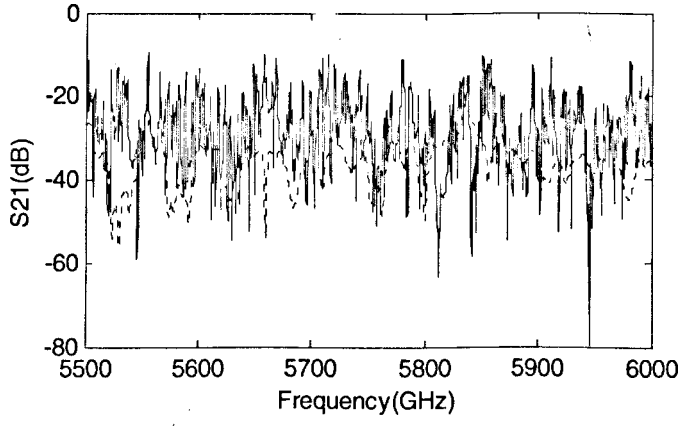

(c)

Fig. 2.9 Measurement results of the S_{21} of an empty cavity (solid line) and this cavity loaded with a circuit board (dotted line). Cavity dimension: 480 mm × 480 mm × 120 mm. Frequency range: (a) 2.5 GHz ~ 3 GHz, (b) 4 GHz ~ 4.5 GHz and (c) 5.5 GHz ~ 6 GHz.

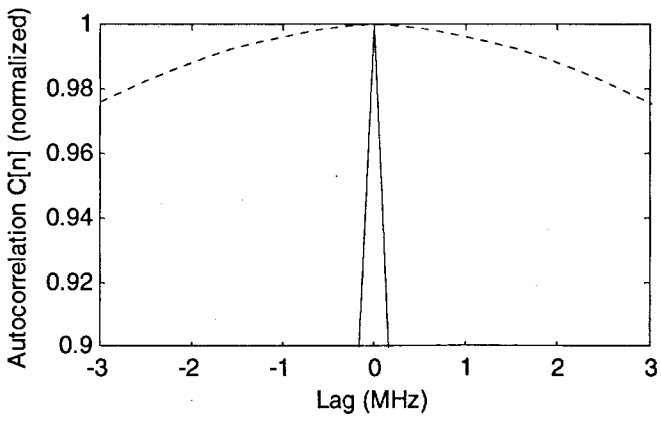

(a)

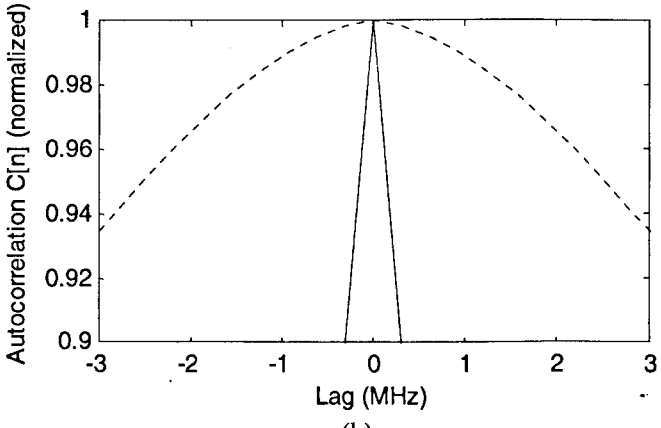

(b)

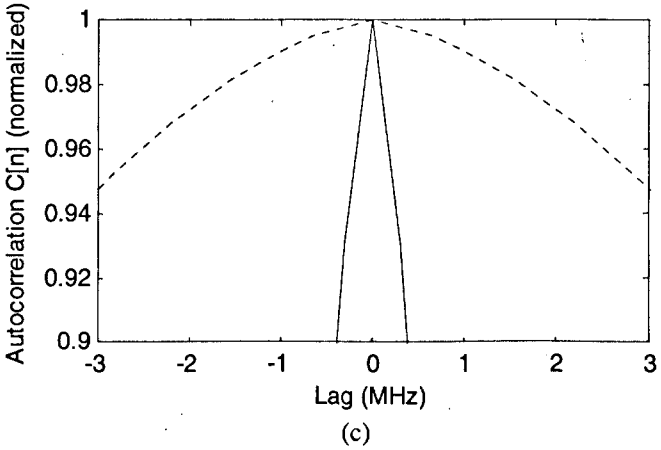

(c)

Fig. 2.10 (a) Autocorrelation results of the S_{21} shown in Fig. 2.9 (a); (b) Autocorrelation results of the S_{21} shown in Fig. 2.9 (b); (c) Autocorrelation results of the S_{21} shown in Fig. 2.9 (c). Solid line: the autocorrelation of the S_{21} of an empty cavity; dotted line: the autocorrelation of the S_{21} of this cavity loaded a circuit board.

The autocorrelation results in Fig. 2.10 imply that the shape of the autocorrelation depends on the energy dissipation inside the cavity: a sharper peak means lower internal energy dissipation. On the contrary, a flatter peak means higher energy

dissipation. More evidence can be found from the autocorrelation results shown in Fig. 2.11. The recent studies on the effects of apertures and human bodies on the propagation and field-statistics inside an aircraft [30] have also shown the width of the autocorrelation function peak increases as the Q decreases, i.e., there are more energy losses inside the cavity.

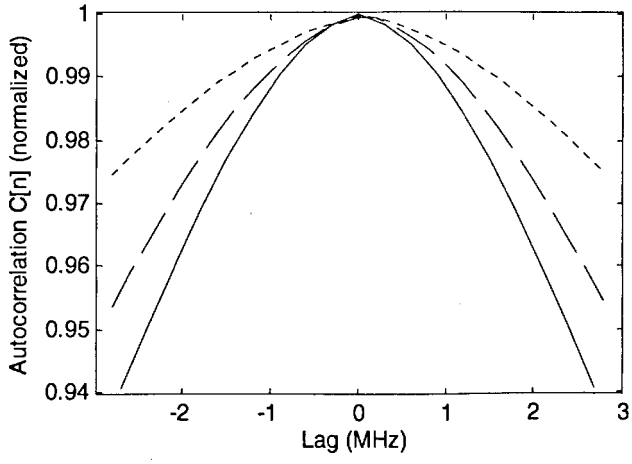

Fig. 2.11 Autocorrelation results of the S_{21} (4 GHz ~ 4.5 GHz) of the cavity with different loads. Solid line: the cavity loaded with one circuit card; dashed line: the cavity loaded with the circuit card and a 160 mm × 100 mm × 5 mm carbon loaded foam; dotted line: the cavity loaded with the circuit card and two 160 mm × 100 mm × 5 mm carbon loaded foams.

To quantify the gross absorption ability of the contents over a certain frequency span, a new parameter width of autocorrelation, *WA*, is proposed, which is defined as the 3-dB bandwidth of the autocorrelation of the frequency response of S_{21}^2 in a defined frequency range. See Fig. 2.12.

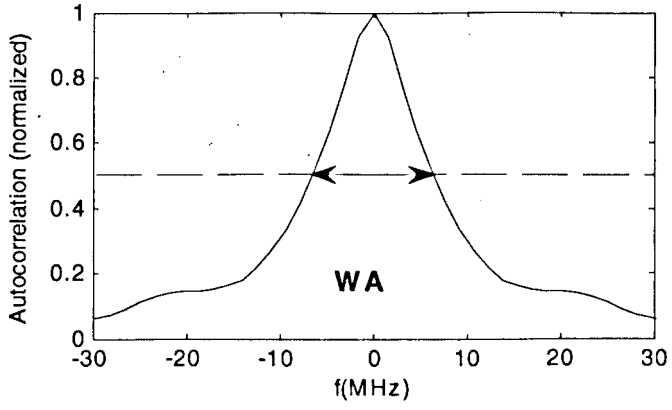

Fig. 2.12 Illustration of definition of *WA*.

2.3.3 The Method to Determine a Suitable RC

Generally, the electromagnetic parameters of materials, such as the permittivity ε and the permeability μ, depend on frequency, i.e. the EM energy loss of materials depends on the frequency. For different materials, the relationship between the loss and frequency is different. A suitable RC should have the similar energy absorption or similar *WA* to that of a typical circuit card in each frequency sub-range of the whole frequency range we are interested in. The frequency range from 1 GHz to 6 GHz is concerned during our measurement. However, over such a broad frequency range, it is not easy to find a RC, of which the *WA* at each frequency sub-range is always close to that of a certain circuit card. So a compromise method is proposed to determine a suitable RC, being illustrated in the following paragraphs.

At first several circuit boards are selected, which are considered as typical contents in most of the equipments and the *WA* of each of these circuit boards is measured. Then the *WA* of the considered RCs with different foam types or thicknesses is also measured separately. Based on the measurement results, the suitable RC is defined as such that at each frequency sub-range, its *WA* should be between the maximum and the minimum *WA* of these circuit boards measured.

During our measurement, the selected circuit boards were two different PC mainboards and two different PC adaptor cards, all of which are multi-layer PCBs made of the same technology and have the similar component density. Both the PC mainboards have the same area 260 mm × 240 mm, which is similar to the total area of the two adaptor cards, 240 mm × 200 mm. For each 200 MHz sub-range, the *WA* of each of the mainboards and the combination of the two adaptors were calculated. To consider the possible effects of the board orientation on the *WA*, every board was also rotated 180^0 about the vertical axis of the circuit plane during the measurement. Thus six frequency responses of *WA(f)* were obtained, as shown in Fig. 2.13. Here *'f'* refers the stop frequency of each frequency sub-range. The envelopes of the maximum *WA* and the minimum *WA* have been also plotted in Fig. 2.13, both of which define the range where the *WA(f)* of a RC should exist. Considering at each measurement, the total area and the component density of the measured circuit

board/boards are similar, the obvious variations between the *WA(f)* imply this measure is sensitive to the energy absorption inside the enclosure.

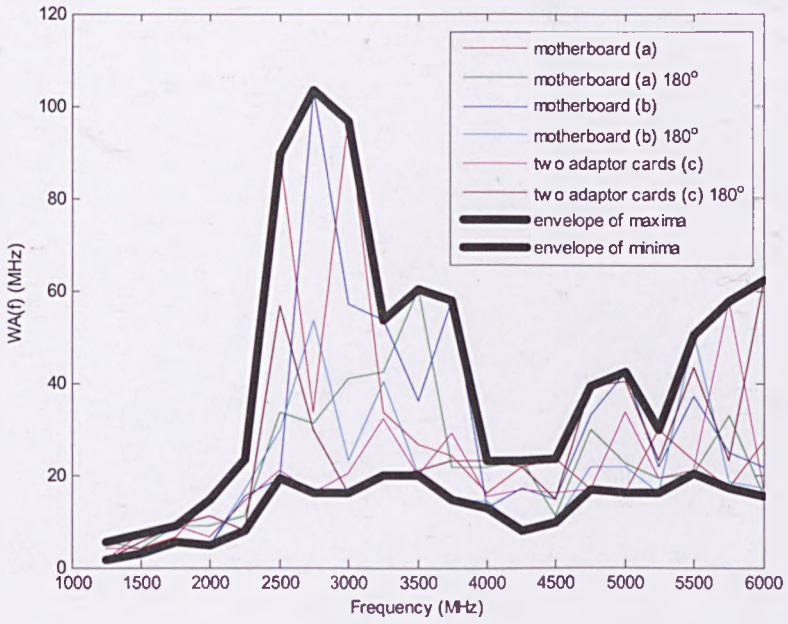

Fig. 2.13 *WA(f)* of various circuit boards with two orientations: 0° and 180°. The thick lines define the range of the *WA(f)* of a suitable RC. Frequency range: 1GHz ~ 6 GHz.

A number of foam sheets (different types and thicknesses) with the same area of the selected mainboard were selected, each of which combined with a PCB laminate was considered as a RC. Examples of the *WA(f)* of these RCs are shown in Fig. 2.14, where 'Foam A' is 10 mm thick and 'Foam B' is 20 mm thick, both of which are made of the same material; 'Foam C' is 10 mm thick and has larger carbon density than that of 'Foam A' and 'Foam B'. Again, the sensitivity of the *WA(f)* to the energy absorption of the contents is expressed by the obvious difference between the *WA(f)* of 'Foam A' with the PCB laminate and the *WA(f)* of 'Foam B' with the PCB laminate. The foam sheets tested here are not commercially available and the exact electromagnetic parameters of each foam sheet are not known. However, the foam sheet of a suitable RC may also be chosen from commercial radio absorption materials (RAM) on the basis of filled polymers, being similar to the foam sheets used here.

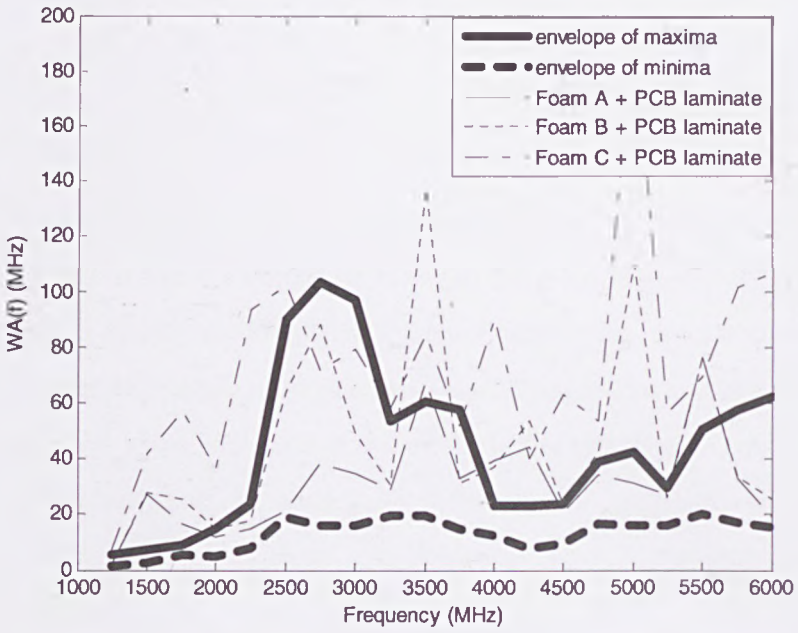

Fig. 2.14 Comparisons between examples of the *WA(f)* of different RCs and the defined range of *WA* given in Fig. 2.13.

Finally, the RC consists of the 'Foam A' and the PCB laminate, of which the *WA(f)* lies in the defined range of *WA* over most of the frequency range we are interested in, was considered as a suitable RC and employed in the following shielding measurements.

2.4 Discussion

In this chapter, a dummy EUT representing a practical electronic equipment is established, which will be used in the sequent shielding measurements. The apertures on the enclosure and the RC used to represent a typical circuit card have been emphasized in the configurations of the dummy EUT.

At frequencies below 1 GHz, it is possible to determine a suitable RC by comparing the S_{21} across a cavity loaded with a RC and the same cavity with a typical circuit card. As frequencies much higher than 1 GHz, due to the large number of resonant modes, it is necessary to adopt a statistical approach to this problem. Here we use autocorrelation of the frequency response of the S_{21} to mitigate the differences between frequencies. Based on the autocorrelation results, a new measure *WA* is

proposed to indicate roughly the absorption ability of the content over a certain frequency range and enable the comparisons between different contents over a much broader frequency range. The measurement results presented here demonstrate the measure *WA* is sensitive to the energy absorption.

During our measurements, a suitable RC is determined as such at each frequency sub-range, the *WA* of the RC should lie between the maximum and the minimum *WA* of several typical circuit cards selected. These cards have similar dimensions and component density. Although individual RCs are required to correspond to the circuit cards with different sizes and various component densities, the RC determined here, having similar absorption properties to those of the selected circuit cards, is considered as a standard content and will be used in all of the following measurement works.

Chapter 3

Radiating Shielding Measurements in an Anechoic Chamber

3.1 Introduction

As discussed in Chapter 2, an equipment enclosure always contains contents that may have effect on the shielding performance of the enclosure, so during the shielding measurement of an equipment enclosure, the contents should be considered in both the reference measurement step and the attenuation measurement step.

In this thesis, the shielding performance of an equipment enclosure will be studied from two approaches: the enclosure's ability to prevent the electromagnetic waves of internal contents from radiating outside and the enclosure's ability to shield the internal contents against external interference, which are named here respectively as radiating shielding and immunity shielding.

From Chapter 3 to Chapter 5, the relevant issues about the radiating shielding will be studied and discussed. To measure the radiating shielding of an equipment enclosure, the radiated fields of the contents without the enclosure and the radiated fields of the enclosure containing the contents should be measured respectively. So the radiating shielding measurement is directly relevant to the radiation measurement.

It is suggested here before proposing any new definition for the radiating shielding, the radiation characteristics of the equipment enclosure containing the contents and these of the contents without the enclosure should be studied at first and a measurement technique suitable for such radiation should be proposed.

Considering that the circuit cards inside an electronic equipment generally produce unintended emissions at low power levels, it is likely the radiation of the equipment may only interfere with other electronic equipment operated in its close proximity, say within the same room. If it is assumed that the interference is only significant

within a few meters of the equipment, the interference victim will be generally located in the radiating near-field region of the enclosure defined in [26] as:

$$0.62\sqrt{D^3/\lambda} \le \rho \le 2D^2/\lambda \quad (3.1)$$

where ρ is the radial distance from the enclosure, D is the largest dimension of the equipment enclosure and λ is the wavelength of the emissions. The boundary between the reactive near-field and the radiating near-field is determined by a distance ρ equal to $0.62\sqrt{D^3/\lambda}$, and the boundary between the radiating near-field and the radiating far-field is determined by a distance ρ equal to $2D^2/\lambda$, which is also termed Rayleigh range.

According to the above discussion, it is significant and suggested here the radiating shielding measurement should be performed in the radiating near-field of the EUT. At frequencies from 1 GHz to 6 GHz, the distances of the inner boundary and the outer boundary of the radiating near-field of a typical 19-inch rack unit, with a largest dimension of 0.48 m, are plotted in Fig. 3.1.

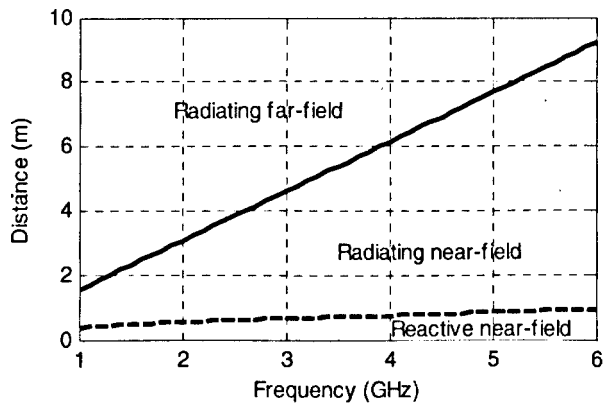

Fig. 3.1 The inner boundary (dashed line) and the outer boundary (solid line) of the radiating near-field of a 19-inch rack unit.

A suitable measurement technique for measuring the radiating shielding of an equipment enclosure in its radiating near-field in an anechoic chamber, i.e., the measurement technique for the radiation of either the equipment enclosure or the equipment contents, is discussed in this chapter. In Section 3.2, based on the theoretical analyses on the radiation properties of an electrically large source in its

radiating near-field, a suitable measurement method for such radiation is proposed and the relevant measurement setup in an anechoic chamber is presented. The measurement results are presented in Section 3.3, which confirm the feasibility of the proposed measurement method. The conclusions about the radiation measurement are presented in Section 3.4.

3.2 Measurement Technique

3.2.1 Radiation Properties of the Dummy EUT and the RC

Because current digital equipment clock frequencies are frequently in excess of 1 GHz, shielding performance of equipment enclosures at higher frequencies is concerned here. Shielding measurements presented in this paper were performed at frequencies from 1 GHz to 6 GHz. At these frequencies, a typical electronic equipment with dimensions of from hundreds of millimetres to one meter is electrically large. Consider an electrically large enclosure with emission source inside. The radiated field distribution around the electrically large enclosure is not a homogeneous plane wave, but expected to express fast spatial variation in its radiating near field due to the Fresnel diffraction from the enclosure. The distance between maxima and minima in the interference pattern may be as small as one quarter wavelength. Such property is illustrated with a simple mathematical model given in Appendix A.

Another property of the radiation of an equipment enclosure is that the polarization of the radiated field is varied and hard to predict. The possible reasons are as follows:

- There are always a number of slots in the walls of a typical equipment enclosure. The slots usually have different orientations, so the polarization of the field radiated from each slot, being perpendicular to the orientation of the slot, also varies.
- The field structure inside an electrically large equipment enclosure is complex due to the large number of excited modes and the effects of the contents. Thus, the phase and the amplitude of the excitation of each slot are unknown and hard to predict.

- The field at each test point is the result of the interference between the radiations of the slots each radiating with various polarizations, amplitudes and phases, so the polarization of the resulting field may vary with test position and cannot be predicted by observation of the enclosure.

Without the effect of the slots, the radiation of the equipment contents, i.e. the circuit cards, may be less complex than those of the equipment enclosure. However, a typical circuit card is also electrically large at frequencies above 1 GHz and usually has complex structure, so its radiated field may also express fast spatial variation and unpredictable polarization due to the Fresnel diffraction. Considering the possibly similar radiation characteristics of the RC to these of the dummy EUT, the following measurement method proposed will be used to determine the radiation of the dummy EUT and the RC respectively.

3.2.2 Measurement Method Proposed

According to the above predication, to match the fast spatial variation of the radiated fields around an electrically large source in its radiating near-field, a measurement antenna should be scanned on a surface encompassing this source, such as a fully spherical scan, of which the scan resolution should be less than the distance between maxima and minima in the radiation pattern. This distance can be determined by Equation (A.5).

Both spherical scan and cylindrical scan are generally adopted during the antenna pattern measurement [26], where the antenna polarization is generally known. The three coordinates (θ , ϕ , ρ) of a spherical coordinate system and the three coordinates (θ, h, r) of a cylindrical coordinate system are plotted respectively in Fig. 3.2.

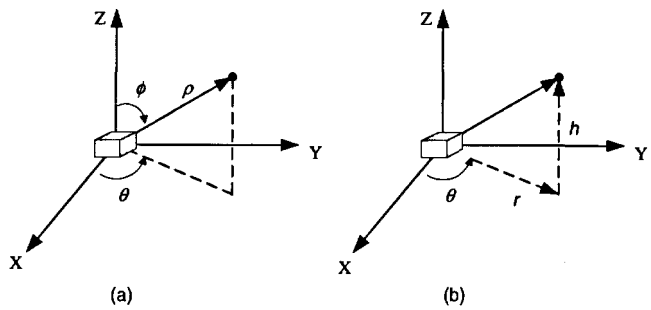

Fig. 3.2 The spherical coordinate system (a) and the cylindrical coordinate system (b).

Consider a spherical scan for the radiation measurement of an electrically large enclosure. Due to the unknown polarization of the radiated field at each test point, it is suggested that the magnitude of the radiating *E*-field at each point can be estimated by:

$$E = \sqrt{E_\theta^2 + E_\phi^2 + E_\rho^2} \,. \quad (3.2)$$

Here E_θ is the azimuth field component, E_ϕ is the zenith field component and E_ρ is the radial field component. It should be notified that in the radiating near field the transverse fields are dominant [26], thus E_ρ is much smaller than the other two components and may be ignored in Equation (3.2), i.e.:

$$E = \sqrt{E_\theta^2 + E_\phi^2} \,. \quad (3.3)$$

The positions of E_θ, E_ϕ and the magnitude of electric field E with different polarizations observed at each test point on the spherical scan surface are plotted respectively in Fig. 3.3. Equation (3.3) can estimate accurately the magnitude of electric field of linear polarization, but will result in the maximum error of 3 dB for that of circular polarization.

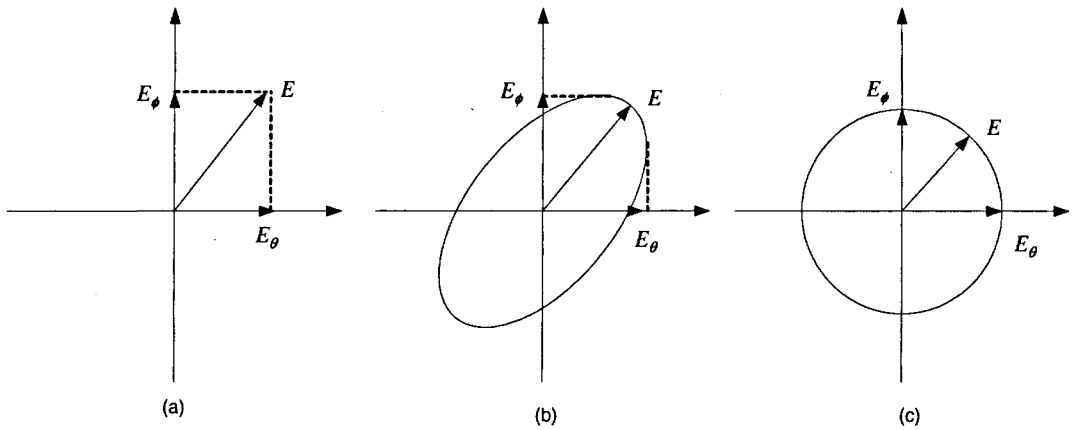

Fig. 3.3 The relationship between E_θ, E_ϕ and E with different polarizations: (a) E_θ, E_ϕ and E with linear polarization; (b) E_θ, E_ϕ and E with elliptical polarization; (c) E_θ, E_ϕ and E with circular polarization.

If a cylindrical scan is used, the magnitude of the radiating E-field at each point can be estimated by:

$$E = \sqrt{E_\theta^2 + E_h^2 + E_r^2} \ . \quad (3.4)$$

Here E_h is the field component along the 'h' coordinate and E_r is the field component along the 'r' coordinate. In the next chapter, the power flow through a cylindrical scan surface is considered. Thus at each test point, the field component tangent to the local surface is required, being expressed as:

$$E = \sqrt{E_\theta^2 + E_h^2} \ . \quad (3.5)$$

3.2.3 Measurement Setup

During the radiating shielding measurement, the dummy EUT was considered as representative of a typical electronic equipment. A comb generator (YES CGE02) was mounted on the RC and the radiation of both the dummy EUT and the RC without the enclosure were measured respectively.

A cylindrical scan was used during our measurement. To validate the cylindrical scan, the measurement antenna was scanned in height and for each antenna height the radiation source, i.e. the dummy EUT or the RC, was rotated for one circle. To ensure the measurements are performed in the radiating near-field of the dummy

EUT, the radius of the cylindrical scan was fixed at 1 meter. There were 200 test points spread evenly on each azimuth cut with circumference of 6.28 m and 40 test points spread evenly in the vertical scan height from 0.6 m below the geometric centre of the dummy EUT to 0.6 m above that geometric centre. Thus, the scan resolution on each direction is about 30 mm. At frequencies from 1 GHz to 6 GHz, the distance between maxima and minima in the measured radiation pattern, which may be derived from Equation (A.5), is always greater than 30 mm. Thus, the scan resolution we used here is considered fine enough to match the spatial variation of the radiation pattern.

At each test point, the measurements were taken with the antenna oriented in both 'θ' and 'h' directions and the magnitudes of E_θ and E_h were recorded respectively. The measurement results of all the test points form a radiation pattern of E_θ and a radiation pattern of E_h on a truncated cylindrical surface, i.e., a cylindrical surface without the two end caps.

The geometry of the cylindrical scan used during our measurement is given in Fig. 3.4, where h is the scan height of the measurement antenna, θ is the rotatic degree of the EUT and r is the radius of the cylindrical scan surface. The area frcm θ=-76° to θ=76° is the one in front of the panel with slots.

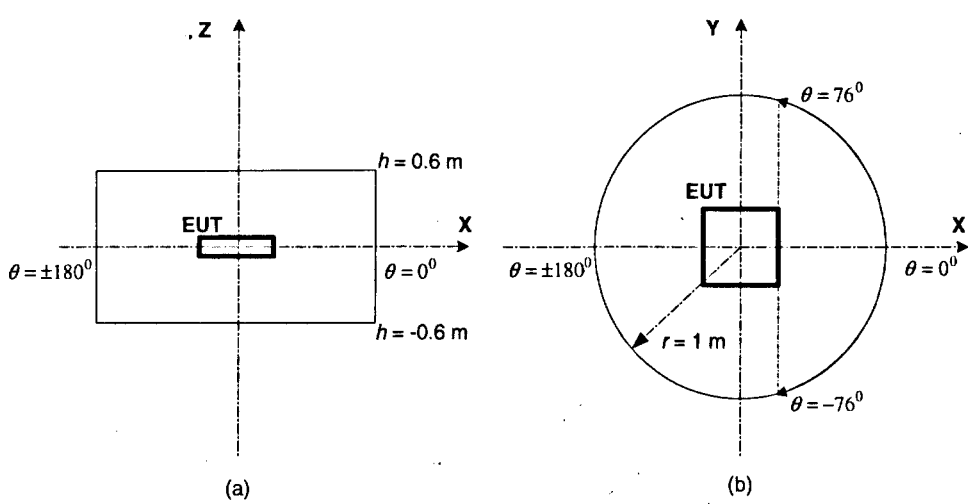

Fig. 3.4 Geometry of the cylindrical scan. (a) side view; (b) top view.

In order to approach to the true field magnitude at each test point, extreme variations of the field along the effective area of the measurement antenna should be avoided,

that is, the maximum dimension of the antenna effective area should be as small as possible to avoid smoothing from convolution with the antenna area. However, the radiation resistance of a short dipole that is a small fraction of a wavelength long is very small [26]. Such antenna usually also exhibits a very high reactance. These will generally result in a high fraction of the input power dissipated in the ohmic losses of the antenna and a mismatch between the short dipole and a typical transmission line. Thus the short dipole is not an efficient radiator or receiver. The size of an efficient antenna must be comparable to the wavelength of the field.

To make a compromise between the above two requirements, a 40 mm balanced dipole was employed during our measurements to measure the possibly detailed radiation pattern. An Agilent spectrum analyser E4404B was used to measure the received signal, which was connected via a coaxial cable and a balun to the dipole during the measurement.

If a dipole is fed directly with a coaxial cable, some of the current may flow on the outside of the shield, changing the radiation or receive pattern of the dipole. The application of balun is to inhibit the unbalanced current outside the shield [26]. The balun used here includes a quarter-wavelength sleeve and a common-mode choke coil. The sleeve was made of copper foil. The choke coil was made of two feeder cables which were twisted together and coiled.

The quarter-wavelength sleeve acts as a quarter-wavelength, short-circuited transmission line, providing infinite impedance at the input end. Thus, the current on the outside of the shield may be blocked. The sleeve works only at frequency where its length is one quarter wavelength, so its bandwidth is limited. However, this problem may be mitigated by the common-mode choke coil, which may suppress the unbalanced current over a broad frequency band.

The diagram of the balun is shown in Fig. 3.5.

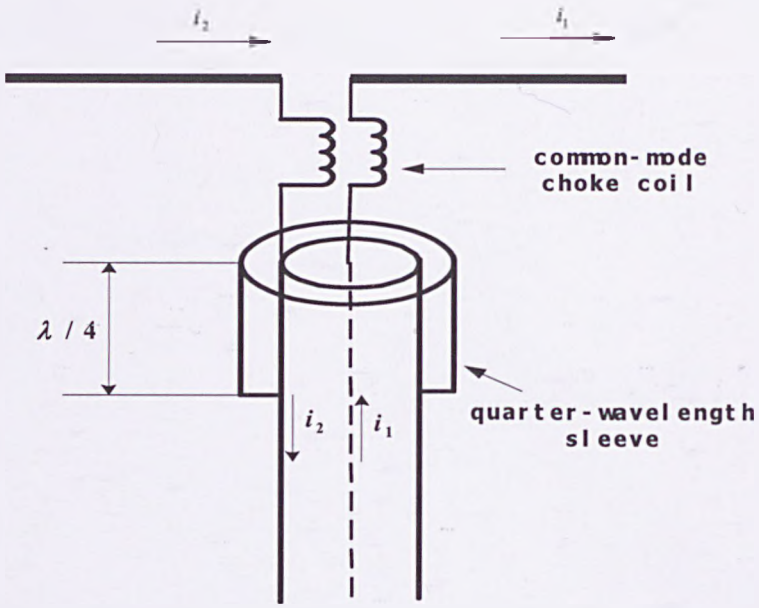

Fig. 3.5 Diagram of a balun consists of a quarter-wavelength sleeve and a common-mode choke coil.

The picture of the dipole and the balun used here is given in Fig. 3.6.

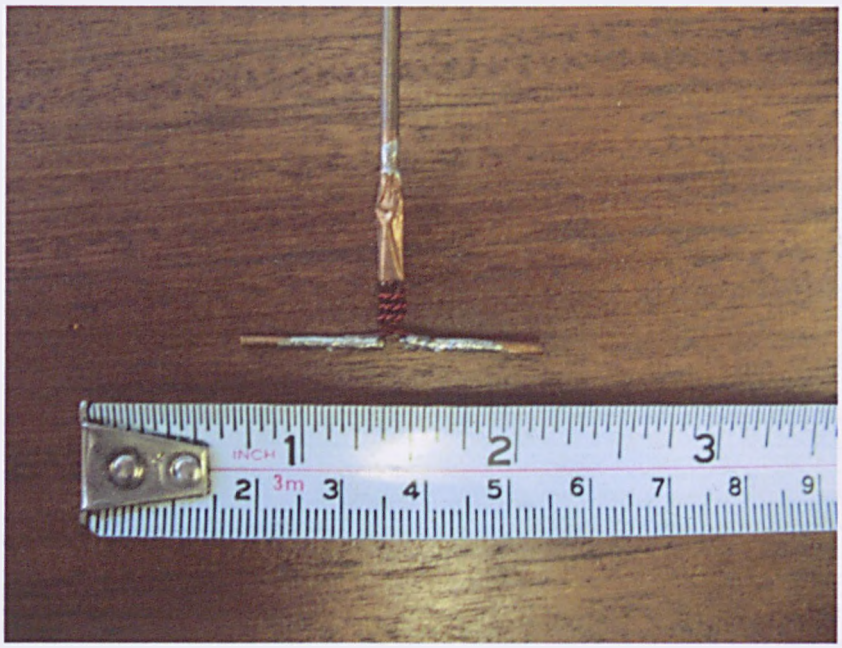

Fig. 3.6 A 40 mm dipole fed with a balun.

The dimensions of the anechoic chamber used were 3.25 m × 2.10 m × 2.05 m. The measurement setup in the anechoic chamber is illustrated in Fig. 3.7.

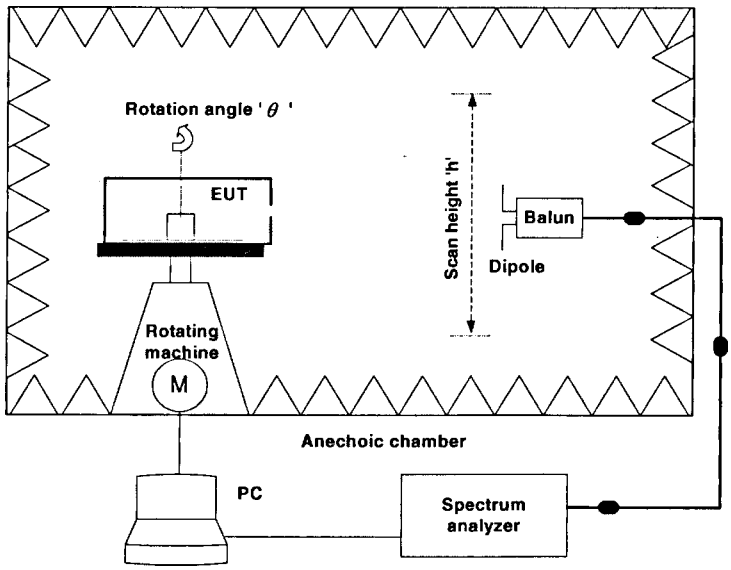

Fig. 3.7 Sketch of measurement setup of the cylindrical scan in an anechoic chamber.

3.3 Measurement Results of Radiation Patterns

3.3.1 Radiation Patterns of the Dummy EUT

Two examples of the radiation patterns measured by the horizontally polarized antenna and the vertically polarized antenna, i.e., the radiation pattern of E_θ and the radiation pattern of E_h, are given respectively in Fig. 3.8.

Obviously, the radiation pattern of E_θ is quite different from that of E_h and the measured field in each plot expresses fast spatial variation. For the data presented in Fig. 3.8, at each test point the ratio of E_θ to E_h is calculated. The cumulative distribution function (CDF) of the calculated ratios expressed in decibels is plotted in Fig. 3.9, indicating these ratios vary over a great range from –20 to +20 dB. Such great variation range implies the polarizations of the radiated fields at different test points are varied and one fixed orientation of the measurement antenna is not sufficient to determine accurately the magnitude of the field.

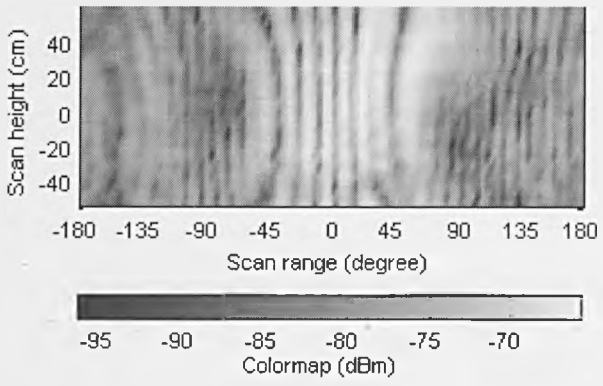

(a)

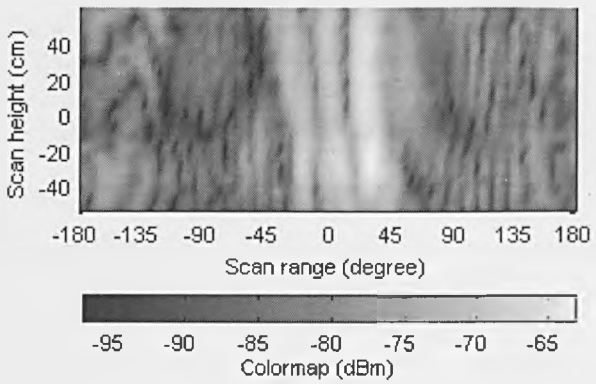

(b)

Fig. 3.8 The radiation patterns of the dummy EUT: (a) E_θ, (b) E_h. Configuration of the slots in the front panel: one CD slot and sixteen short slots. Frequency: 3 GHz. Source position: 1.

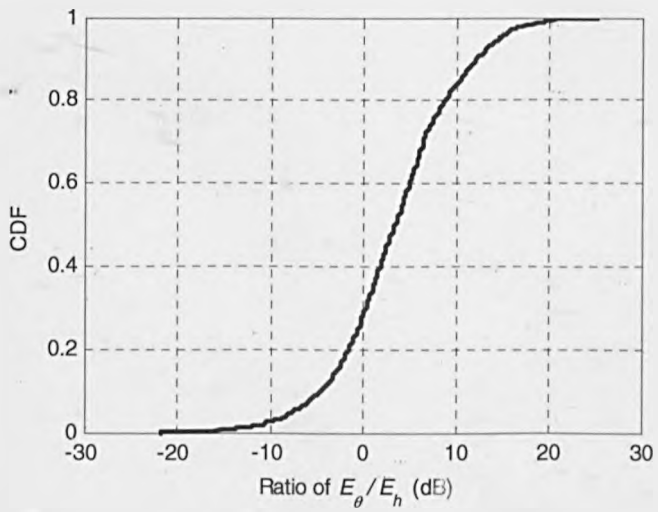

Fig. 3.9 The CDF of the ratio of E_θ / E_h expressed in decibels. Configuration of the slots in the front panel: one CD slot and 16 short slots. Frequency: 3 GHz. Source position: 1.

Three E patterns of the dummy EUT with three different slot configurations measured at 3 GHz are given respectively in Fig. 3.10. For the data presented in

Fig. 3.10, the magnitude of the E at each test point is derived from Equation (3.5), being the field component tangent to the local scan surface.

It can be seen in Fig. 3.10 no matter how many slots three are in the front panel, the radiation pattern of the electrically large enclosure in its radiating near-field is quite complex. This implies the complexity of the radiation pattern results not only from the interferences of the line-of-sight radiations from the slots, but also from the diffraction of the enclosure, itself acting as an electrically large source.

During our measurements, only the front panel with slots was used to radiate EM field. However, the radiation patterns shown in Fig. 3.10 indicate that the field strength measured at the scan area behind the front panel, i.e., the scan area from -180° to -76° and from +76° to +180°, is comparable to the field strength measured at the scan area in front of the panel, i.e., the scan area from –76° to +76°. This is mainly due to the diffraction of the whole enclosure. More E patterns measured at 6 GHz are given in Fig. 3.11. Comparisons between Fig. 3.10 and Fig. 3.11 indicate that the higher frequency, the less radiated field appears behind the front panel via diffraction. In Fig. 3.11(c), a typical interference pattern with a number of cycles can be observed at the area in front of the panel with slots.

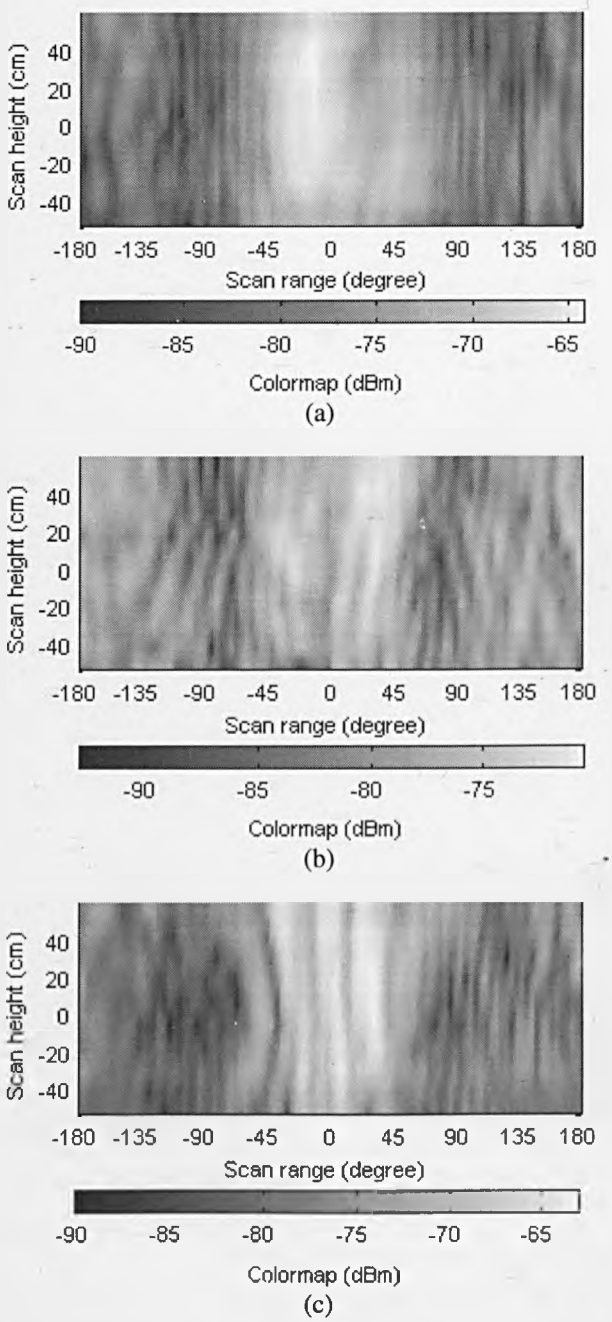

Fig. 3.10 The *E* patterns of the dummy EUT. Configuration of the slots in the front panel: (a) two rectangular slots, (b) one CD slot and (c) one CD slot and sixteen short slots. Frequency: 3 GHz. Source position: 1.

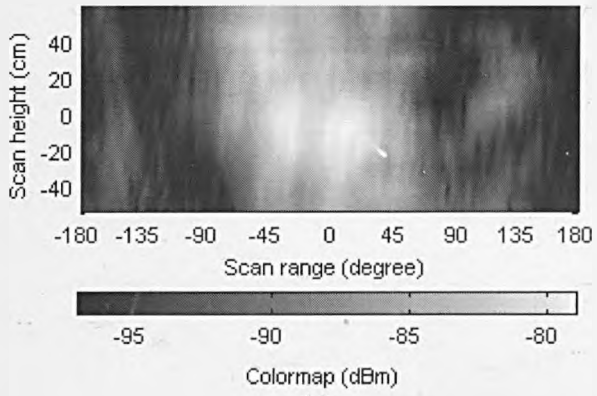

(a)

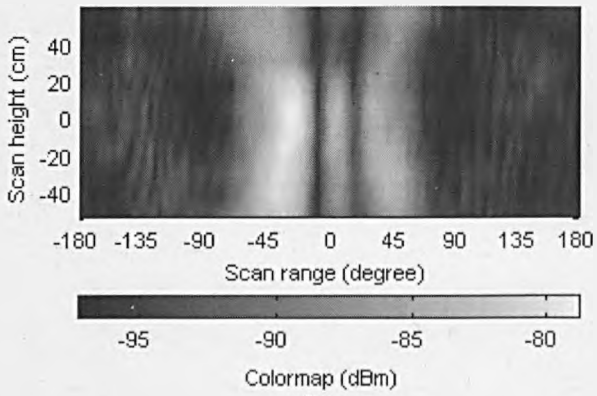

(b)

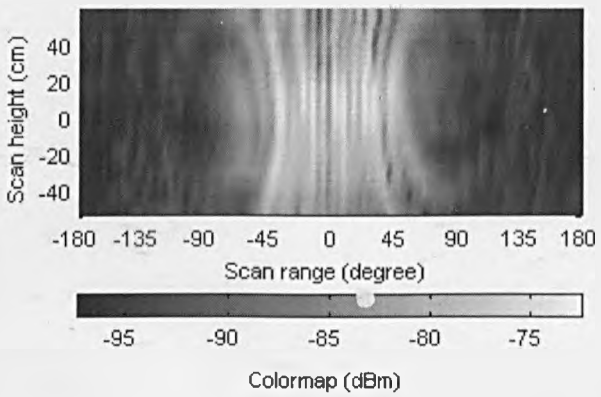

(c)

Fig. 3.11 The *E* patterns of the dummy EUT. Configuration of the slots in the front panel: (a) two rectangular slots, (b) one CD slot and (c) one CD slot and sixteen short slots. Frequency: 6 GHz. Source position: 1.

3.3.2 Radiation Patterns of the RC

Two examples of the radiation pattern of E_θ and the radiation pattern of E_h of the RC are shown in Fig. 3.12. It can be seen that without the enclosure, the radiation of the RC also varies dramatically.

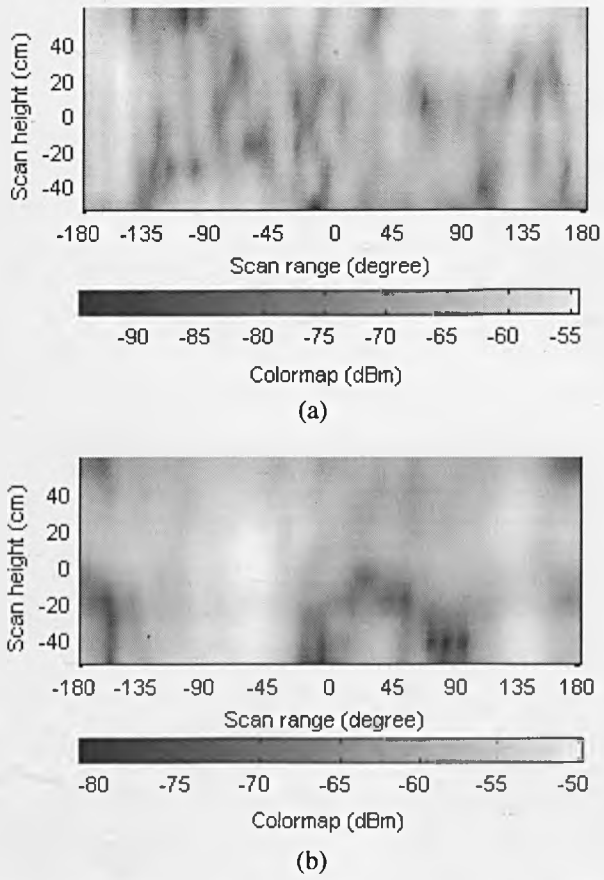

Fig. 3.12 The radiation patterns of the RC: (a) E_θ, (b) E_h. Frequency: 3 GHz. Source position. 1.

For the data presented in Fig. 3.12, at each test point the ratio of E_θ to E_h is calculated. The CDF of the ratios expressed in decibels is plotted in Fig. 3.13, which also illustrate the various polarizations of the radiated fields of the RC. In terms of the fast spatial variation and the various polarizations of the electric fields, the radiation characteristics of the RC are similar to these of the dummy EUT.

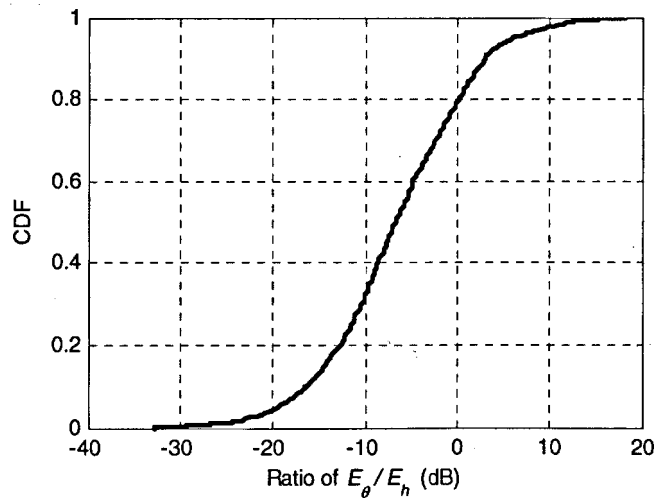

Fig. 3.13 The CDF of the ratio of E_θ / E_h of the RC. Frequency: 3 GHz. Source position: 1.

It can be seen in Fig. 3.13 about 80% of the ratio values in dB are negative, meaning at most of the test points the vertical component of the electric field is dominant. This is mainly due to the radiation of the CGE02 being vertically polarized. However, the plot shown in Fig. 3.9 indicates only about 30% of the ratio values in dB are negative, indicating that due to the effects of the enclosure and the slots, the polarization of the radiated field may be changed greatly,

During our measurement, 3 different configurations of slots, 6 different source positions and 6 different frequencies were considered. Thus 108 E patterns of the dummy EUT and 36 E patterns of the RC were obtained, all of which are given in Appendix B.

3.4 Discussion

Considering the radiations of a typical electronic equipment are generally at low power levels, such equipment may only interfere with other electronic systems located in its proximity. According to Equation (3.1), such interference is likely triggered in the radiating near-field of the equipment at frequencies above 1 GHz. Thus, the radiating shielding measurement of an equipment enclosure in its radiating near-field is concerned here.

At frequencies above 1 GHz, both the dummy EUT and the RC are electrically large. The measurement results indicate that the radiated fields of the dummy EUT in its

radiating near-field express fast spatial variation and the polarizations of the radiated fields at different test points are various. Such complexity results from both the interference of the line-of-sight radiation of the slots and the diffraction of the enclosure. The longer the wavelength, the more obvious diffraction of the enclosure. However, the shorter wavelength, the more detailed the interference pattern that results from the line-of-sight radiation of the slots. The RC also expresses similar radiation characteristics as those of the dummy EUT, resulting from the Fresnel diffraction.

To measure the complex radiation of either the dummy EUT or the RC in an anechoic chamber, an antenna scan on a spherical or cylindrical surface surrounding this source with a fine scan resolution is required. The scan resolution may be determined by Equation (A.5). The various polarizations of the radiated field at different test points also mean one fixed orientation of the measurement antenna is not sufficient to determine accurately the magnitude of the field. The magnitude of the radiating *E*-field at each test point may be determined by Equation (3.2) or Equation (3.4), requiring the measurements are taken with the antenna oriented at three mutually orthogonal directions. In terms of a cylindrical scan, the field component tangent to the local scan surface may be determined by Equation (3.5), requiring the measurements are taken with the antenna at two orthogonal orientations. Such measurement is time consuming and its significance is doubtable. Consider the radiation measurement of an equipment with the maximum dimension of 0.6 m. If the measurement distance is 1 m, to obtain the detailed information of the radiation of this equipment at 6 GHz, the scan resolution should be less than 25 mm and at least 20106 test points on a spherical surface surrounding this source at a radius of 1 m are required.

The difference between Fig. 3.9 and Fig. 3.13 indicates that due to the effects of the apertures of an equipment enclosure, the radiation polarization of the enclosure containing a source is likely to be different from that of the source. This implies that the conventional SE measurement technique based on one fixed orientation of the measurement antenna is not appropriate for equipment enclosures.

The complex radiation of either the dummy EUT or the RC also mean that the conventional definition SE based on a single ratio of fields is not suitable to evaluate the radiating shielding ability of an equipment enclosure. This problem is solved in Chapter 4, where several new definitions are considered and compared and finally one of these definitions is proposed for the radiating shielding.

A method for the radiation measurement of equipment at frequencies above 1 GHz has been proposed in the recent edition of CISPR 16-2-3 [31], where an anechoic chamber is the assumed test environment. According to this method, if the EUT is encompassed by the 3 dB beam width of the measurement antenna, only one azimuth scan around the EUT is required and the additional antenna height scan is not necessary. However, the complex diffraction pattern around an electrically large EUT shown in this chapter implies such measurement method is technically incorrect. The deficiency of this method will be illustrated in Appendix C, and the measurement technique proposed here for radiating shielding is also suggested to determine the maximum radiation of an electrically large source.

Chapter 4

Definitions of Radiating Shielding

4.1 Introduction

The conventional SE measurement of an equipment enclosure in anechoic chambers relates the field at a certain position (generally in the centre of the enclosure) inside the enclosure emptied to the external threat field [20], [24], [25]. The external radiating source fixed at a certain test point should have the same polarization as the internal measurement antenna and during the attenuation measurement step should face directly to the slots of the equipment enclosure. If an internal radiating source is placed in the centre of the enclosure, an external measurement antenna is required and should be directed to the slots of the enclosure during the attenuation measurement. Generally, the equipment contents are not involved in the conventional SE measurement. Based on such a measurement technique, a typical SE value of the equipment enclosure is obtained, being a single ratio of the electric field measured when the enclosure is absent to that measured when the enclosure is present.

However, such measurement technique has several weaknesses. Consider an external radiating source being used during the SE measurement. Firstly, different incidence angles and polarizations of the external fields mean various excitations on apertures of the tested enclosure, resulting in different attenuated fields inside the enclosure and so different SE results. Secondly, if the tested enclosure is electrically large, the complex field structure within the enclosure means that the SE also depends on the test position and orientation of the measurement antenna inside the enclosure. Similarly, if an internal radiating source is employed during the SE measurement, the complex diffraction pattern of the enclosure shown in Chapter 3 means that the SE result is dependent on the position and orientation of the measurement antenna outside the enclosure. In addition, different internal source position stands for different excitation on the apertures and so has effects on the shielding ability of the enclosure.

As discussed in Chapter 2, the equipment contents also have effects on the shielding performance of equipment enclosures and should be involved in the shielding measurement.

In a word, the conventional SE measurement technique is inadequate because it does not account for the effects of the contents, the position of the radiating source, and the position and orientation of the measurement antenna. It is suggested here that the measurement technique proposed in Chapter 3 to determine the radiation pattern of an electrically large equipment may also be used to measure the shielding performance of an equipment enclosure.

Moreover, the complex radiation pattern of the dummy EUT means that a number of E_{ref} values may be obtained during the reference measurement step. Here E_{ref} is the magnitude of the field radiated from the dummy EUT. The complex radiation pattern of the RC also means that a number of E_{att} values may be obtained during the attenuation measurement step, where E_{att} is the magnitude of the field radiated from the RC only. The complex radiation patterns of both the dummy EUT and the RC imply that the equipment enclosure expresses various attenuations, namely, shielding performances, on the radiated fields of the contents. Thus, the definition of SE determined by a single ratio of electric fields is not appropriate for this situation.

The aim of this chapter is to propose a suitable definition for the radiating shielding of an equipment enclosure. It is suggested here that an ideal shielding definition of an equipment enclosure should be related to all the measured E_{ref} and E_{att} values and also be able to express the shielding variation of the enclosure. To achieve this aim, several definitions for the various shielding performances of an equipment enclosure are considered here.

At first, based on the ratio between E_{ref} and E_{att}, three new definitions are proposed in Section 4.2, each of which consists of a number of elements, expressing the detailed shielding performances of an equipment enclosure.

Secondly, another new definition, shielding of radiating power *(SRP)*, is considered in Section 4.3, which consists of only two parameters the average shielding of radiating power *(ASRP)* and the enhancement factor $E.F._{95th}$. This definition is used

to indicate both the average shielding performance and the worst shielding performance.

In Section 4.4 examples of the measurement results of these considered definitions and the typical SE values are presented and compared, which illustrate the rationality of the definition of *SRP*.

The advantages and disadvantages of these definitions are summarized in Section 4.5 and finally *SRP* is proposed as a suitable definition for the radiating shielding.

4.2 Three New Definitions for the Detailed Shielding Performances

4.2.1 Definition Descriptions

As stated above, E_{ref} is used to indicate the electric field strength obtained during the reference measurement step and E_{att} is the electric field strength obtained during the attenuation measurement step. It should be notified that both E_{ref} and E_{att} are derived from Equation (3.5).

Consider a cylindrical scan used for a radiating shielding measurement, which consists of n rows (n different scan heights) and m columns (m different scan angles). Here symbol i is assigned as the row index and j is the column index. Then symbol $E_{ref}(i, j)$ is used to represent the E_{ref} at the $(i, j)th$ test point on the cylindrical scan surface during the reference measurement step, and $E_{att}(i, j)$ is used to represent the E_{att} at the $(i, j)th$ test point on the same cylindrical scan surface during the attenuation measurement step. Consequently, an $n \times m$ matrix $\boldsymbol{E}_{ref}$ with entries $E_{ref}(i, j)$ may be obtained in the reference measurement step and an $n \times m$ matrix $\boldsymbol{E}_{att}$ with entries $E_{att}(i, j)$ may be obtained in the attenuation measurement step.

To involve all the measured E_{ref} and E_{att} values, the first suggested shielding definition is shielding of radiating fields in positions (***SRFP***), being defined as an $n \times m$ matrix with entries $SRFP(i, j)$. Here $SRFP(i, j)$ is the ratio of $E_{ref}(i, j)$ to $E_{att}(i, j)$, both of which are measured at the same test point, i.e. the $(i, j)th$ test point

on the cylindrical scan surface. The matrix ***SRFP*** can be obtained by the array right division (i.e. the element-wise division) E_{ref}./ E_{att}:

$$SRFP = E_{ref} / E_{att}. \quad (4.1)$$

The complex radiation patterns of the RC and the dummy EUT shown in Chapter 3 imply that the enclosure has effects on both the magnitudes and directions of the radiated fields of the RC. That is, it may be assumed that the $E_{att}(i, j)$ measured at the $(i, j)th$ test point is the attenuation result of the $E_{att}(i', j')$ measured at any test point. Here the coordinates (i', j') may be different from (i, j), or be same as (i, j). To include all the possible conditions, the second definition shielding of radiating fields (***SRF***) is defined as a set which contains all of the possible ratios of E_{ref}/E_{att}, i.e.,

$$SRF = \{E_{ref} / E_{att}\}. \quad (4.2)$$

Another definition named as shielding of radiating fields in order (***SRFO***) is also developed. Two arrays $E_{ref, desc}$ and $E_{att, desc}$ are required in this definition, where $E_{ref, desc}$ is an array in which all the measured E_{ref} values are arranged in descending order and $E_{att, desc}$ is an array in which all the measured E_{att} values are arranged in descending order. The definition shie lding of radiating fields in order, ***SRFO***, is defined as the element-by-element right division $E_{ref, desc}$ ./ $E_{att, desc}$:

$$SRFO = E_{ref, desc} ./ E_{att, desc} \quad (4.3)$$

According to Equation (4.3), the *'i'th* element in the array ***SRFO*** is the ratio of the *'i'th* maximum E_{att} to the *'i'th* maximum E_{ref}. It is assumed in this definition that the *'i'th* maximum E_{att} is the attenuated result of the *'i'th* maximum E_{ref}. That is, the first maximum E_{att} is assumed as the attenuated result of the first maximum E_{ref}, the second maximum E_{att} is assumed as the attenuated result of the second maximum E_{ref}, and so on. It should be noted that generally the position of the *'i'th* maximum E_{ref} is different from that of the *'i'th* maximum E_{att}. So the elements in ***SRFO*** cannot be related with the elements in ***SRFP***, each of which is the ratio of the E_{ref} to the E_{att} measured at the same test position.

According to the above three definitions, both shielding of radiating fields in positions, ***SRFP***, and shielding of radiating fields in order, ***SRFO***, consist of n × m elements, and shielding of radiating fields, ***SRF***, consists of $n^2 \times m^2$ elements. The

large number of elements in each of these definitions implies there may be great differences between these elements. That is, although the shielding variation of an equipment enclosure may be expressed by each of these definitions, the overall shielding ability of the enclosure cannot be defined by these definitions. It can be proved that the variation range of the elements in ***SRF*** should be greater than that in ***SRFP***, and the variation range of the elements in ***SRFP*** should be greater that in ***SRFO***, i.e.:

$$SRF_{max} - SRF_{min} > SRFP_{max} - SRFP_{min} > SRFO_{max} - SRFO_{min} \quad (4.4)$$

where $SRFP_{max}$, $SRFO_{max}$ and SRF_{max} are the maximum elements in ***SRFP***, ***SRFO*** and ***SRF*** respectively, and $SRFP_{min}$, $SRFO_{min}$ and SRF_{min} are the minimum elements in ***SRFP***, ***SRFO*** and ***SRF*** respectively.

4.2.2 Measurement Results

The examples of a matrix $\boldsymbol{E}_{ref}$ obtained in the reference measurement step and a matrix $\boldsymbol{E}_{att}$ obtained in the attenuation measurement step are plotted in Fig. 4.1. In the following contents of this chapter, for convenience, all the results of the proposed shielding definitions are expressed in decibels.

The matrix ***SRFP*** resulted from the data matrices given in Fig. 4.1, is plotted in Fig. 4.2. Fig. 4.2 indicates the *SRFP* also expresses fast spatial variation around the EUT, varying between -10 decibels to 30 decibels. This means a small displacement of the measurement antenna may result in a significant difference between the measurement results of *SRFP*. In other words, in terms of the conventional SE measurement of an equipment enclosure, a reliable measurement repeatability is not expected.

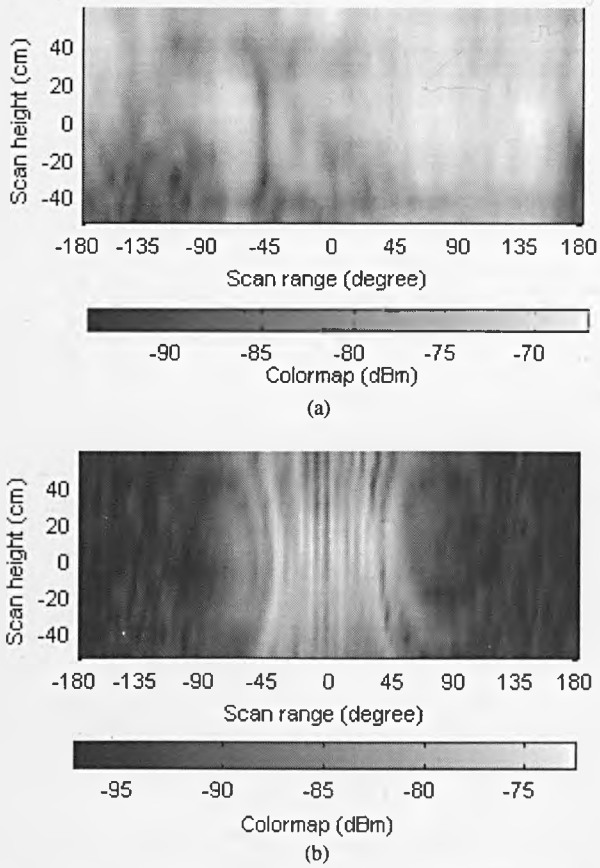

Fig. 4.1 (a) Radiated *E* pattern obtained in the reference measurement step; (b) Radiated *E* pattern obtained in the attenuation measurement step. Configuration of the slots: one CD slot and 16 short slots. Frequency: 6 GHz. Source position: 1.

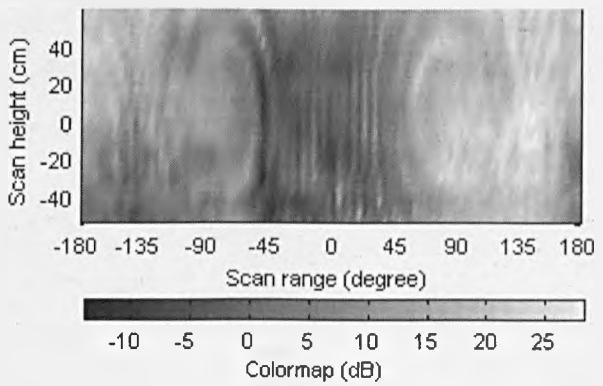

Fig. 4.2 The pattern of matrix ***SRFP*** derived from the data matrices presented in Fig. 4.1.

The CDFs of the elements of ***SRFP, SRFO*** and ***SRF*** derived from the data matrices presented in Fig 4.1 are plotted respectively in Fig. 4.3.

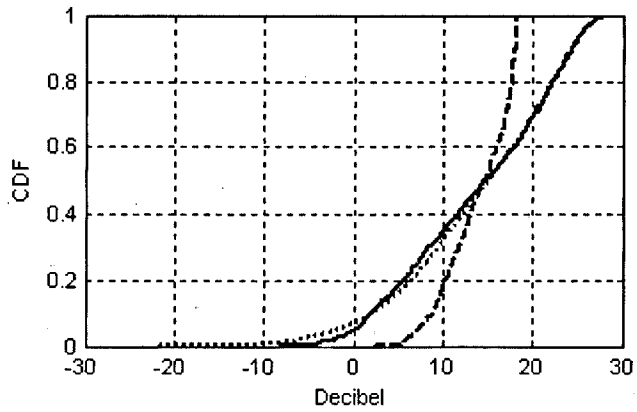

Fig. 4.3 Solid line: the CDF of the elements in ***SRFP***; Dashed line: the CDF of the elements in ***SRFO***; Dotted line: the CDF of the elements in ***SRF***. ***SRFP, SRFO*** and ***SRF*** are derived from the data matrixes presented in Fig 4.1.

Obviously, the difference between the SRF_{max} and SRF_{min} is larger than the difference between the $SRFP_{max}$ and $SRFP_{min}$, which is larger than the difference between $SRFO_{max}$ and $SRFO_{min}$. The elements in each of the three definitions express an obvious variation of the shielding performance of an equipment enclosure, which may be more than 50 dB, meaning these definitions cannot give a defined indication of the shielding ability of n equipment enclosure.

More CDFs of the elements of the measured ***SRFP, SRFO*** and ***SRF*** are given respectively in the three plots of Fig. 4.4. In each plot, the solid line is the CDF of the results of the dummy EUT with two rectangular slots, the dashed line is the CDF of the results of the dummy EUT with one CD slot and the dotted line is the CDF of the results of the dummy EUT with one CD slot and sixteen shot slots. The obvious differences between the dashed line and the dotted line in each plot illustrate as more slots are introduced in an enclosure, the gross shielding performance of the enclosure deteriorates.

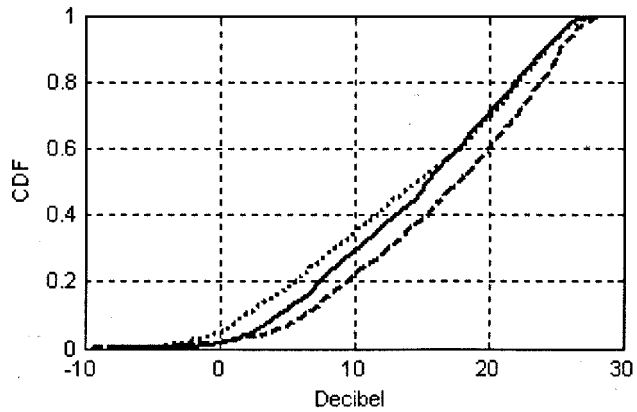

(a)

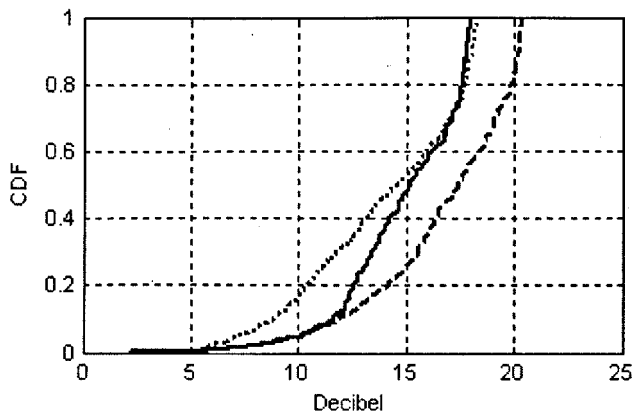

(b)

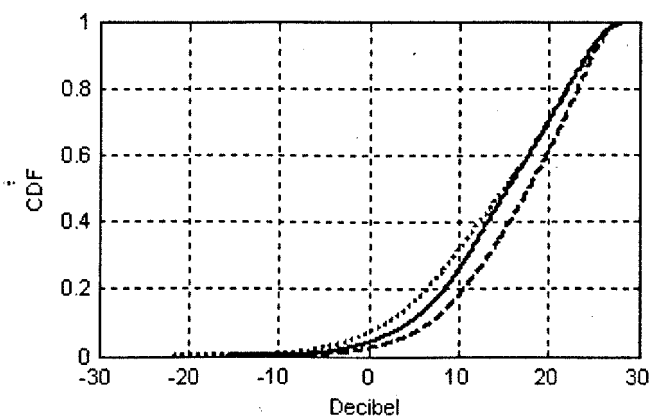

(c)

Fig. 4.4 (a) The CDF of the elements of ***SRFP***; (b) The CDF of the elements of ***SRFO***; (c) The CDF of the elements of ***SRF***. In each plot, the solid line is the CDF of the results of the dummy EUT with two rectangular slots, the dashed line is the CDF of the results of the dummy EUT with one CD slot and the dotted line is the CDF of the results of the dummy EUT with one CD slot and sixteen shot slots. Frequency: 6 GHz. Source position: 1.

4.3 A New Definition Shielding of Radiating Power for the Average and Worst Shielding Performances

4.3.1 Definition Descriptions

Although the detailed shielding performances of an equipment enclosure may be expressed by the three definitions given in the above section, in practice, a single parameter used to indicate the overall shielding ability of an equipment enclosure may be more useful to an engineer, which enables direct comparisons between different equipment enclosures. But the shielding variation of the equipment enclosure should also be considered in the expression of the shielding definition.

To achieve the above aims, the new definition shielding of radiating power (*SRP*) proposed here consists of two parameters: the average shielding of radiating power (*ASRP*) representing the average shielding performance of an equipment enclosure and the enhancement factor $E.F._{95th}$ representing the variation of the radiating power densities of the enclosure in its radiating near-field.

In detail, the *ASRP* is defined as the ratio between P_{ref} the total radiated power measured in the reference measurement step to P_{att} the total radiated power measured in the attenuation measurement step

$$ASRP = \frac{P_{ref}}{P_{att}}. \quad (4.5)$$

This measure takes no account of the field or power density variation and is a measure of the ratio of the average radiated power densities.

The enhancement factor $E.F._{95th}$ is defined as

$$E.F._{95th} = \frac{p_{95th}}{p_{ave}} \quad (4.6)$$

where p_{95th} is the upper 95th percentile of the power densities on a whole spherical or cylindrical surface around the EUT and p_{ave} is the average power density on the same area around the EUT.

The enhancement factor $E.F._{95th}$ is analogous to the probable maximum directivity D_{max} of an enclosure measured in its radiating far-field as given in [32], except here we use p_{95th} to replace the maximum power density p_{max} and the relevant measurement is performed in the radiating near-field around the enclosure. There are two reasons why the p_{95th} rather than the p_{max} is applied in the definition of the $E.F._{95th}$:

- Firstly, in terms of the radiated field pattern measured in an anechoic chamber, the accuracy of the maximum field depends on the number of test points used [31], [33]. In other words, the 'true' value of the maximum radiated field of a EUT cannot be obtained. So it is more precise to describe the maximum field as an estimate, which the field measured will not exceed. Here p_{95th} is chosen as an estimate of the maximum field p_{max}, which implies there is only about 5% possibility that the measured values may exceed it.
- Secondly, the 95th percentile value includes all but 5% of the test area and so can be estimated accurately from a sufficiently large scan resolution. However, the maximum value may strongly depend on the scan resolution. The statistic results presented in [34] have shown that for a certain scan resolution, the uncertainty of the measured p_{95th} are much less than that of the measured p_{max}.

Comparing the average shielding performance defined in Equation (4.5), it is suggested here that the worst shielding performance of the enclosure may be determined by $ASRP/E.F._{95th}$.

As described in Chapter 3, during the radiation pattern measurement in the anechoic chamber, the measurement antenna was scanned on a truncated cylindrical surface centred the EUT and the measurement distance was in the radiating near-field of the EUT. In the radiating near-field the transverse fields are dominant and the ratio between E-field and H-field is close to the intrinsic impedance of free space (120π ohms), so the power flow density at each test point on the cylindrical surface, p, may be estimated by

$$p = \frac{E^2}{120\pi}. \quad (4.7)$$

Here E is the electric field strength derived from Equation (3.5). The total radiated power may be determined by the integration of the power density p on the whole surface around the EUT. In terms of the truncated cylindrical scan used here, the total power flow through the scan area, P, can be estimated by:

$$P = \sum p \cdot \Delta x \cdot \Delta y \quad (4.8)$$

where Δx is the scan step on azimuth direction and Δy is the scan step on vertical direction, respectively.

Based on Equation (4.7) and (4.8), both the *ASRP* and the $E.F._{95th}$ can be derived from the measured electric fields. The *ASRP* may give an overall evaluation of the shielding performances of an equipment enclosure and it is suggested here the ratio of $ASRP/E.F._{95th}$ may be used to indicate the worst shielding performance. Generally, the best shielding performance of an equipment enclosure is not concerned because this is not likely to be the cause of an EMC or EMI problem. Thus, the shielding variation of an equipment enclosure may be expressed effectively by the combination of *ASRP* and $ASRP/ E.F._{95th}$.

4.3.2 Measurement Results

During the radiating shielding measurement, 3 different combinations of slots, 6 different source positions and 6 different frequencies were considered. Thus, 108 *ASRP* values were obtained during the measurements in the anechoic chamber, which are plotted in Fig. 4.5. The data in Fig. 4.5 indicate that the *ASRP* of a typical equipment enclosure is generally less than 30 dB, much less than the SE of a screened enclosure, which is usually close to 100 dB. Comparisons between the *ASRP* values in Fig. 4.5 (b) and these in Fig. 4.5 (c) also indicate that the *ASRP* of the enclosure deteriorates as more slots are introduced, especially at higher frequencies. Obviously *ASRP* also depends on the internal source positions. At each frequency, even for the same configuration of slots, there are apparent differences

between the *ASRP* values of different source positions, which may be more than 10 dB.

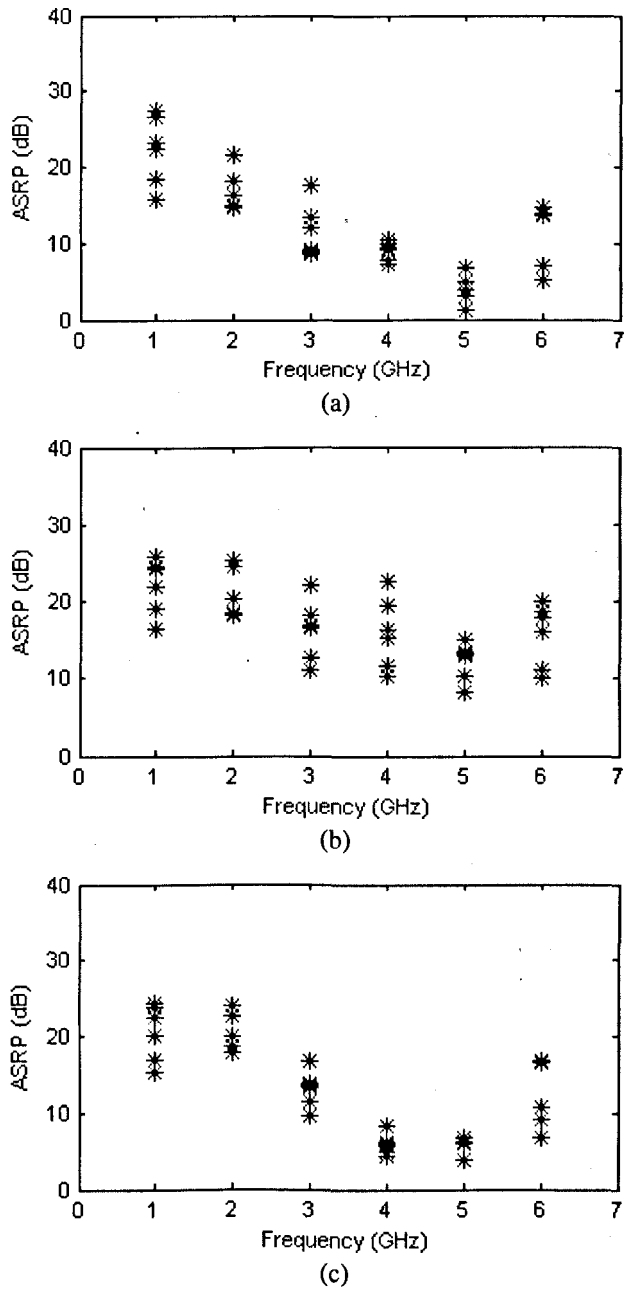

Fig. 4.5 The *ASRP* values obtained during the meaurements in the anechoic chamber. The 'asterisk' markers represent the measured *ASRP* values. Configuration of slots in the front panel: (a) two rectangular slots, (b) one CD slot only and (c) one CD slot and 16 short slots.

Similarly, 108 $E.F._{95th}$ values were obtained during the measurements in the anechoic chamber. The results of $E.F._{95th}$, together with the results of $E.F._{max}$ (p_{max}/p_{ave}), are plotted in Fig. 4.6. Here both $E.F._{95th}$ and $E.F._{max}$ are expressed in linear form.

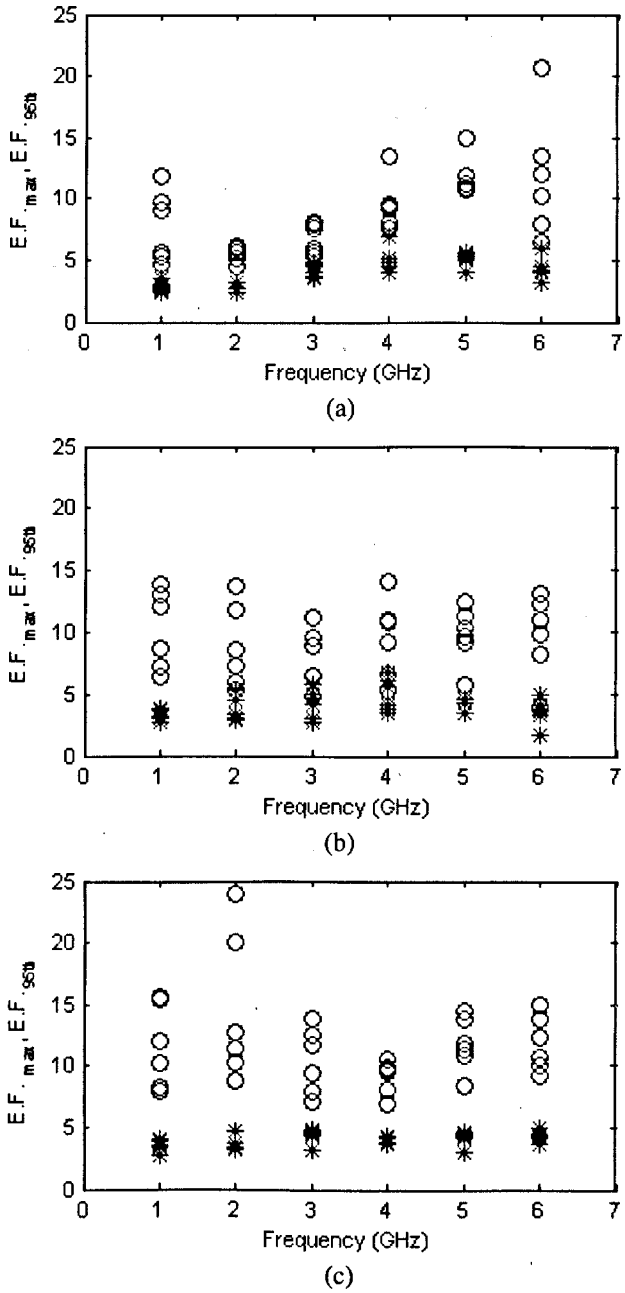

Fig. 4.6 The $E.F._{95th}$ (the 'asterisk' markers) and the $E.F._{max}$ (the 'circle' marker) values obtained during the measurements in the anechoic chamber. Configuration of slots in the front panel: (a) two rectangular slots, (b) one CD slot only and (c) one CD slot and 16 short slots.

The three plots in Fig. 4.6 indicate most of the $E.F._{95th}$ results vary between 2 and 5, regardless of the frequency, source position and the configuration of the slots. The mean of all the $E.F._{95th}$ is 4.01 and the relevant standard deviation is 0.97. However, the $E.F._{max}$ varies dramatically for different frequencies, source positions or configurations of the slots. The maximum difference between the $E.F._{max}$ presented

in Fig. 4.6 is 19.96. It seems the $E.F._{95th}$ may be estimated roughly using a single value, whereas the $E.F._{max}$ varies greatly and cannot be represented by a single value.

4.4 Comparisons between Results of Different Definitions

Some measurement results derived from the four definitions proposed here and the corresponding typical SE values are given in Table. 4.1. All the values are in decibels.

Table 4.1. Measurement results of *SRP*, SE, $SRFP_{max}$, $SRFP_{min}$, $SRFO_{max}$, $SRFO_{min}$, SRF_{max} and SRF_{min} at different frequencies. Configuration of the slots in the front panel: one CD slot and sixteen short slots. Source position: 1. All the values are in decibels.

Proposed definitions of radiating shielding		**1 GHz**	**2 GHz**	**3 GHz**	**4 GHz**	**5 GHz**	**6 GHz**
SRP	*ASRP*	20.1	24.0	16.8	4.3	5.9	10.8
	ASRP/ E.F.$_{95th}$	14.8	18.3	10.1	-2.1	-0.8	3.8
SE		15.4	36.4	1.4	-1.0	2.0	-1.2
SRFP	$SRFP_{max}$	35.1	42.5	37.6	30.7	28.8	28.7
	$SRFP_{min}$	-3.4	2.4	2.9	-24.3	-12.4	-8.0
SRFO	$SRFO_{max}$	22.6	27.8	20.7	10.9	12.9	18.3
	$SRFO_{min}$	14.9	13.6	13.4	0.0	1.0	2.6
SRF	SRF_{max}	37.9	44.9	40.2	36.4	33.3	29.9
	SRF_{min}	-3.4	-13.6	-12.1	-31.9	-26.3	-21.5

The data shown in Table 4.1 indicate at each frequency, the *ASRP* is always between the maximum element and the minimum element of ***SRFP***, ***SRFO*** or ***SRF***, and the worst shielding performance determined by *ASRP/E.F.*$_{95th}$ is close to $SRFO_{min}$.

The typical SE values in Table 4.1 result from the conventional SE measurement technique described in the beginning of this chapter. During the SE measurement, the emission source CGE02 was employed and placed in the tested enclosure during the attenuation step. The emission pattern of CGE02 is similar to that of a dipole. It can

be seen the typical SE value obtained is usually less than the corresponding *ASRP* value. The main reason is as follows:

During the reference step of the traditional SE measurement, the radiated field at a certain distance from the CGE02 is measured, from which the power density derived should be close to the average power density at the same distance derived from the total radiated power of the CGE02. However, during the attenuation step of the traditional SE measurement, the external measurement antenna is generally faced to the slots of the enclosure and thus located in the area occupied by the line-of-sight radiations of the slots, where the radiated fields are generally much larger than other areas. Consequently, the power density derived from the measured electric field is generally larger than the average one at the same distance derived from the total radiated power of the enclosure. These result in that the measured SE value is generally less than the corresponding *ASRP* value and so tends to underestimate the overall shielding ability of the equipment enclosure. However, the constructive interferences of the line-of-sight radiations also imply a pretty small electric field may be obtained during the attenuation step of the traditional SE measurement, which may result in the SE value is much higher than the corresponding *ASRP* value, as the examples of 2 GHz given in Table 4.1.

4.5 Discussion

Because of the complex and detailed radiation patterns of both the equipment enclosure and the equipment contents, the SE value based on a single ratio of electric fields strongly depends on the position of the measurement antenna and is not expected to give a reasonable estimation of the overall shielding ability of an equipment enclosure. A single SE value cannot express the various shielding performances of an equipment enclosure either.

Three new definitions: ***SRFP*** based on a matrix, ***SRFO*** based on an array and ***SRF*** based on a set, are suggested respectively to indicate the detailed shielding performances of an equipment enclosure. One disadvantage of these definitions is to determine each of these definitions, a number of measurements in an anechoic chamber as described in Section 3.2 are required, which are time consuming and so

uneconomic. The second disadvantage is the large differences between the elements included in each definition imply it is hard to use these definitions to give a defined indication of the shielding ability of an equipment enclosure and thus the significance of the application of these definitions is in doubt.

To cope with the above difficulties, another new definition *SRP* is proposed, which consists of two parameters the *ASRP* representing the average shielding performance of an equipment enclosure and the enhancement factor $E.F._{95th}$ expressing the power density variation of the enclosure in its radiating near-field. The characteristics of this definition are as follows:

- The *ASRP* gives a defined indication of the overall shielding ability of an equipment enclosure, which enables an engineer to directly compare the shielding abilities of different enclosures, or study the effects of other factors, such as the frequency and the source position, on the overall shielding ability of an equipment enclosure. The measurement results of *ASRP* indicate that the radiating shielding ability of an equipment enclosure depends on not only the slots configuration and frequency, but also the source position.
- As shown in Table 4.1, the worst shielding performance may be indicated by the ratio of $ASRP/E.F._{95th}$. Considering the best shielding performance of an equipment enclosure is generally not of concern, the shielding variation of this enclosure may be described by the combination of the *ASRP* and the ratio of $ASRP/E.F._{95th}$. It can be seen in Fig. 4.6 the $E.F._{95th}$ values of the dummy EUT are relative stable, regardless of the frequency, source position and the configuration of the slots. This implies the $E.F._{95th}$ may be statistically estimated. The value of $E.F._{95th}$ is also limited and so there is no significant difference between the *ASRP* and the worst shielding performance defined by $ASRP/E.F._{95th}$. Thus, it is also suggested here the shielding performance of an equipment enclosure may be simply determined by *ASRP*.
- It has been shown in [4], [15] the radiating power of a radiator may be measured swiftly in a reverberation chamber. Thus, to determine the *SRP*, the time consuming measurement in an anechoic chamber may be replaced by the combination of a swift power measurement in a reverberation chamber and a

statistical estimate of the $E.F._{95th}$. The measurement technique of the *ASRP* in a reverberation chamber and the estimation of the $E.F._{95th}$ of a practical equipment enclosure will be detailed in Chapter 5.

Each of the three definitions ***SRFP***, ***SRFO*** and ***SRF*** requires a number of measurements in anechoic chambers, being time consuming. Comparing with these definitions, the definition *ASRP* may not only be determined in anechoic chambers using the same time-consuming measurement method, but also be determined swiftly in reverberation chambers. So the definition *ASRP* is more practical for an engineer and proposed as the definition of the radiating shielding of an equipment enclosure.

Chapter 5

ASRP Measured in a Reverberation Chamber and the Estimate of the $E.F._{95th}$

5.1 Introduction

As discussed in Chapter 4, the shielding of radiating power, *SRP*, of an equipment enclosure may be derived from the radiation patterns measured in an anechoic chamber. However, the relevant measurements as described in Chapter 3 are time consuming. The aim of this chapter is to find a fast way to determine the *SRP*.

It has been illustrated in [4], [15], that the total radiated power of an arbitrary source may be measured in a reverberation chamber. Comparing the measurement technique in the anechoic chamber proposed in Chapter 3, the reverberation chamber measurement avoids the antenna scan on a surface that encompasses the EUT. Thus, reverberation chamber may be an alternative environment to swiftly measure the average shielding of radiating power, *ASRP*. In Section 5.2, an overview of reverberation chamber measurements, the measurement setup of *ASRP* in a reverberation chamber and the measurement results are presented.

However, the reverberation chamber measurement cannot give the detailed information of the radiated fields of a EUT, such as the maximum field or the directivity. This difficulty is well recognized and some efforts have been performed to overcome the limitations of reverberation chamber measurements: several theory-based equations have been proposed in [32] to estimate the maximum directivity D_{max} of an EUT in its far-field. Using the total radiated power measured in a reverberation chamber and estimated D_{max}, the maximum radiated field of the tested EUT can also be estimated.

However, the angular field distribution of a radiating source in its far-field is different from that in its radiating near-field [26]. Consequently, the D_{max} measured

in the far field should be different from the enhancement factor $E.F._{95th}$ measured in the radiating near-field. That is, the estimated D_{max} given in [32] cannot be used to represent the $E.F._{95th}$ of an EUT in its radiating near-field. Here to determine the $E.F._{95th}$ of a practical enclosure, the point source modelling technique described in [34] is employed to simulate the emission pattern of an equipment enclosure with various slot distributions. Numerous simulations are performed and based on the measurement and simulation results, the estimate of the $E.F._{95th}$ of a practical enclosure is finally determined. By combining the *ASRP* measured in a reverberation chamber and the estimated $E.F._{95th}$, the *SRP* of an equipment enclosure may be determined quickly. The associated contents are presented in Section 5.3.

The conclusions about the *ASRP* measurement in the reverberation chamber and the estimation of the $E.F._{95th}$ of a practical enclosure are illustrated in Section 5.4.

5.2 *ASRP* Measured in a Reverberation Chamber

5.2.1 Description of the Reverberation Chamber Measurement

A reverberation chamber is an electrically large, high-Q cavity where enough modes are required to be excited during the measurement and thus the field pattern within the chamber is highly detailed. The internal fields may be statistically uniform due to mechanical stirring [35] or frequency stirring [36]. Although frequency stirring is much faster than mechanical stirring, it is not applicable to emissions measurement. Mechanical stirring is suitable for both emissions and immunity measurements and thus is used more widely.

During the mechanical stirring, a mode stirrer inside the chamber is rotated to alter the boundary conditions and thus change the detailed field pattern within the chamber. Then if measurements are taken at a sufficient number of the stirrer positions over one complete rotation, a statistical uniformity of the internal fields is achieved. That is, the measured field statistics are independent of the position, polarization and directivity of the radiation source.

To ensure there are sufficient modes excited in the reverberation chamber during the measurement, the lowest usable frequency (LUF) required for a working

reverberation chamber can be determined empirically as the one at least 3 times the first resonance frequency of the reverberation chamber. The resonant frequencies (modal resonance frequencies) of a rectangular reverberation chamber f_{mnp} (in hertz) can be calculated from the Helmholtz equation:

$$f_{mnp} = \frac{c_0}{2}\sqrt{\left(\frac{m}{a}\right)^2 + \left(\frac{n}{b}\right)^2 + \left(\frac{p}{d}\right)^2} \quad (5.1)$$

where m, n and p are integers; a is the length, b is the width and d is the height of the reverberation chamber, all of which are in metres; c_0 is the speed of light in free space (3×10^8 m/s).

The lowest usable frequency, LUF, may be also determined as the frequency below which there are at least 60 modes inside the reverberation chamber. The number of possible resonant modes N_m below the frequency f (in hertz) for a rectangular reverberation chamber can be given approximately by [15]:

$$N_m = \frac{8\pi abdf^3}{3c_0^3} - \frac{(a+b+d)f}{c_0} + \frac{1}{2} \quad (5.2)$$

5.2.2 Measurement Setup for *ASRP*

The statistically uniform and isotropic field distribution inside a reverberation chamber allows the determination of the total radiated power of a radiating EUT. To measure the radiated power, the time consuming antenna scan on a coverage encompassing the EUT and the consideration of the orientations of the measurement antenna in an anechoic chamber may be replaced by the swift stirrer rotation in the reverberation chamber. In other words, the reverberation chamber is an ideal environment that can measure the total radiated power swiftly, regardless of the radiation pattern. Consequently, the *ASRP* can also be determined quickly by the reverberation chamber measurement.

Consider the radiated power measurement in a reverberation chamber. The amount of the power radiated by an EUT placed in a reverberation chamber can be determined by measuring the amount of the power received by the receive antenna and correcting for chamber losses [4]:

$$P_{EUT} = \frac{\langle P_{RXEUT} \rangle}{CCF} \quad (5.3)$$

Where P_{EUT} is the radiated power from the EUT; $\langle P_{RXEUT} \rangle$ is the received power measured by the receive antenna averaged over one stirrer rotation; CCF is the chamber calibration factor.

To determine *CCF*, a separate reference measurement under the same chamber conditions is required. During the measurement, a known power P_t is transmitted from a transmit antenna and P_r is the power measured by a receive antenna. Then the *CCF* is determined by

$$CCF = \frac{\langle P_r \rangle}{\langle P_t \rangle} \quad (5.4)$$

Where $\langle P_r \rangle$ is the average received power over one stirrer rotation, $\langle P_t \rangle$ is the transmitted power averaged over one stirrer rotation;

According to Equation (5.3) and (5.4), P_{EUT} is determined by:

$$P_{EUT} = \langle P_{RXEUT} \rangle \cdot \frac{\langle P_t \rangle}{\langle P_r \rangle} \quad (5.5)$$

The measurement setup of the radiated power of a EUT in a reverberation chamber is given in Fig. 5.1. The mechanically stirred reverberation chamber used here has dimensions 4.70 m × 3.00 m × 2.37 m (a × b × d). According to Equation (5.1), the first resonant frequency of the reverberation chamber is about 59 MHz. Thus, the LUF determined by three times the first resonance frequency is about 177 MHz, which is well below 1 GHz, i.e. the lowest frequency we are interested in. According to Equation (5.2), about 10000 resonant modes may exist below 1 GHz in this chamber. Measurements were taken at 32 stirrer positions over one complete stirrer rotation.

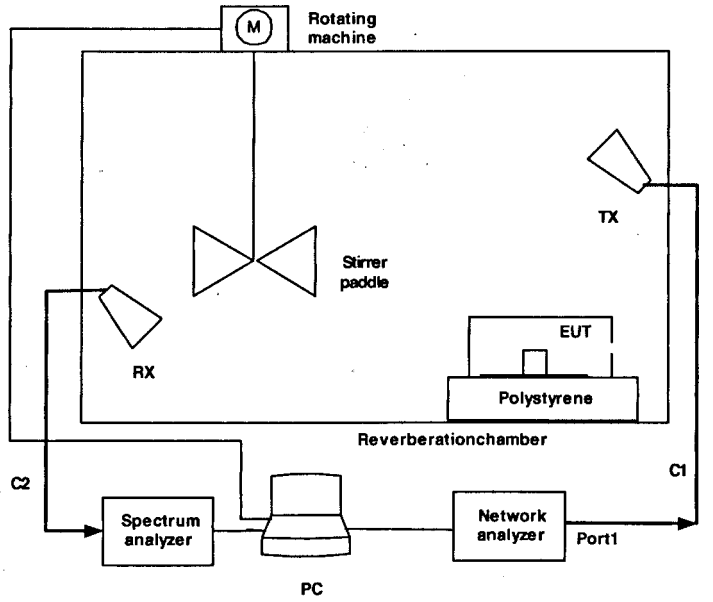

Fig. 5.1 Measurement setup of the radiated power of a EUT in a reverberation chamber.

An Agilent spectrum analyser E4404B was employed to measure the P_r and a Hewlett Packard network analyser 8753D was employed to generate a fixed output power P_{out}, which also enables a simultaneous measurement of the transmit antenna reflection coefficient S_{11}. Then $\langle P_t \rangle$ is determined by:

$$\langle P_t \rangle = P_{out} \cdot L_{C1} \cdot \left(1 - \langle S_{11}^2 \rangle\right) \cdot \eta_{TX} \quad (5.6)$$

Where L_{C1} is the loss of cable C1, η_{TX} is the antenna efficiency factor of the transmit antenna and $\langle S_{11}^2 \rangle$ is the average result of S_{11}^2 for one rotation of the stirrer. The value of η_{TX} is generally given by the antenna manufacturer. If the manufacturer's data is not available, then the η_{TX} can conservatively be assumed to be 0.75 for a log periodic antenna and 0.9 for a horn antenna.

The relevant measurement procedure for the radiated power of the EUT is as follows:

1) Set output power of port 1 of the network analyser: P_{out}.
2) For each stirrer position, record the reading of S_{11} on the network analyser and the reading of P_r on the spectrum analyser. Calculate the average results $\langle S_{11}^2 \rangle$ and $\langle P_r \rangle$ respectively for one rotation of the stirrer. Then $\langle P_t \rangle$ may be derived from Equation (5.6).

3) Disconnect cable C1 from network analyser and connect C1 with a 50 Ω load. Switch on the power of the EUT. Then record the reading of P_{RXEUT} on the spectrum analyser for each stirrer position. Derive the average of P_{RXEUT}, $\langle P_{RXEUT} \rangle$. Using $\langle P_r \rangle$, $\langle P_t \rangle$ and $\langle P_{RXEUT} \rangle$ measured, the radiated power of the EUT P_{EUT} can be determined by Equation (5.5).

According to the above measurement procedure, the radiated power of an EUT without its enclosure and that of the EUT with the enclosure can be measured respectively. Consequently, the *ASRP* of the enclosure can be determined by the ratio of the measurement results in these two measurement steps.

It should be mentioned that $\langle P_t \rangle$ obtained during the reference measurement step should be same as that obtained during the attenuation measurement step, provided the P_{out} of the network analyser is fixed. Thus, in terms of the determination of *ASRP*, $\langle P_t \rangle$ is not required because it is eliminated during the calculation of *ASRP*.

5.2.3 Measurement Results

The *ASRP* values obtained during the measurement in ıe anechoic chamber have been given in Fig. 4.5. Theoretically, the *ASRP* measured in the reverberation chamber should be equivalent to that measured in the anechoic chamber because both are based on the estimates of total radiated power. By subtracting each *ASRP* value measured in the anechoic chamber to the relevant one measured in the reverberation chamber, we got the difference values, which are plotted in Fig. 5.2.

For the data presented in Fig. 5.2, about 67% of the difference values are within ±5 dB and 97% are within ±10dB. The *ASRP* measured in the anechoic chamber is comparable with that measured in the reverberation chamber.

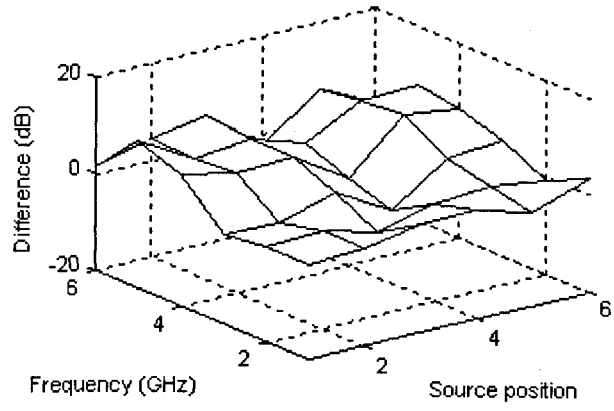

(a)

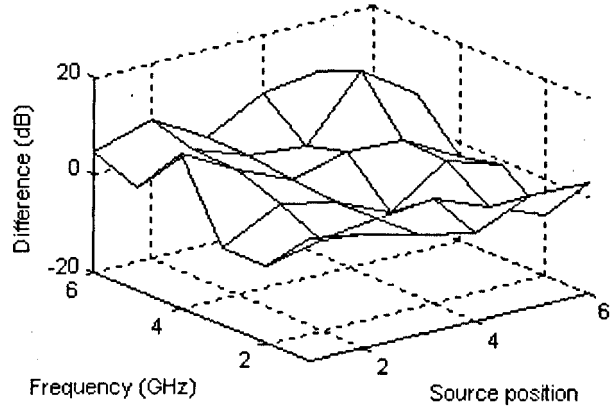

(b)

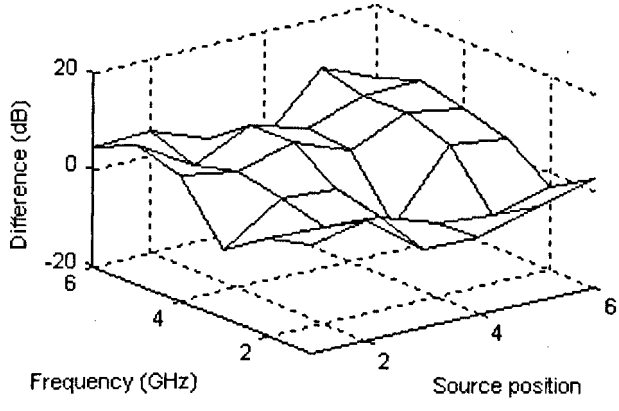

(c)

Fig. 5.2 The plot of the difference between *ASRP* measured in the anechoic chamber and that measured in the reverberation chamber. Configuration of the slots in the front panel: (a) two rectangular slots, (b) one CD slot only and (c) one CD slot and 16 short slots.

During scanning the measurement antenna on a truncated cylindrical surface around the EUT in an anechoic chamber, the emission power above and below the EUT was

missed. The radius and height of the cylindrical surface are respectively 1 m and 1.2 m. Thus, the solid angle subtended at the geometric centre of the dummy EUT by one end cap of the cylindrical surface is 2.6 steradians. Consequently, the ratio of the solid angles covered by the two end caps of the cylindrical surface to the solid angle of a sphere (i.e., 4π steradians) is about 0.42, implying that a considerable fraction of the radiated power may be missed using the cylindrical scan proposed here. It can be predicted that a better agreement between the *ASRP* measured in the anechoic chamber and that measured in the reverberation chamber may be obtained by a complete spherical scan around the EUT in the anechoic chamber.

5.3 The $E.F._{95th}$ of a Practical EUT

5.3.1 The Simulated $E.F._{95th}$ of the Dummy EUT

As discussed in Chapter 3, to get the detailed information of the radiated fields of an equipment enclosure in its radiating near-field, a fully spherical scan or cylindrical antenna scan around the enclosure with a fine scan resolution and two orthogonal orientations of the measurement antenna at each test point are required, which is time consuming.

Here the point source modelling technique that can simulate the radiation pattern of an EUT is used to replace part of the measurement work. This modelling used a simple array of point sources arranged over the surface of a simulated EUT to estimate the radiated emissions from the EUT. The sources are allowed to have random amplitudes within the range 0 to 1 and random phases within the range 0 to 2π. The details of the point source modelling technique may be found in [34]. An example of a Matlab program based on this technique is given in Appendix E, which can simulate the radiation pattern of an EUT with two holes.

The radiation patterns measured by the truncated cylindrical scan around the dummy EUT, as the examples shown in Fig 3.6, Fig 3.8 and Fig 3.9, indicate that although some EM energy appeared in the scan area behind the panel with slots via diffraction, the majority of the EM energy was radiated in front of the panel with slots because of the direct radiation from the slots and the reflection by this panel. This is especially

obvious at frequencies above 3 GHz. The measurement results given in Fig. 5.3 indicate the ratio of the radiated power on the cylindrical scan surface in front of the panel with slots (the scan area from θ=-76° to θ=76°) to the radiated power on the whole scan surface is generally about 90% at frequencies above 3 GHz and about 60% at frequencies below 3 GHz.

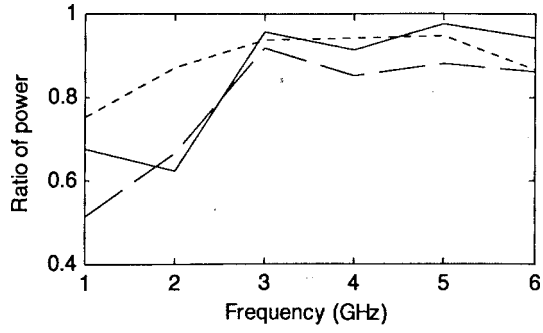

Fig. 5.3 The ratio of the power measured on the cylindrical scan surface in front of the panel with slots to that measured on the whole scan area. Solid line: two rectangular slots; dashed line: one CD slot; dotted line: one CD slot and 16 shot slots. Source position: 2.

The examples of the radiation pattern measured on the scan surface in front of the panel with slots and the equivalent one simulated are given in Fig. 5.4(a) and Fig. 5.4(b) respectively.

Because in each run of the simulation the amplitude and phase of the point source radiation are assigned randomly, the simulated radiation pattern may be different from the measured one. To be comparable with Fig. 5.4(a), Fig. 5.4(b) was chosen from a number of runs of simulation. Both figures have a typical interference pattern with seven cycles.

Whereas it is not expected for the radiation pattern, the statistics $E.F._{95th}$ can be predicted accurately by the modelling technique. During our simulation, for each configuration of slots and each frequency, to compare the $E.F._{95th}$ values derived from the measured radiation patterns from 6 internal source positions, the simulation program has also been run 6 times, and 6 $E.F._{95th}$ values were derived from the simulated radiation patterns. The $E.F._{95th}$ results from simulations, together with these from measurements, are plotted in Fig. 5.5. Here all the $E.F._{95th}$ results are expressed in linear form.

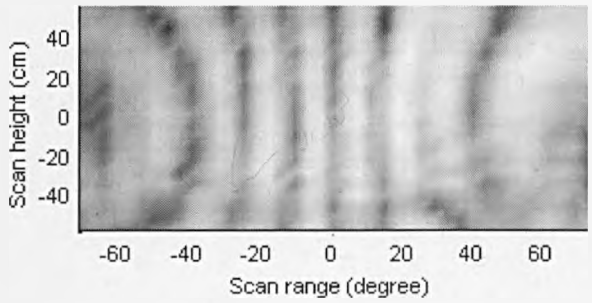

(a)

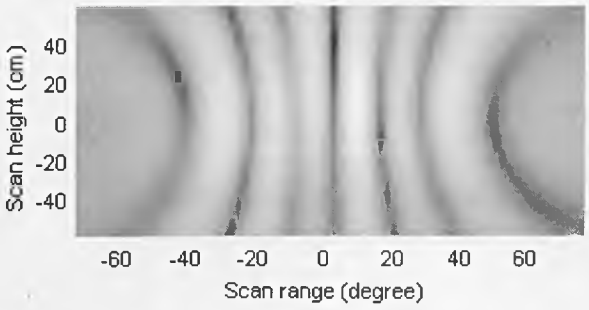

(b)

Fig. 5.4 (a) The measured radiation pattern and (b) the relevant simulation result based on point source modelling technique. Configuration of the slots: one CD slot and 16 short slots. Source position: 1. Frequency: 3 GHz. Scan range: -76~+76 degree.

The three plots in Fig. 5.5 indicate the $E.F._{95th}$ measured is similar to that simulated. The mean and the standard deviation of the simulated $E.F._{95th}$ results are 4.53 and 0.82 respectively, being close to the mean and the standard deviation of the measured $E.F._{95th}$ results, which are 4.01 and 0.97 respectively. The reason why the simulated $E.F._{95th}$ is slightly larger than the measured value is that during the simulation we presume that the power radiated on the scan area in front of the panel with slots is 100% of the radiated power on the whole one, but in fact it is about 90% at frequencies above 3 GHz and about 60% at frequencies below 3 GHz. So far, the radiated field in the scan area behind the front panel via diffraction cannot be simulated by the point source modelling technique.

The agreement between the $E.F._{95th}$ derived from the emission pattern measured and that derived from the emission pattern simulated confirms the feasibility of the modelling technique used here.

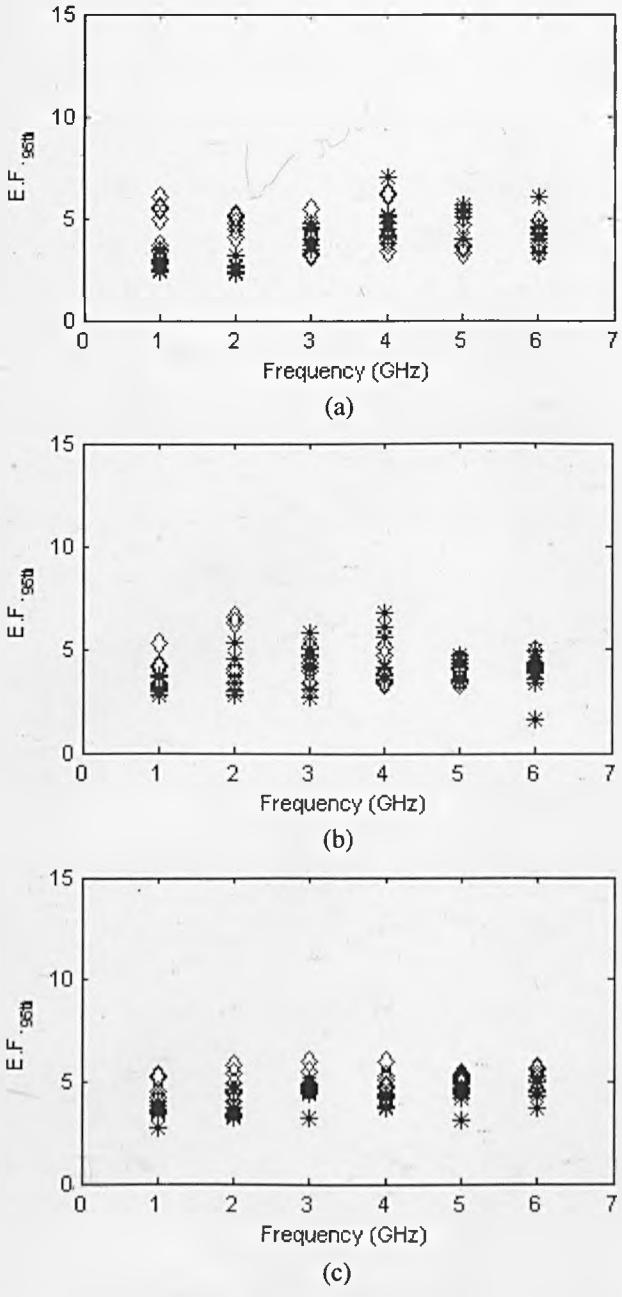

Fig. 5.5 The plots of the $E.F._{95th}$ versus frequency. The 'asterisk' and the 'diamond' markers mean the $E.F._{95th}$ derived from the radiation pattern measured and simulated respectively. Configuration of the slots in the front panel: (a) two rectangular slots, (b) one CD slot only and (c) one CD slot and 16 short slots.

5.3.2 The Simulated $E.F._{95th}$ of a Practical EUT

It is the extreme condition that all the slots are located on only one side of the enclosure, resulting in the majority of the radiated power being focused on the area in

front of this side. The $E.F._{95th}$ of a practical enclosure, on 6 sides of which a number of slots are generally distributed at random, should be less than that of the dummy EUT tested here.

Here the radiation patterns on a truncated cylindrical surface around an enclosure, on 6 sides of which 12 holes are randomly distributed, have been simulated. The dimensions of the simulated enclosure are same as the dummy EUT. The $E.F._{95th}$ and the $E.F._{max}$ derived from the simulation results, together with the theoretical estimation of the D_{max} in the far-field given in [32] are plotted in Fig. 5.6, where the sphere radius 'r' of the enclosure is 0.345 m (based on the enclosure diagonal) and k is the wave number. The frequency range considered is between 1 GHz and 6 GHz, so 'kr' varies between 7.23 and 43.38.

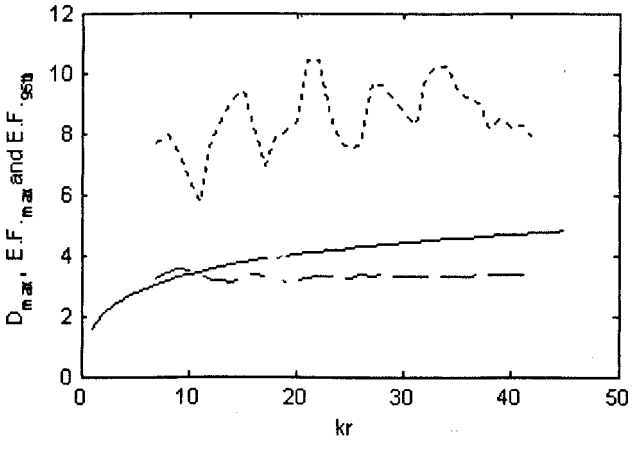

Fig. 5.6 The plot of D_{max}, $E.F._{max}$ *and* $E.F._{95th}$ vs. kr. The solid line: the theoretical estimation of D_{max} in the radiating far-field; the dotted line: the $E.F._{max}$ results from simulated emission pattern in the radiating near-field; the dashed line: the $E.F._{95th}$ results from simulated emission pattern in the radiating near-field. Test distance: 1 m.

It can be seen in Fig. 5.6 that the $E.F._{max}$ of a practical enclosure in its radiating near-field is much higher than the D_{max} in the far-field and varies between 5 and 11. Comparing with $E.F._{max}$ in the radiating near-field, $E.F._{95th}$ is relative stable, and varies between 2 and 4.

More $<E.F._{95th}>$ results from simulated radiation patterns at different test distances and frequencies are given in Fig. 5.7. Here the $<E.F._{95th}>$ is the mean of the $E.F._{95th}$

over 20 runs. The dashed line is the plot of the Rayleigh distance vs. frequency determined by Equation (3.1).

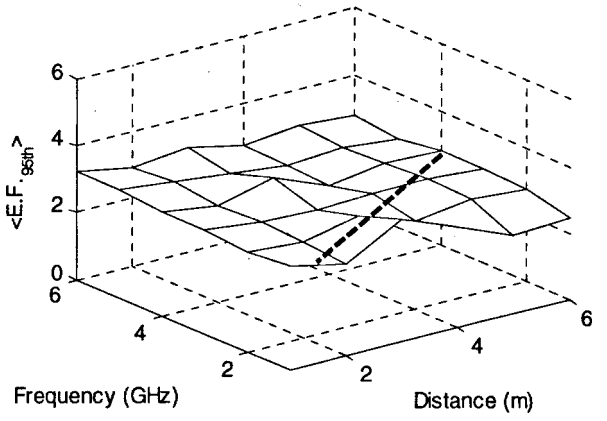

Fig. 5.7 The plot of $<E.F._{95th}>$ derived from simulated radiation patterns at different frequencies and different distances. The dashed line is the plot of the Rayleigh distance vs. frequency.

The radiating near-field is located at the left of the dashed line and the radiating far-field is at the right. The simulation results indicate that over a broad range around the Rayleigh distance, the $<E.F._{95th}>$ still varies between 2 and 4. In terms of the definition *SRP*, to ensure the worst shielding performance of a practical equipment enclosure in its radiating near-field can be estimated, a value of 4 is suggested as the estimate of the $E.F._{95th}$.

The estimate of the $E.F._{95th}$ derived from numerous simulation and measurement results is an empirical value. Because rigorous solutions to three dimensional near-field diffraction problems are rare [37], so far the theory-based estimates of $E.F._{95th}$ cannot be given.

Considering the slots of an equipment enclosure are randomly distributed on its surface, it is quite possible that a truncated cylindrical scan is not sufficient to always meet the maximum emission, for example, as all the slots are located on one side and this side just faces one of the cylinder end caps. However, during our simulation, although 12 holes are randomly distributed on the surface of the EUT, the $E.F._{95th}$ results from the simulated emission patterns on the truncated cylindrical surface are relatively stable. This implies a partial scan can promise a relative accurate estimate of the $E.F._{95th}$ even if such scan cannot meet the maximum emission.

5.3.3 Prediction of the P_{95th} of the Dummy EUT

During the EMC tests, the maximum emission from the EUT is usually required to be determined. Although the maximum emission can be measured directly in an anechoic chamber by a whole cylindrical scan or spherical scan around the EUT, such a measurement is time consuming and thus is uneconomic. If the total radiated power P_{EUT} and the $E.F._{95th}$ of an equipment enclosure are known, then the p_{95th} of the enclosure over the sphere of radius r in free-space can be given by:

$$p_{95th} = E.F._{95th} \cdot \frac{P_{EUT}}{4\pi \cdot r^2} \quad . \quad (5.5)$$

It has been indicated in subsection 5.3.1 that the average of the $E.F._{95th}$ results of the dummy EUT is close to 4 and the standard deviation of these results is less than 1. Thus, a value of 4 is used here as the estimate of the $E.F._{95th}$ of the dummy EUT. P_{EUT} can be measured in a reverberation chamber. Then the p_{95th} of the dummy EUT can be estimated by Equation (5.5). The differences between the p_{95th} estimated and the p_{95th} measured in the anechoic chamber are given in Fig. 5.8.

For the data presented in the three plots in Fig. 5.8, approximately 90% of the absolute differences are less than 5 dB, and approximately 70% of the absolute differences are less than 3dB. The similarity between the p_{95th} measured and that estimated confirms the viability of the estimated $E.F._{95th}$.

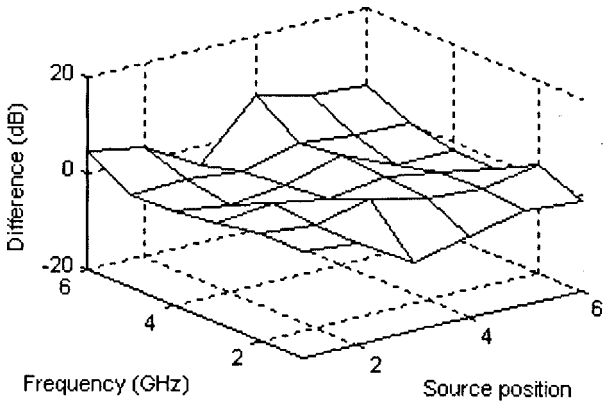

(a)

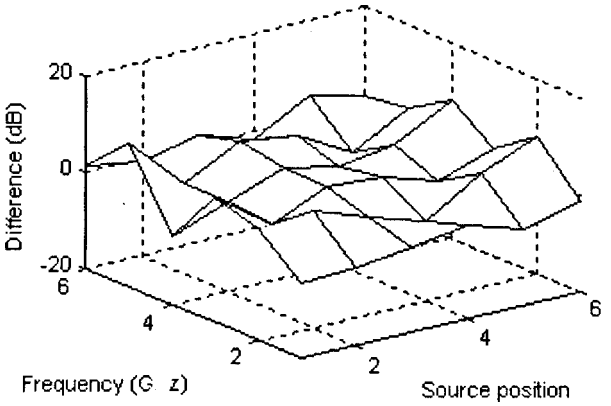

(b)

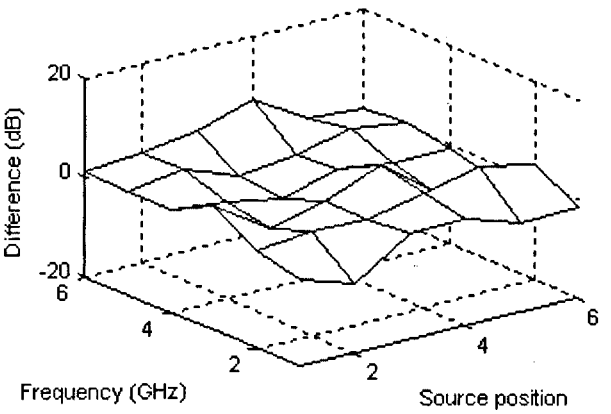

(c)

Fig. 5.8 The difference (dB) between P_{95th} estimated and that measured in the anechoic chamber. Configuration of the slots in the front panel: (a) two rectangular slots, (b) one CD slot only and (c) one CD slot and 16 short slots.

5.4 Discussion

It has been shown that the *ASRP* measured in a reverberation chamber is close to that measured in an anechoic chamber. The reverberation chamber is therefore proposed as an ideal test environment in which either the total radiated power or the *ASRP* can be determined swiftly.

The enhancement factor $E.F._{95th}$ can be used to determine the worst shielding performance and the possible maximum emission from the enclosure in its radiating near-field. Numerous simulation results indicate that $E.F._{95th}$ of a practical enclosure is relative stable, varying between 2 and 4 for various internal source positions, frequencies, configurations of slots and test distances. In order to ensure the worst shielding performance of a practical equipment enclosure in its radiating near-field can be estimated, 4 is suggested as the estimate of the $E.F._{95th}$. By combining the total power measured in the reverberation chamber with the estimate of the $E.F._{95th}$, the upper 95^{th} power density at a given distance can also be predicted accurately according to Equation (5.5).

In a word, the time consuming measurement of *SRP* in an anechoic chamber may be replaced by the combination of a swift measurement of the *ASRP* in a reverberation chamber and a given estimate of the $E.F._{95th}$.

Chapter 6

Immunity Shielding Measurements in a Small Reverberation Chamber

6.1 Introduction

During the shielding measurements described in the previous three chapters, an internal emission source was employed and a new measure *SRP* was proposed to evaluate the radiating shielding, i.e. the ability of an equipment enclosure to shield against the radiation of the equipment contents.

In most other papers about measuring or simulating the shielding performance of an equipment enclosure, such as [16], [18], [25], the enclosure is illuminated by the EM wave derived from an external transmit antenna and an internal receive antenna is used to measure the attenuated signal. That is, the ability of the enclosure to shield against the external threat field is measured. Such ability is termed as immunity shielding in this thesis. During the immunity shielding measurement of an electrically small enclosure [25], both the transmit and the receive antennas are fixed, and the SE is defined as the ratio of the electric fields measured by the receive antenna. It has been shown in [16] that for an electrically large enclosure, the spatial variation of the field within the enclosure should be considered, implying the movement of the receive antenna inside the enclosure is required. It has also been suggested in [18] that the equipment contents should be involved during the shielding measurement.

Moreover, in the scenario of the EMI between equipments described in Chapter 3, it is likely that the victim equipment is in the Fresnel diffraction region of the source equipment, so the structure of the field incident on the victim is complex. Thus, the immunity shielding measurement should also take into account the effects of the incidence angle and the polarization of the incident wave.

The effect of incidence angles and polarizations of the incident waves on the shielding performance of a large enclosure with apertures has been considered in [22], where a reverberation chamber is chosen as the test environment for the shielding measurement. During the measurement, a stirrer and a transmit antenna are placed outside the enclosure, and a receive antenna and another stirrer are placed inside the tested enclosure. The SE is determined by the ratio of the incident power density to the power density in the enclosure, representing the overall shielding performance of the enclosure for various incidence angles and polarizations of the incident waves. Such measurement technique implies that the field variations both inside and outside the enclosure have been averaged.

Although reverberation chamber is an ideal test environment for the immunity shielding measurement of an enclosure, the measurement method proposed in [22] is not applicable to a practical equipment enclosure whose volume is generally not large enough to hold both a measurement antenna and a stirrer. To cope with this difficulty, a new measure shielding of absorption cross section (*SACS*) is proposed, being the ratio of the average absorption cross section of the equipment content in the absence of the enclosure to the one in the presence of the enclosure. During the measurement of *SACS* in reverberation chambers, no measurement facilities are required to be placed inside the tested enclosure. The measurement setup is shown in Fig. 6.1.

The measurement of *SACS* in reverberation chambers implies that all the possible incidence angles and polarizations have been considered and averaged. The measure *SACS* also implies the field variation on the equipment contents have been averaged. However, the measurement results presented here indicate that it is not easy to measure accurately the absorption cross section of the equipment content inside the enclosure, especially as the enclosure with small apertures. So far, the measurement technique proposed here is only applicable to enclosures with large apertures.

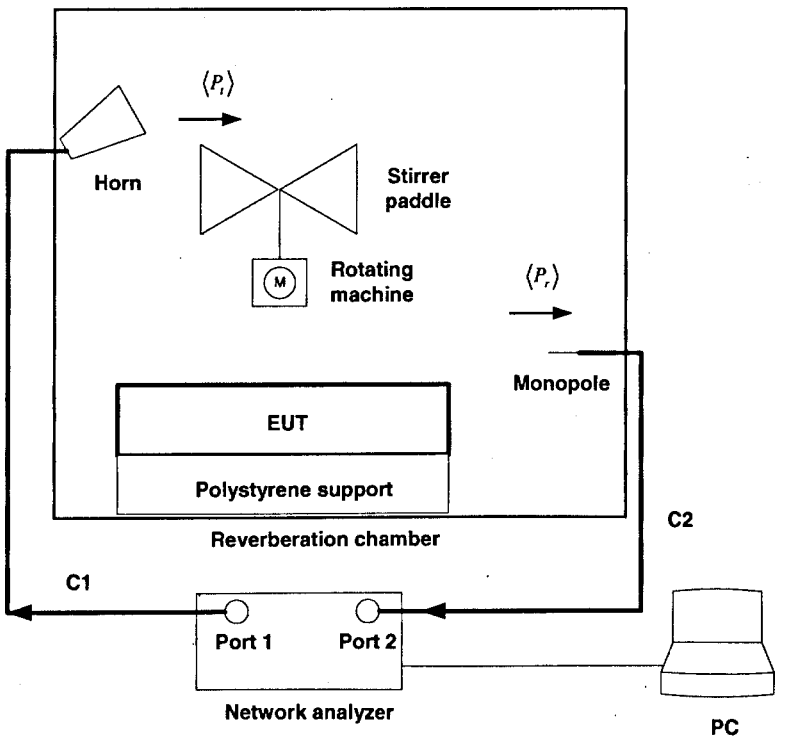

Fig. 6.1 Measurement setup of *SACS* of an enclosure in a reverberation chamber.

During the measurement of *SACS*, both the transmit and receive antennas are placed outside the tested enclosure and the measurement result is not power but average absorption cross section. Thus, the measurement of *SACS* proposed here is not the reciprocal of the measurement of shielding of radiating power, *SRP*, which was proposed in Chapter 4. The measurement of *SACS* is also not the reciprocal of the typical SE measurement of an enclosure, which generally accounts for only one test point and one fixed polarization.

The organization of this chapter is as follows. The definition of *SACS* and the associated parameters are introduced in Section 6.2. The relevant measurement setup and measurement procedure are illustrated in Section 6.3 and 6.4 respectively. The measurement results are given in Section 6.5. The disadvantages and advantages of this new measure are discussed in Section 6.6.

6.2 A New Definition *SACS* Proposed for the Immunity Shielding

6.2.1 Definition Descriptions

In electromagnetism, absorption cross section, σ, refers to the ability of an object to absorb the EM energy. Generally, the absorption cross section of an object depends on the frequency, field polarization and the geometry and EM properties of the object. Here the proposed definition shielding of average cross section, *SACS*, is defined as:

$$SACS = \frac{\langle \sigma_{c,out} \rangle}{\langle \sigma_{c,in} \rangle} \quad (6.1)$$

where $\langle \sigma_{c,out} \rangle$ is the average value of the absorption cross section of the equipment content outside the enclosure over a certain frequency range, and $\langle \sigma_{c,in} \rangle$ is the average value of the absorption cross section of the equipment content inside the enclosure over the same frequency range.

The $\langle \sigma_{c,out} \rangle$ may be calculated by

$$\langle \sigma_{c,out} \rangle = \frac{1}{N} \sum_{i=1}^{N} \langle \sigma_{ci,out} \rangle \quad (6.2)$$

where $\langle \sigma_{ci,out} \rangle$ is at each frequency the absorption cross section of the equipment content outside the enclosure, N is the number of the spot frequencies in the considered frequency range. The $\langle\ \rangle$ of $\langle \sigma_{ci,out} \rangle$ means an average over all possible incidence angles and polarizations of the incident wave.

Similarly, $\langle \sigma_{c,in} \rangle$ may be calculated by

$$\langle \sigma_{c,in} \rangle = \frac{1}{N} \sum_{i=1}^{N} \langle \sigma_{ci,in} \rangle \quad (6.3)$$

where $\langle \sigma_{ci,in} \rangle$ is at each frequency the absorption cross section of the equipment content inside the enclosure.

The definition of *SACS* addresses the average shielding performance over a certain frequency range and takes account for the spatial variation of the field on the contents and the effects of the incidence angle and polarization of the incident wave.

6.2.2 Relationship between Absorption Cross Section and Q Factor

The absorption cross section of a lossy object, σ, which is directly related to the absorbed power, can be derived from the quality factor Q of the reverberation chamber loaded with this object. The relationship between σ and the Q factor of the reverberation chamber has been discussed in [22], which will also be introduced briefly in the following paragraphs taken directly from [22].

Generally, the Q of a cavity may be defined as

$$Q = \varpi U_s / P_d \quad (6.4)$$

where ϖ is the excitation (angular) frequency, U_s is the steady-state energy in the cavity, and P_d is the dissipated power in the cavity.

If the reverberation chamber is used as the test environment, the Q factor of the reverberation chamber can be expressed as:

$$Q = \frac{16\pi^2 V}{\lambda^3} \frac{\langle P_r \rangle}{P_t} \quad (6.5)$$

where V is the chamber volume, $\langle P_r \rangle$ is the averaged power received by the receive antenna and P_t is the transmitted power from the transmit antenna. For the calculation convenience, (6.5) can also be expressed as

$$Q = \frac{16\pi^2 V \langle S_{21}^2 \rangle}{\lambda^3} \quad (6.6)$$

where $\langle S_{21}^2 \rangle$ is the mean square of the measured forward transmission coefficient between the transmit and receive antennas.

The dissipated power inside a reverberation chamber P_d can be written as the sum of four terms:

$$P_d = P_{d1} + P_{d2} + P_{d3} + P_{d4} \quad (6.7)$$

where P_{d1} is the power dissipated in the chamber walls, P_{d2} is the power absorbed by loading objects within the cavity, P_{d3} is the power lost through aperture leakages, and P_{d4} is the power dissipated in the loads of receiving antennas.

Combining (6.4) and (6.7), the inverse of Q of the chamber can be expressed as

$$Q^{-1} = Q_1^{-1} + Q_2^{-1} + Q_3^{-1} + Q_4^{-1} \quad (6.8)$$

where

$$Q_1 = \varpi U_s / P_{d1},\ Q_2 = \varpi U_s / P_{d2},\ Q_3 = \varpi U_s / P_{d3} \text{ and } Q_4 = \varpi U_s / P_{d4}.$$

The Q_2 results from the absorption cross section of the loading objects is determined by

$$Q_2 = \frac{2\pi V}{\lambda \langle \sigma \rangle}. \quad (6.9)$$

Again, the $\langle\ \rangle$ of $\langle \sigma \rangle$ indicates an average over all possible incidence angles and polarizations of the incident wave.

6.3 Measurement Setup

To ensure a sufficient sensitivity to the loaded lossy object, a small reverberation chamber with dimensions of 800 mm × 700 mm × 600 mm (a × b × c) was used as the test environment. A ridged horn (EMCO 3115) and an 18 mm monopole were used as the transmit antenna and the receive antenna respectively, and a Hewlett Packard network analyser 8753D was used to measure the S_{21} between these two antennas.

Evaluating Equation (5.1) shows that the first resonant frequency f_{110} of the small reverberation chamber is 284.73 MHz. Thus, the LUF of the small reverberation chamber determined by 3 times the first resonance frequency is about 854 MHz, which is just below the lowest test frequency considered during our measurement,

1000 MHz. According to Equation (5.2), about 100 modes exist in this small reverberation chamber at frequencies below 1000 MHz.

The boundary conditions at any highly conducting surface require that the tangential component of electric field is approximately zero at the surface, so the field uniformity cannot be achieved as walls of a reverberation chamber or other conducting contents are approached. To get the desired field uniformity, it is recommended in IEC 61000-4-21 [4] that the equipment tested shall be more than one quarter of the wavelength of the lowest test frequency (75mm at 1GHz) from the chamber walls, antennas and stirrer. During our measurement the enclosure was supported 80 mm above the chamber floor by a polystyrene plate, and the front panel with slots was 120 mm away from the chamber sidewall. There are two reasons for using a polystyrene plate as the support. Firstly, polystyrene is non-conductive material and thus the electric field near the polystyrene is not necessary to be normal to its surface. Secondly, polystyrene has no EM energy absorption when an electromagnetic wave impinges on it. That is, the application of the polystyrene plate will not reduce the working volume and the Q factor of the reverberation chamber.

The relative positions of the antennas, the mode stirrer, the polystyrene plate and the enclosure inside the small reverberation chamber are shown in Fig. 6.2.

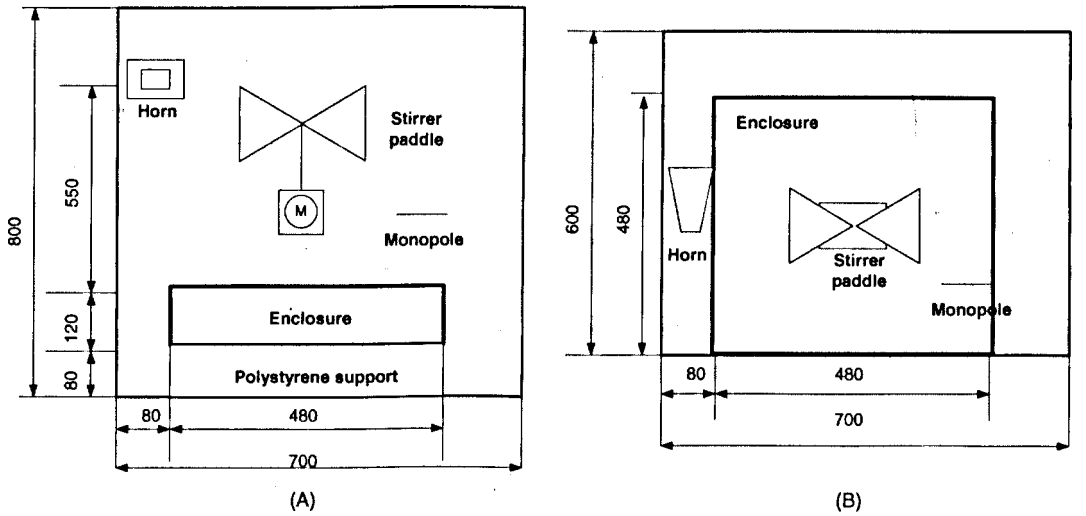

Fig. 6.2 Geometry of the measurement setup in the small reverberation chamber. All dimensions in millimeters. (A): side view; (B): top view.

The enclosure of the dummy EUT used for the radiating shielding measurement was also employed here. Two different slots arrangements in the front panel were used during the measurement, as shown in Fig. 6.3.

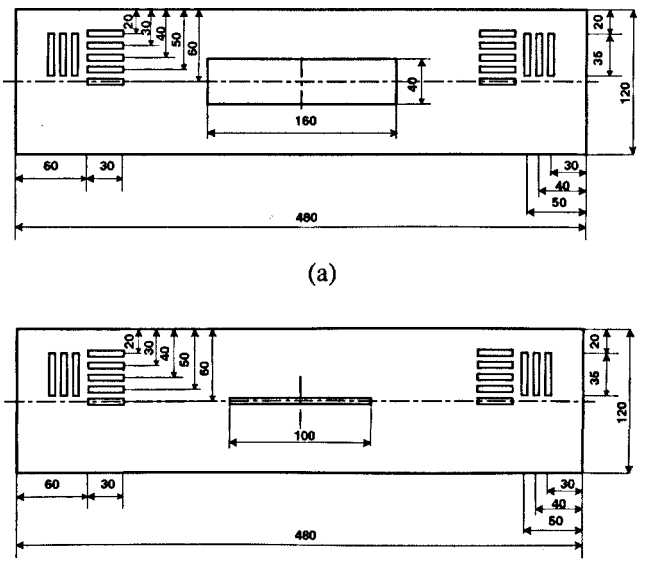

(a)

(b)

Fig. 6.3 Geometry of the front panels used for the measurement of *SACS*. (a) one big slot (160 mm × 40 mm) and 16 short slots (30 mm × 5 mm or 35 mm × 5 mm), (b) one CD slot (100 mm × 5 mm)and 16 short slots same as those in (a). All dimensions in millimeters.

To test the effects of different loads on the shielding performance of the enclosure, both the RC of the dummy EUT and a large carbon foam block were considered as the equipment contents. The RC has dimensions of 300 mm × 240 mm × 10 mm. The carbon foam block is a truncated pyramid, of which the bottom dimensions are 320 mm × 320 mm, the top dimensions are 110 mm × 110 mm and the height is 100 mm. The volume of the carbon foam block is much larger than the RC, implying a larger value of absorption cross section may be measured. Fig. 6.4 gives the picture of the RC and the large carbon foam block.

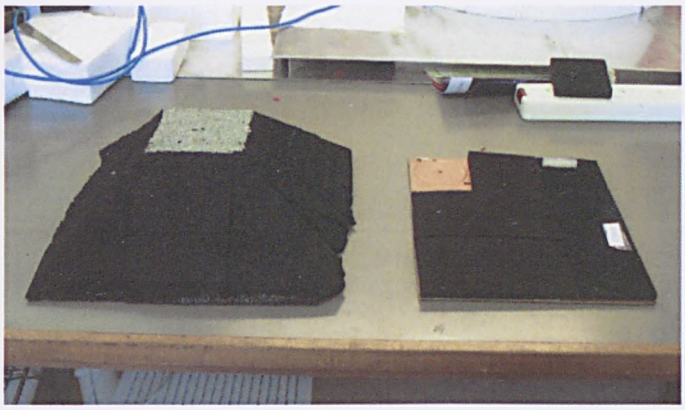

Fig. 6.4 The large carbon foam (left) and the RC (right) used as different loads of the enclosure tested.

6.4 Measurement Procedure

To determine *SACS* of an equipment enclosure in a reverberation chamber, three measurement steps are required, which are detailed as follows.

A. Calibration measurement

In this step, only the empty enclosure is put inside the reverberation chamber as the loading object, and for each stirrer position the transmission coefficient $S_{21,e}$ between the horn and the monopole is recorded.

Combining (6.6), (6.8) and (6.9), we find:

$$\frac{\lambda^3}{16\pi^2 V}\frac{1}{\left\langle S_{21,e}^2\right\rangle} = Q_1^{-1} + \frac{\lambda\left\langle\sigma_{ei}\right\rangle}{2\pi V} + Q_3^{-1} + Q_4^{-1} \quad (6.10)$$

where $\left\langle\sigma_{ei}\right\rangle$ is the absorption cross section of the enclosure measured in this step.

B. Reference measurement

In this step, both the enclosure with the content are put inside the reverberation chamber with the content is located outside the enclosure. For each stirrer position, the transmission coefficient $S_{21,c}$ is recorded, and (6.8) can be expressed as

$$\frac{\lambda^3}{16\pi^2 V}\frac{1}{\left\langle S_{21,c}^2\right\rangle} = Q_1^{-1} + \frac{\lambda\left\langle\sigma_{ei}\right\rangle}{2\pi V} + \frac{\lambda\left\langle\sigma_{ci,out}\right\rangle}{2\pi V} + Q_3^{-1} + Q_4^{-1}. \quad (6.11)$$

Then $\langle \sigma_{ci,out} \rangle$ can be derived by subtracting (6.10) from (6.11):

$$\langle \sigma_{ci,out} \rangle = \frac{\lambda^2}{8\pi} \left(\frac{1}{\langle S_{21,c}^2 \rangle} - \frac{1}{\langle S_{21,e}^2 \rangle} \right). \quad (6.12)$$

C. Shielding measurement

In this measurement step, the content is put inside the enclosure and the forward transmission coefficient $S_{21,eut}$ is recorded for each stirrer position. Then (6.8) can be expressed as

$$\frac{\lambda^3}{16\pi^2 V} \frac{1}{\langle S_{21,eut}^2 \rangle} = Q_1^{-1} + \frac{\lambda \langle \sigma_{ei} \rangle}{2\pi V} + \frac{\lambda \langle \sigma_{ci,in} \rangle}{2\pi V} + Q_3^{-1} + Q_4^{-1} \quad (6.13)$$

and the absorption cross section of the equipment content inside the enclosure, $\langle \sigma_{ci,in} \rangle$, can be derived by subtracting (6.10) from (6.13), that is,

$$\langle \sigma_{ci,in} \rangle = \frac{\lambda^2}{8\pi} \left(\frac{1}{\langle S_{21,eut}^2 \rangle} - \frac{1}{\langle S_{21,e}^2 \rangle} \right). \quad (6.14)$$

It is expected that as objects with increasing absorption are placed inside the reverberation chamber, the smaller the value of $\langle S_{21}^2 \rangle$ obtained, that is, $\langle S_{21,e}^2 \rangle > \langle S_{21,eut}^2 \rangle > \langle S_{21,c}^2 \rangle$. Thus, according to (6.12) and (6.14), both $\langle \sigma_{ci,out} \rangle$ and $\langle \sigma_{ci,in} \rangle$ should be positive and due to the shielding performance of the enclosure, $\langle \sigma_{ci,out} \rangle$ should be larger than $\langle \sigma_{ci,in} \rangle$.

During our measurements, 401 test points were adopted for every 100 MHz frequency range and measurements were taken at 240 positions over one complete stirrer rotation.

6.5 Measurement Results

6.5.1 Shielding of Average Cross Section of the Enclosure with Large Slots

At first, the *SACS* of the enclosure with the front panel shown in Fig 6.3 (a) was measured. Examples of $\langle \sigma_{ci,out} \rangle$ and $\langle \sigma_{ci,in} \rangle$ of the RC are plotted in Fig. 6.5 (a) and those of the pyramidal foam block are plotted in Fig. 6.5(b).

As discussed above, $\langle \sigma_{ci,out} \rangle$ should be always larger than $\langle \sigma_{ci,in} \rangle$ and both of them should be positive. However, it can be seen in Fig. 6.5(a) a few $\langle \sigma_{ci,out} \rangle$ are less than the corresponding values of the $\langle \sigma_{ci,in} \rangle$. The possible reason is due to the limited energy absorption of the RC at some frequencies, the reverberation chamber is not sensitive enough to test the difference between $S_{21,c}$ and $S_{21,eut}$. Such experimental error may be reduced as the RC is replaced with a larger lossy object. It can be seen in Fig. 6.5(b) that at each frequency, the $\langle \sigma_{ci,out} \rangle$ is always larger than the $\langle \sigma_{ci,in} \rangle$.

When either the truncated pyramid foam block or the RC is placed inside the enclosure, its energy absorption may be too small due to the shielding performance of the enclosure. Thus, in some cases the reverberation chamber is not sensitive enough to test the difference between $S_{21,e}$ and $S_{21,eut}$, which may result in a negative $\langle \sigma_{ci,in} \rangle$. For the data presented in Fig. 6.5(a) and (b), about 13% and 17% of the measured $\langle \sigma_{ci,in} \rangle$ are negative respectively.

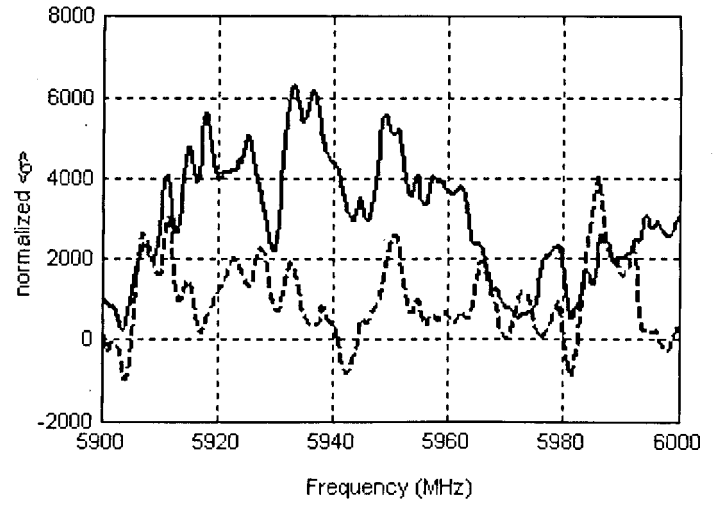

(a)

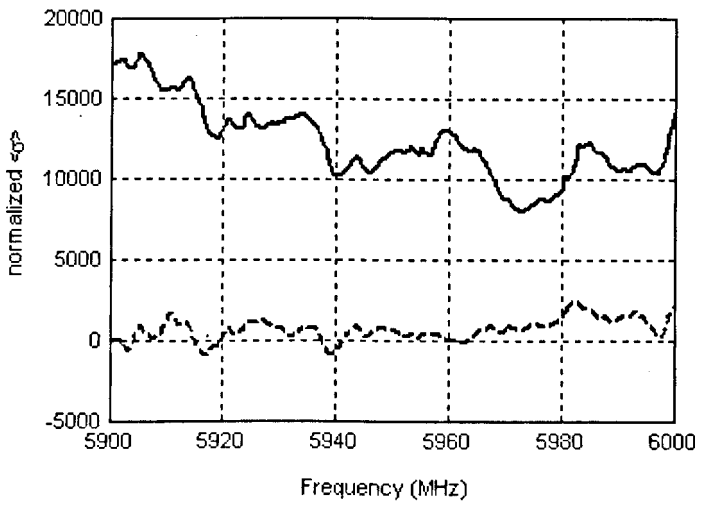

(b)

Fig. 6.5 The measurement results of $\langle \sigma_{ci,out} \rangle$ and $\langle \sigma_{ci,in} \rangle$ of the RC (a) and those of the truncated pyramid foam block (b). The solid line: $\langle \sigma_{ci,out} \rangle$; the dashed line: $\langle \sigma_{ci,in} \rangle$. Both $\langle \sigma_{ci,out} \rangle$ and $\langle \sigma_{ci,in} \rangle$ have been normalized to $\lambda^2/8\pi$. Configuration of the slots in the front panel is shown in Fig. 6.3(a).

The experimental error of either $\langle \sigma_{ci,in} \rangle$ or $\langle \sigma_{ci,out} \rangle$ can be mitigated during the calculation of the *SACS*, where both $\langle \sigma_{ci,in} \rangle$ and $\langle \sigma_{ci,out} \rangle$ are averaged over a certain frequency range. For the following data presented, the *SACS* is derived from the average results of $\langle \sigma_{ci,in} \rangle$ and $\langle \sigma_{ci,out} \rangle$ over 100 MHz.

Examples of the derived *SACS(f)* values, together with several *ASRP* values, are given in Fig. 6.6. Here *'f'* in *SACS(f)* refers the stop frequency of each frequency range of 100 MHz.

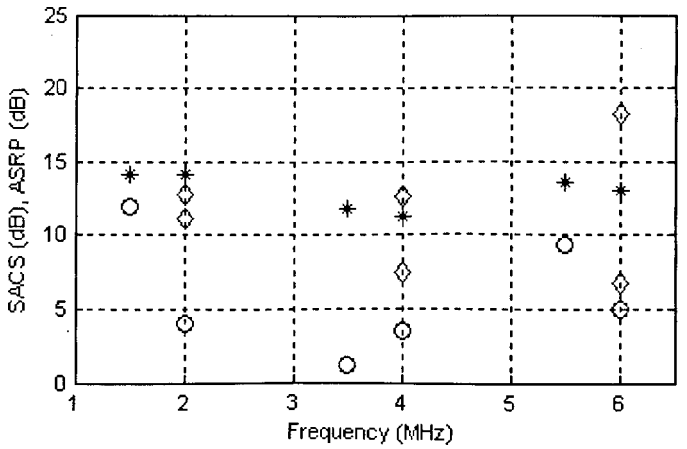

Fig. 6.6 Some results of *SACS* and *ASRP* of the enclosure with the front panel shown in Fig. 6.3(a). At each frequency, the 'asterisk' marker is the *SACS* value of the enclosure with the truncated pyramid foam block; the 'circle' marker is the *SACS* value of the enclosure with the RC; the 'diamond' markers are the *ASRP* values of the enclosure for two difference source positions on the RC.

It can be seen in Fig. 6.6 that the higher the energy absorption of the equipment contents, the larger shielding performance the enclosure exhibits. That is, the shielding performance of an enclosure depends on its Q factor. This conclusion coincides with that given in [22], where the theory and measurement results illustrate that the SE of a large enclosure with apertures depends on the internal loss of the enclosure. The *ASRP* values, depending on the source position, are quite different from the corresponding *SACS* values.

6.5.2 Shielding of Average Cross Section of the Enclosure with Small Slots

Secondly, consider the shielding measurement of the enclosure with the front panel shown in Fig. 6.3(b). It can be predicted that when the 160 mm × 40 mm slot in the front panel is replaced by a 100 mm × 5 mm CD slot, because less power is coupled

inside the enclosure, the measurement error of $\langle \sigma_{ci,in} \rangle$ may be increased. The examples of measurement results of $\langle \sigma_{ci,in} \rangle$ and $\langle \sigma_{ci,out} \rangle$ are given in Fig. 6.7.

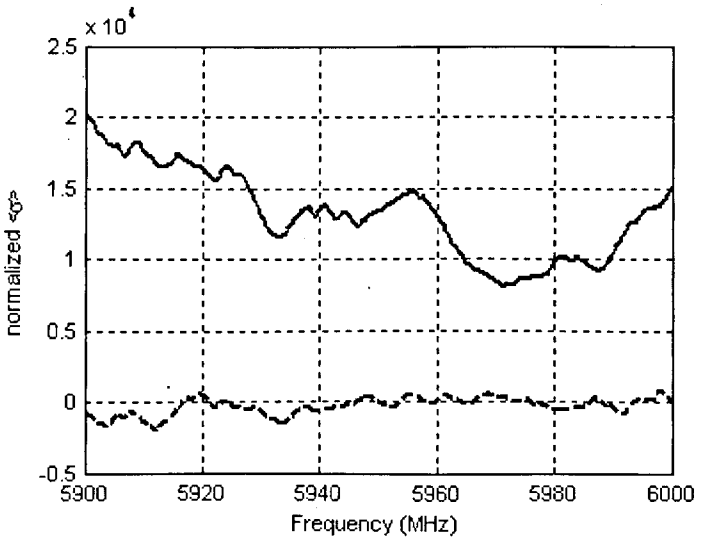

Fig. 6.7 The measurement results of $\langle \sigma_{ci,out} \rangle$ and $\langle \sigma_{ci,in} \rangle$ of the truncated pyramid foam block. The solid line: $\langle \sigma_{ci,out} \rangle$; the dashed line: $\langle \sigma_{ci,in} \rangle$. Both $\langle \sigma_{ci,out} \rangle$ and $\langle \sigma_{ci,in} \rangle$ have been normalized to $\lambda^2/8\pi$. Configuration of the slots in the front panel is shown in Fig. 6.3 (b).

For the data given in Fig. 6.7, only about 35% of the measured $\langle \sigma_{ci,in} \rangle$ values are positive and the linear *SACS* value calculated at this frequency band is -40. Obviously, the measurement technique proposed here is not sufficient to estimate the shielding performance of an enclosure with smaller apertures.

6.6 Discussion

The new measure *SACS* proposed here can give an ensemble estimation of the immunity shielding performance of an equipment enclosure with large apertures over a defined frequency range. A reverberation chamber with small dimensions is suggested as the test environment.

This measure shows several promising advantages: firstly, during the measurement no receive antenna is required inside the enclosure, thus the shielding performance of an equipment enclosure with limited volume can be measured easily and the possible

effect of the receive antenna and the connected cabling on the shielding performance of the enclosure is avoided; secondly, the *SACS* measured in a reverberation chamber implies all the possible incidence angles and polarizations of the incident fields have been considered; thirdly, the absorption cross section of the equipment contents also implies the field variation on the content has been considered and averaged.

However, the absorption cross section of the enclosure with internal contents, $\langle \sigma_{ci,in} \rangle$, is usually very small and not easily tested by the reverberation chamber. To reduce the measurement error of $\langle \sigma_{ci,in} \rangle$, three methods are adopted during the measurement. Firstly, a small sized reverberation chamber is employed to ensure a sufficient sensitivity to the loaded lossy object. Secondly, besides the RC, a larger absorber has also been used as the equipment content, which may increase the value of $\langle \sigma_{ci,in} \rangle$. Thirdly, the measured $\langle \sigma_{ci,in} \rangle$ values are averaged over a certain frequency range. In spite of these efforts, the measurement error of $\langle \sigma_{ci,in} \rangle$ of an enclosure with small apertures is still unacceptable. Being limited by the measurement accuracy of the test equipment, so far the measurement technique proposed here is only applicable to enclosures with large apertures. A new measurement technique or the improvement of the current measurement equipment is required to validate this measure.

The measurement results also illustrate that the *SACS* of an equipment enclosure depends on the equipment contents: the larger energy absorption of the equipment contents, the higher *SACS* of the enclosure exhibits. It can be predicted the shielding ability of an equipment enclosure with apertures will approach to zero if there are no contents inside the enclosure, say, the energy loss inside the enclosure is close to zero.

Besides the *SACS* used to indicate the average immunity shielding performance, the worst immunity shielding performance is also important and should be expressed. To derive the worst immunity shielding performance, further experimental and theoretical studies are required to get the possible maximum field or the field distribution inside the tested enclosure.

Chapter 7

Conclusions

7.1 Introduction

An overview of the SE measurement standards for materials and those for large screened enclosures is given in Chapter 1. It has been shown the current SE measurement standards for large screened enclosures are not suitable for equipment enclosures. The main problems are:

- There are always a number of apertures on an equipment enclosure. Incident fields with various polarizations and incidence angles mean different excitations on the apertures, which may result different shielding performance of the enclosure. These variations should be expressed during the shielding measurement;
- Equipment contents usually occupy a high fraction of the equipment enclosure volume, which disturb the internal field structure and reduce the Q-factor of the enclosure. Thus, during the shielding measurement of an equipment enclosure, the equipment contents should be considered;
- The limited empty volume of many equipment enclosures means that the measurement antenna is not easily placed and moved inside.

The aim of this thesis was to propose a suitable definition, together with the associated measurement technique, for evaluating the shielding performance of an equipment enclosure. To achieve this, different measurement techniques associated with different test environments are developed and several definitions based on the measurement results from these measurement techniques are proposed. The test environments considered in this thesis are: a medium sized anechoic chamber with dimensions of 3.25 m × 2.10 m × 2.05 m; a medium sized reverberation chamber

with dimensions of 4.70 m × 3.00 m × 2.37 m; and a small sized reverberation chamber with dimensions of 0.80 m × 0.70 m × 0.60 m.

The contents of this chapter are organized as follows. The conclusions on each chapter of this thesis will be presented in Section 7.2. Comparisons between the measurement techniques proposed in this thesis will be summarized in Section 7.3, together with some suggestions for the future work related with the shielding measurement of equipment enclosures.

7.2 Conclusions on Individual Chapters

7.2.1 The Dummy EUT

To ensure the proposed shielding measurement techniques are appropriate to practical electric equipment enclosures, the dummy EUT used here has a similar structure and comparable electromagnetic properties to a typical electronic equipment. This EUT was employed during the shielding measurements in all the three measurement environments considered here.

Previous experimental and theoretical work [17], [18], [19] has indicated that the equipment contents may disturb the fields and absorb the EM energy inside the enclosure, having effects on the shielding performance of the enclosure. Thus, it is suggested here the equipment contents should be involved during the shielding measurement of an equipment enclosure. However, different contents, such as the circuit cards with various dimensions and component densities, may result in different shielding performances of the same enclosure. To enable the designers to compare the shielding performance of different enclosures, a standard RC is required.

However, the previous technique proposed in [18] cannot determine a suitable RC at frequencies above 1 GHz, at which an equipment enclosure is usually electrically large and thus the frequency response of S_{21} between two antennas inside the enclosure is too complex to be compared with others. This difficulty may be solved by applying autocorrelation to the measured S_{21}. A statistical approach based on the autocorrelation results is proposed here to determine a suitable RC at frequencies above 1 GHz.

The measurement results indicate that the combination of a PCB laminate and a suitable carbon loaded foam may has the similar absorbing properties to a typical circuit card over a broad frequency range, and so can be looked as a RC representing a circuit card.

7.2.2 Radiation Measurements in an Anechoic Chamber

During our measurements, two approaches were considered to determine the radiating shielding and immunity shielding of the dummy EUT. In the first approach, to measure the radiating shielding of the enclosure of the dummy EUT, i.e. the ability of the enclosure to prohibit the radiating contents from interfering other equipments, a radiating source was mounted on the RC and the radiations of both the dummy EUT and the RC were measured respectively. Thus, the radiating shielding measurement is directly related to the radiation measurement.

It is suggested here that the proposed measurement technique should correspond to the current equipment technologies. Firstly, because current digital equipment clock frequencies are frequently in excess of 1 GHz, the measurement technique for radiating shielding at frequencies above 1 GHz was considered in this thesis. At these frequencies, both an equipment enclosure with dimensions of from hundreds of millimetres to one meter and a typical circuit card with dimensions of hundreds of millimetres are electrically large. Secondly, considering that a circuit card usually produces unintended emissions at low power levels, it is likely that the radiated fields of a typical electronic equipment can only interfere other equipments located in its proximity. Thus, according to Equation (3.1), it is suggested here that the radiating shielding measurement of an equipment enclosure should be performed in its radiating near-field at frequencies above 1 GHz.

The radiation characteristics of an electrically large equipment enclosure in its radiating near-field are as follows:

- The amplitude of the radiated field generally exhibits fast spatial variation due to the interference between the line-of-sight radiations from the enclosure slots and the diffraction of the enclosure in its radiating near-field. The distance between the electric field maxima and the minima may be close to $\lambda/4$. The complex

radiation pattern implies it is hard to predict either the direction or the magnitude of the maximum electric field.

- The complex field structure inside an electrically large enclosure and the effect of apertures mean that the polarizations of the radiated fields at different observation points are various and hard to be predicted.

To measure such radiated fields in an anechoic chamber, the measurement antenna should scan on an area encompassing the EUT with the scan resolution less than $\lambda/4$, and at each test point two measurements should be taken with the antenna oriented at two orthogonal directions respectively. At frequencies above 1 GHz, thousands of test points at 1 m test distance may be required and thus the measurement is time consuming.

The complex radiation patterns obtained also imply the measurement method of equipment emissions proposed in CISPR 16-2-3, i.e., an antenna scan on one azimuth circle around the EUT encompassed by the 3 dB beam width of the antenna, is not sufficient to determine the maximum emission of an equipment. The radiating shielding measurement technique proposed here, i.e., an antenna scan on a surface encompassing the EUT, may be also used to determine the maximum radiation of equipment. The associated discussions are given in Appendix C.

7.2.3 Considered Definitions for Radiating Shielding

The complex and detailed radiation patterns of both the dummy EUT and the RC mean the measured SE value strongly depends on the test position of the measurement antenna and so a good measurement repeatability of the SE is not expected. In other words, the shielding performance of an equipment enclosure generally expresses fast spatial variation. However, both the traditional SE measurement technique and the definition of SE based on one ratio of electric fields cannot indicate such variation.

An antenna scan on a cylindrical surface centred on the EUT was suggested at first to measure the shielding performance of the EUT. To indicate the detailed shielding performances of an equipment enclosure, three new definitions shielding of radiating

fields in positions (***SRFP***), shielding of radiating fields in order (***SRFO***) and shielding of radiating fields (***SRF***) were considered, each of which is a collection of a number of ratios of the electric fields measured. However, the measurement results indicate that there are generally large differences in the elements in each of three definitions, which may be more than 50 dB, meaning the shielding ability of an equipment enclosure cannot be defined by these definitions.

To cope with this difficulty, a simple definition shielding of radiating power (*SRP*) is proposed, consisting of two parameters the average shielding of radiating power (*ASRP*) and the enhancement factor $E.F._{95th}$. In detail, the *ASRP* is defined as the ratio between the total radiated power measured as the enclosure is absent to the total radiated power measured as the enclosure is present, giving a defined indication of the overall shielding ability of an equipment enclosure. The enhancement factor $E.F._{95th}$ is defined as the ratio between the upper 95^{th} percentile of the power densities measured on a scan area encompassing the EUT in the radiating near-field and the averaged power density on the same area, being analogous to the maximum directivity D_{max} of an antenna in its radiating far-field. The ratio between the *ASRP* and $E.F._{95th}$ can be used to represent the worst shielding performance of an equipment enclosure in its radiating near-field. The best shielding performance of an enclosure is generally not of concern as it is the worst one that causes EMI or EMC problems. Thus, the shielding variation of an equipment enclosure may be expressed effectively by the combination of the *ASRP* and the ratio of $ASRP/E.F._{95th}$.

Comparisons between the measurement results of ***SRFP***, ***SRFO***, ***SRF*** and *SRP* indicate that the results of *ASRP* are always between the maximum and the minimum elements of the other three definitions for detailed shielding performances and the results of $ASRP/E.F._{95th}$ are always close to the results of $SRFO_{min}$, i.e. the worst shielding performance determined by ***SRFO***. Considering the *SRP* can provide more useful information and has the potential to be determined swiftly by other means, this definition is finally proposed for the radiating shielding of equipment enclosures.

It has also been shown that the typical SE value is generally less than the corresponding *ASRP* value, meaning the SE results from the conventional SE

measurement technique are prone to underestimate the overall shielding ability of an equipment enclosure.

7.2.4 Radiating Shielding Measurements in a Reverberation Chamber and Prediction of the Enhancement Factor

To determine the *SRP* of an equipment enclosure in an anechoic chamber, both the emission pattern on a cylindrical or spherical surface centred on the equipment and that centred on the equipment content are required. The associated measurements are time consuming. Thus to achieve a quick estimate of the *SRP*, another method is proposed. In detail, the *ASRP* may be determined in a reverberation chamber, which is an environment to measure the total radiated power swiftly, regardless of the emission pattern. The *ASRP* measured in the reverberation chamber should be equivalent to that measured in the anechoic chamber because both are based on the estimates of total radiated power. It has been shown in Section 5.2 that about two-thirds of the difference values between the *ASRP* measured in the reverberation chamber and the equivalent one measured in the anechoic chamber with a truncated cylindrical scan are within ±5 dB and almost all are within ±10dB.

It has been shown in Section 4.3 that the $E.F._{95th}$ of the dummy EUT is relative stable, regardless of the frequency, source position and the slot configurations. This implies that the $E.F._{95th}$ may be estimated roughly by a single value. However, the $E.F._{95th}$ of the dummy EUT, of which only one panel with slots was used to radiate EM energy, cannot be used to represent the $E.F._{95th}$ of a practical enclosure, on 6 sides of which a number of slots could be randomly distributed. Here point source modelling technique is employed to simulate the emission patterns of a practical enclosure with various slots distributions, from which the $E.F._{95th}$ can be derived. Numerous simulation results indicate the $E.F._{95th}$ of a practical enclosure is also relative stable, which varies between 2 and 4 for various frequencies, distributions of slots and test distances. To ensure a safe estimation of the worst shielding performance, a value of 4 is suggested as the estimate of $E.F._{95th}$.

Considering the $E.F._{95th}$ of a practical enclosure is generally less than 4, the difference between the worst shielding performance defined by $ASRP/E.F._{95th}$ and the

ASRP is not significant. Thus, the shielding performance of an equipment enclosure may be described only by the *ASRP*, being more convenient. The small $E.F._{95th}$ values also mean the directive characteristics of an electrically large equipment in its radiating near-field are not obvious.

The estimate of the $E.F._{95th}$ given in this thesis and the estimate of D_{max} given in [32] provide a complete profile of the ratio between the possible maximum power density to the average power density of an electrically large source from its radiating near-field to far-field.

It has also been shown in Section 5.3 that combining the total power measured in the reverberation chamber with the estimate of the $E.F._{95th}$, an accurate estimate of the p_{95th} of equipment in its radiating near-field can be derived from Equation (5.5). Our results indicate that the differences between the estimated p_{95th} and the measured p_{95th} are usually within ±5 dB.

7.2.5 Immunity Shielding Measurements in a Small Sized Reverberation Chamber

The second approach considered during our shielding measurements is to measure the immunity shielding of an equipment enclosure, i.e. the ability of the enclosure to protect the internal content against the external threat field. Thus, during the shielding measurement, both the equipment content and the enclosure containing this content should be illuminated with the external fields.

The proposed measure *SACS* is the ratio of the average absorption cross section of the equipment content over a certain frequency range as the enclosure is absent to that as the enclosure is present. The small sized reverberation chamber is chosen as the test environment due to two reasons described as follows:

- The shielding performance of an equipment enclosure with apertures depends on the polarization and incidence angle of the incident field. As the scenario of the EMI between equipments described in Chapter 3, the victim equipment should be located in the Fresnel diffraction region of the source equipment. Thus, the incident fields with various polarizations and incidence angles

should be presented during the shielding measurement, which may be imitated by the complex field structure inside the reverberation chamber.

- The quality factor Q of a reverberation chamber depends on its internal loss [22]. During the shielding measurement, as the contents or the enclosure is introduced inside the chamber, the Q or the internal field of the chamber will be decreased. The smaller chamber, the more sensitive the internal field is to the objects introduced inside.

This measure implies the incident fields with various incidence angles and polarizations and the field variation on the equipment contents have been accounted. Another advantage of this measure is during the measurement, no receive antenna is placed inside the enclosure. Thus, the shielding ability of an electrically large but physically small equipment enclosure can be measured easily without the considerations of the antenna movement inside the enclosure and the possible effect of the receive antenna on the shielding performance of the enclosure

The disadvantage of this measure is as the enclosure is present, the average absorption cross section of the equipment content is not easily tested in the reverberation chamber, especially as the enclosure with small apertures implicitly has a high shielding performance. So far the measurement technique proposed here is only applicable to enclosures with large apertures. Thus this measure is suggested prudently here due to its limited applications.

It has been shown in Section 6.5 that the shielding of an equipment enclosure depends on the equipment contents. For the same enclosure, a higher *SACS* is obtained as the internal content has larger loss. Similar conclusion has also been illustrated in [22], where the enclosure tested is a larger 1.75 m × 0.629 m × 0.514 m cavity with a circular aperture of radius 1.4 cm and the internal contents are several salt-water spheres of radius 6.6 cm. It has also been shown the *SACS* values are quite different from the corresponding *ASRP* values, implying the measurement of *SACS* is not the reciprocal of the measurement of *ASRP*.

7.3 General Conclusions and Future Work

It has been illustrated that to evaluate the shielding performance of equipment enclosures, the proposed measurement technique should account for the spatial variation of the fields inside and outside the enclosure and the presence of the equipment contents, being quite different from the measurement technique proposed in the current IEEE STD 299 for large screened enclosures. The field variation includes both magnitude variation and polarization variation. In fact, the field variation also may exist within a large screened enclosure and should be considered in the shielding measurement technique for large screened enclosures.

During the radiating shielding measurement, the spatial variation inside the enclosure is expressed here by different source positions on the RC. The fast spatial variation of the radiations of an equipment enclosure may be detected by an antenna scanning on an area encompassing the enclosure with a sufficient scan resolution in anechoic chambers or be averaged during the measurement in reverberation chambers. The definition *ASRP* proposed here implies that spatial variation of the radiated fields has been averaged. Such measure gives an indication of the overall radiating shielding of an equipment enclosure.

However, it has been shown the difference between the *ASRP* determined by the truncated cylindrical scan in the anechoic chamber and the corresponding one determined in reverberation chamber is still considerable, which may be more than 5 dB. The possible reason is the emission power above and below the EUT was missed during the truncated cylindrical scan. It is expected that a better agreement between the measurement results in these two environments may be obtained if a fully spherical scan is performed in the anechoic chamber. Considering the application of anechoic chambers is much wider than that of reverberation chambers, a quick and relatively accurate determination of the *ASRP* in anechoic chambers is also useful and necessary. Such requirement may be solved by a fully spherical scan with hybrid scan resolutions, i.e. a relative fine scan resolution on the area facing the equipment side with slots and a relative coarse scan resolution on the area facing the

equipment side with no slot. To realise such a method, further measurements and relevant statistical study on the measurement results are required.

The reverberation chamber, where the complex field structure may be used to mimic the incident fields with various polarizations and incidence angles, is also suggested as an ideal test environment to measure the immunity shielding of an equipment enclosure. The definition *SACS* proposed here implies that not only the incidence angles and polarizations of incident fields, but also the field variation on the contents have been averaged. Such measure gives an indication of the overall immunity shielding of an equipment enclosure. However, the maximum field strength inside the enclosure, which is the most likely origin of an EMI, is also important and should be studied. To get the maximum field or the field distribution inside an equipment enclosure, new measurement technique or the application of numerical modelling technique, such as TLM or FDTD, is required.

It has been shown the measurement technique proposed here for *SACS* is only applicable to equipment enclosures with large slots. In the future study, either a new measurement technique or the improvement of the accuracy of the current measurement facilities is required to expand the application of this measure. The measurement technique proposed in [22] may be also used to determine the immunity shielding of equipment enclosures. However, it is not easy to arrange both a stirrer and a measurement antenna inside a practical equipment enclosure, which volume is generally limited and occupied partially by equipment contents. So the feasibility of such measurement technique should be tested before its application.

Very recently, a frequency stirred reverberation chamber approach for SE measurement of enclosures was proposed by Holloway et al in [38], which indicates that the frequency stirring approach gives the same results as the mode stirring approach, but is more efficient than the latter due to avoiding the movement of the mode stirrer. However, to ensure the enclosure may be well stirred through frequency stirring, enough mode density inside the tested enclosure is required during the measurement. Thus, the measurement frequency range of the tested enclosure is limited, especially for enclosures with small dimensions. Only a large

enclosure with dimensions of 1.49 m × 1.16 m × 1.45 m was tested in [38]. To validate the frequency stirring approach, more enclosures with different dimensions should be tested and the measurement results from this approach should be compared with those from other approaches.

Appendix A

The Criterion of One Quarter Wavelength Scan Resolution

For an electrically large radiating structure, the diffraction pattern measured in its radiating near-field may exhibit fast spatial variation. It is expected that the minimal distance between the maximum field and the minimum field may be close to $\lambda/4$.

To illustrate the above assumption, a simple model is given in the following figure, which shows the paths of the emissions from the two ends of an EUT to the maximum point and the adjacent minimum point on the scan plane.

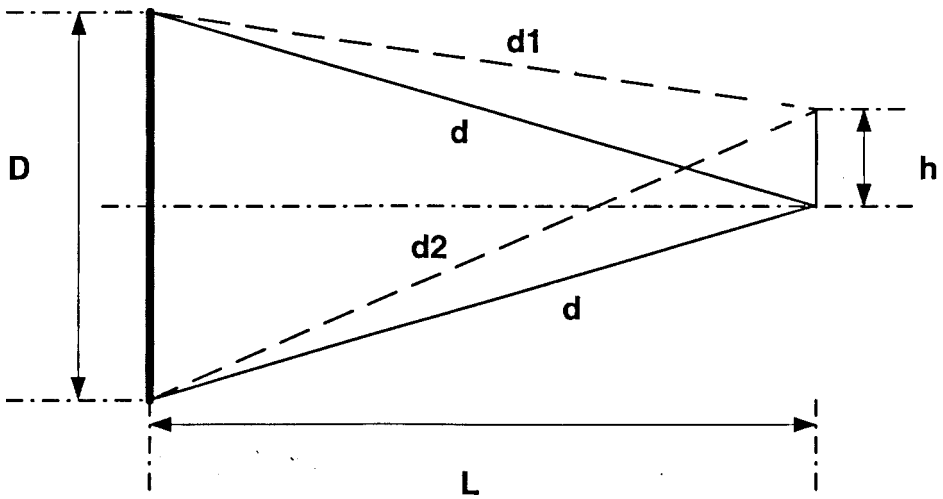

Fig. A.1. Paths geometry of the emissions from the two ends of an EUT to the maximum point and the adjacent minimum point.

In Fig. A.1, D is the maximum dimension of the EUT, L is the measurement distance. For the case where the emissions are in phase, the maximum field will be seen at the centre line. Assume the distance between the maximum point and the adjacent

minimum point is h. Then the phase difference between the two incident waves at the minimum point is equal to π:

$$\frac{2\pi}{\lambda}(d2-d1)=\pi. \quad \text{(A.1)}$$

That is,

$$d2-d1=\frac{\lambda}{2} \quad \text{(A.2)}$$

where

$$d2=\left[L^2+\left(\frac{D}{2}+h\right)^2\right]^{\frac{1}{2}} \quad \text{(A.3)}$$

and

$$d1=\left[L^2+\left(\frac{D}{2}-h\right)^2\right]^{\frac{1}{2}}. \quad \text{(A.4)}$$

Combining (A.2), (A.3) and (A.4), (A.5) is obtained

$$h^2=\frac{\lambda^2}{16}\times\left(1+\frac{L^2}{D^2-\frac{\lambda^2}{4}}\right). \quad \text{(A.5)}$$

Because $L\geq 0$,

$$h\geq\frac{\lambda}{4}. \quad \text{(A.6)}$$

It can be seen in (A.5) that h decreases as L decreases. To enable the detailed diffraction pattern to be tested or an accurate estimate of the maximum field, the scan resolution should be at least as small as h.

During the radiating near-field measurement, L is generally comparable with D, so h is relative small, which implies a fine scan resolution is required. For the extreme case L=0, h is equal to $\lambda/4$. Thus, a scan resolution of $\lambda/4$ is required.

Equation (A.5) can also been expressed as:

$$\frac{h}{\lambda}=\frac{1}{4}\times\left(1+\frac{\left(\frac{L}{\lambda}\right)^2}{\left(\frac{D}{\lambda}\right)^2-\frac{1}{4}}\right)^{1/2} \quad . \quad \text{(A.7)}$$

Obviously, h/λ is only determined by L/λ and D/λ. Several plots of h/λ against L/λ for various D/λ are given below in Fig. A.2.

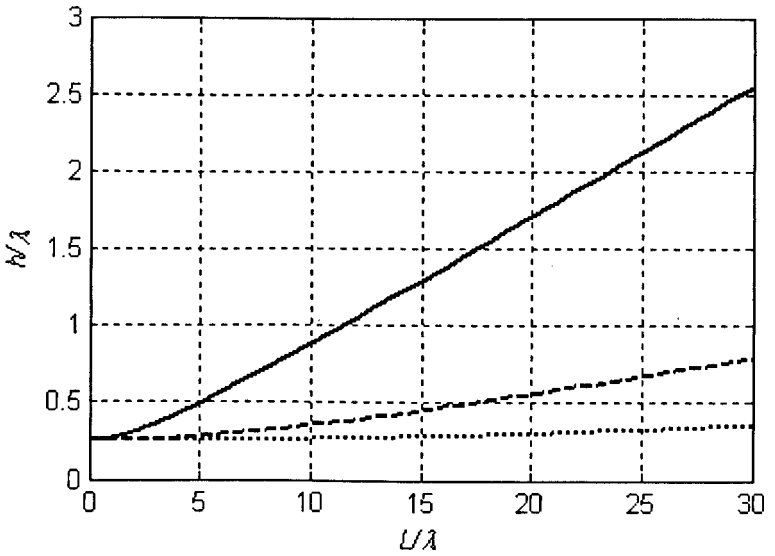

Fig. A.2. Plots of h/λ against L/λ for various D/λ. Solid line: D/λ=3; dashed line: D/λ=10; dotted line: D/λ=30.

The three plots shown in the above figure indicate that for a certain D/λ, the h/λ increases as the L/λ increases, or for a certain L/λ, the h/λ decreases as the D/λ increases. According to Equation (A.7) or the indication of the dotted line, when the D is comparable to or larger than L, the h/λ is close to 1/4 for various values of L/λ.

Appendix B

Radiation Patterns Measured in the Anechoic Chamber

In the following figures, all the radiation patterns measured in the anechoic chamber are presented. There are 6 subplots in each figure, corresponding to the measurement results of 6 different source positions respectively. The arrangement of the positions of the subplots in each figure is given as below.

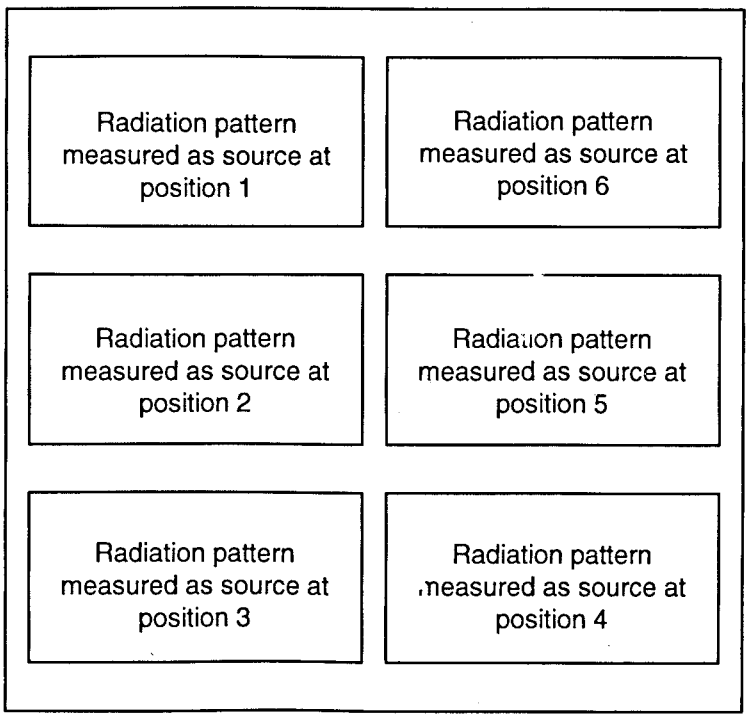

Fig. B.1. The relative positions of the subplots in each figure.

B.1 Radiation Patterns of the Dummy EUT with the Front Panel Shown in Fig. 2.1 (a)

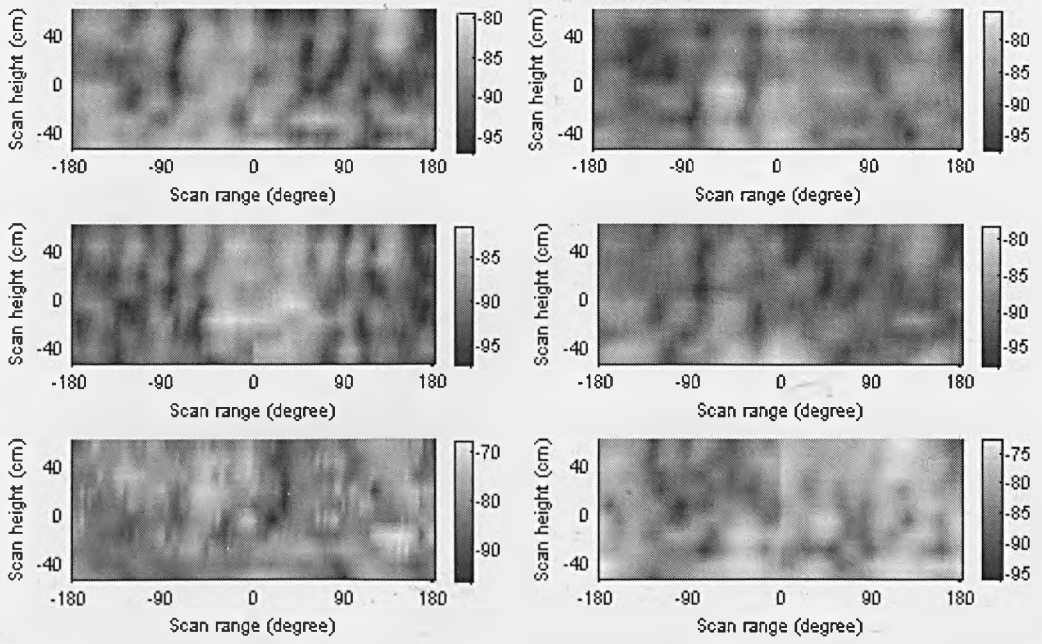

Fig. B.2. Radiation patterns of the dummy EUT with the front panel shown in Fig. 2.1(a). Frequency: 1 GHz.

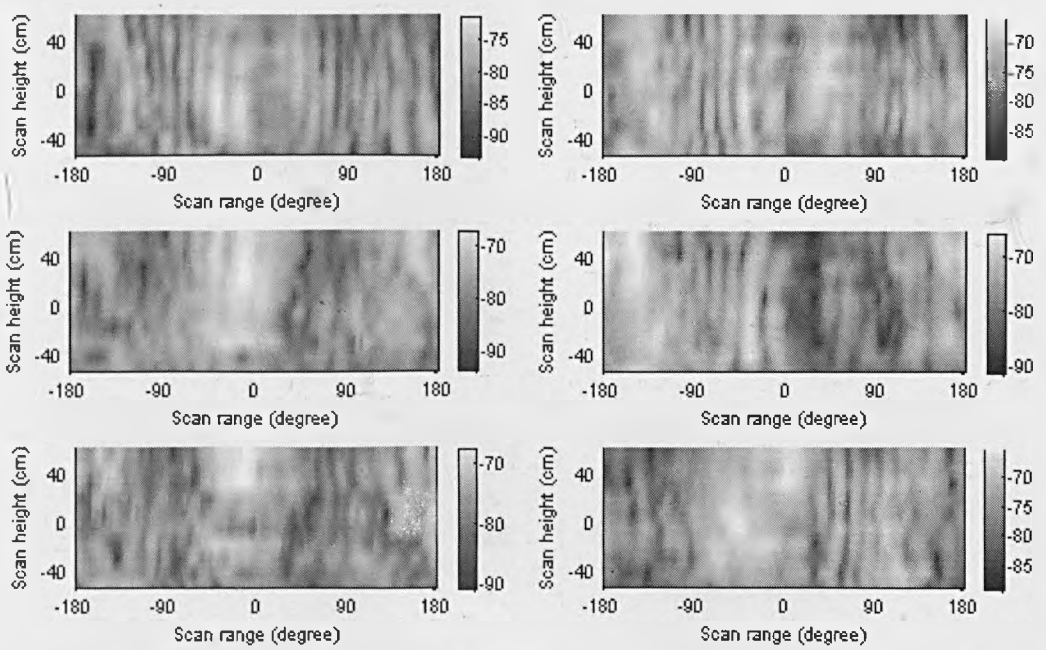

Fig. B.3. Radiation patterns of the dummy EUT with the front panel shown in Fig. 2.1(a). Frequency: 2 GHz.

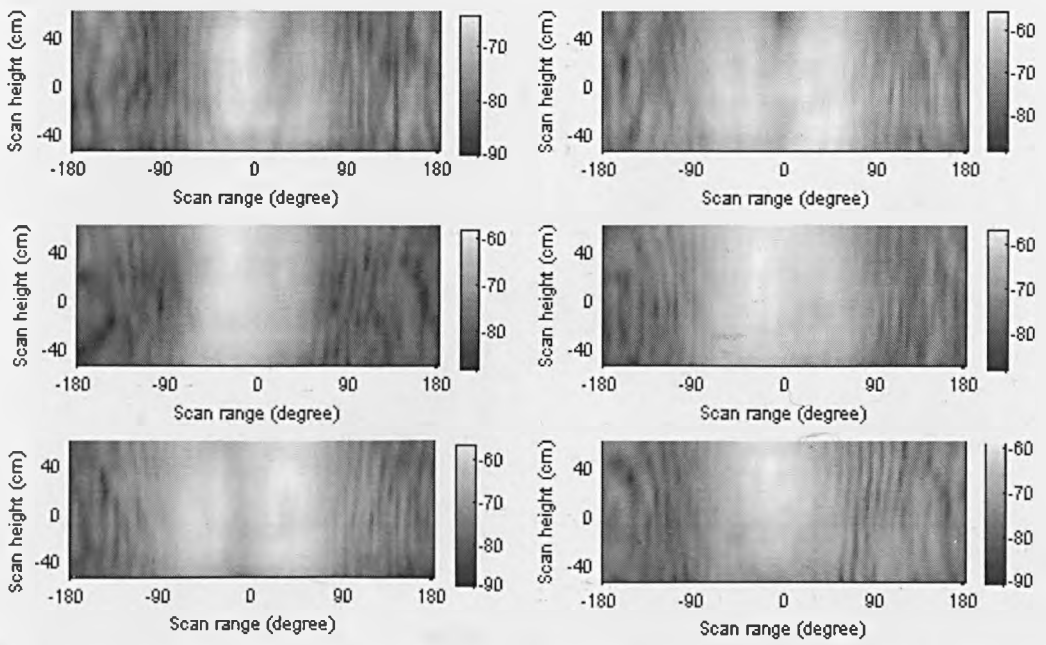

Fig. B.4. Radiation patterns of the dummy EUT with the front panel shown in Fig. 2.1(a). Frequency: 3 GHz.

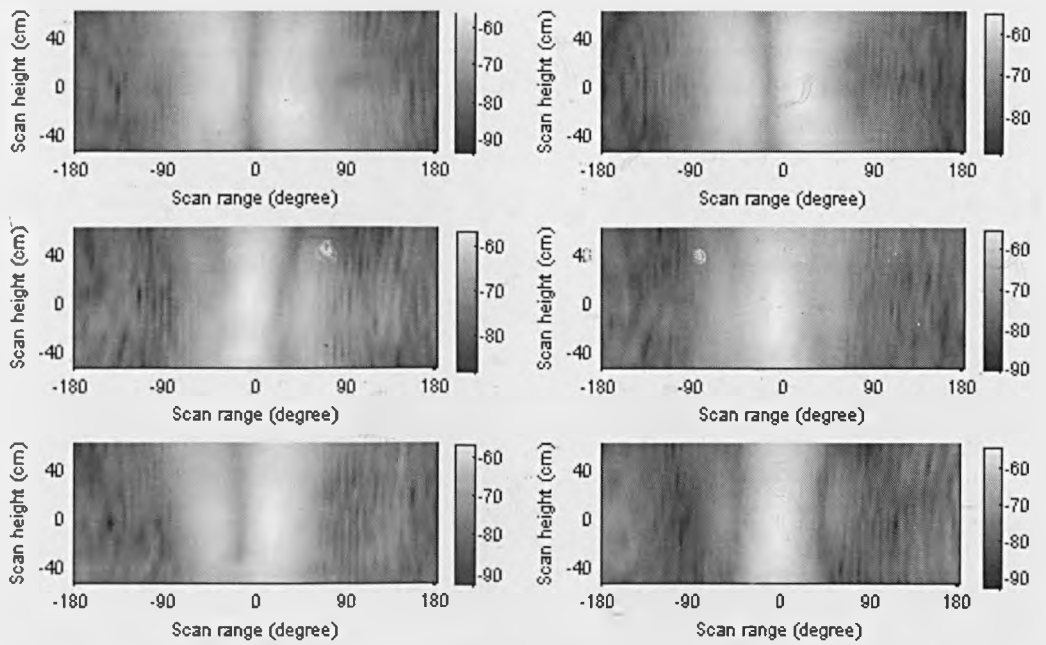

Fig. B.5. Radiation patterns of the dummy EUT with the front panel shown in Fig. 2.1(a). Frequency: 4 GHz.

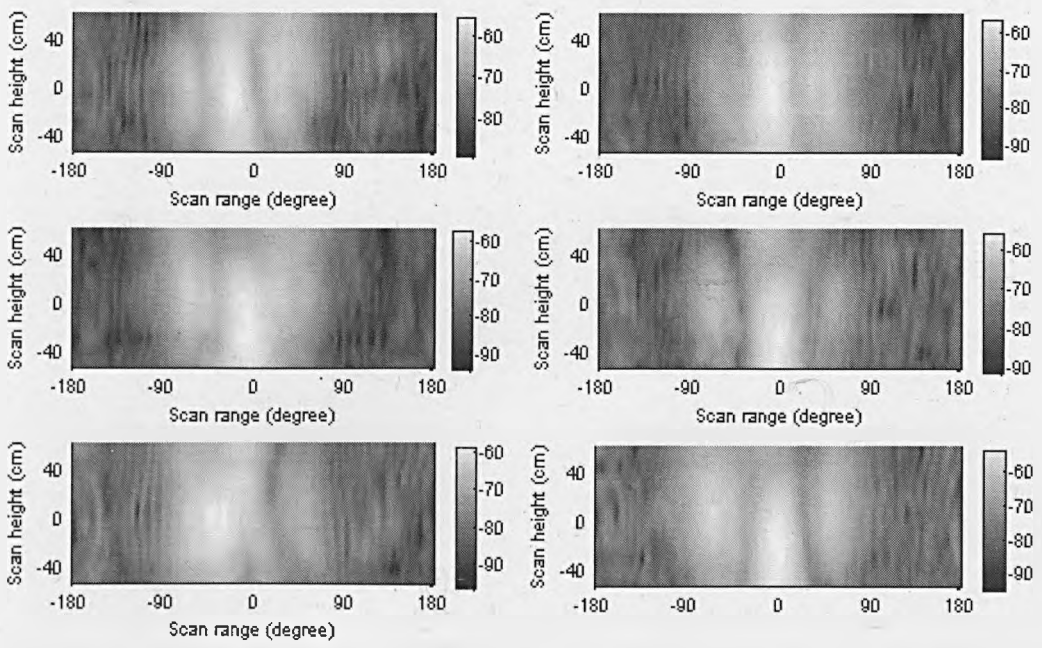

Fig. B.6. Radiation patterns of the dummy EUT with the front panel shown in Fig. 2.1(a). Frequency: 5 GHz.

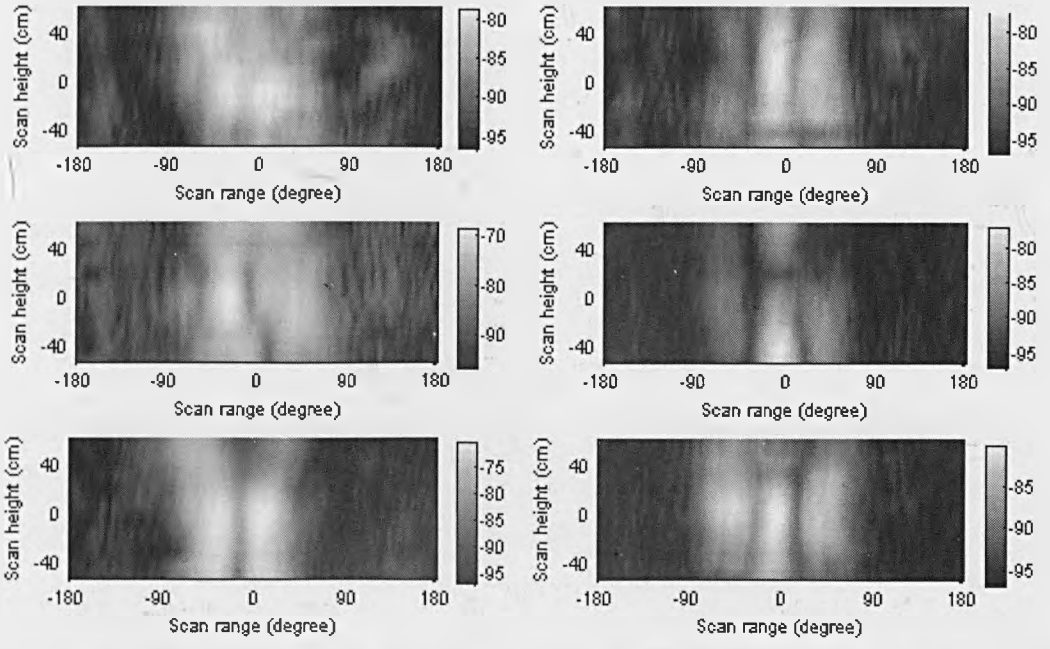

Fig. B.7. Radiation patterns of the dummy EUT with the front panel shown in Fig. 2.1(a). Frequency: 6 GHz.

B.2 Radiation Patterns of the Dummy EUT with the Front Panel Shown in Fig. 2.1 (b)

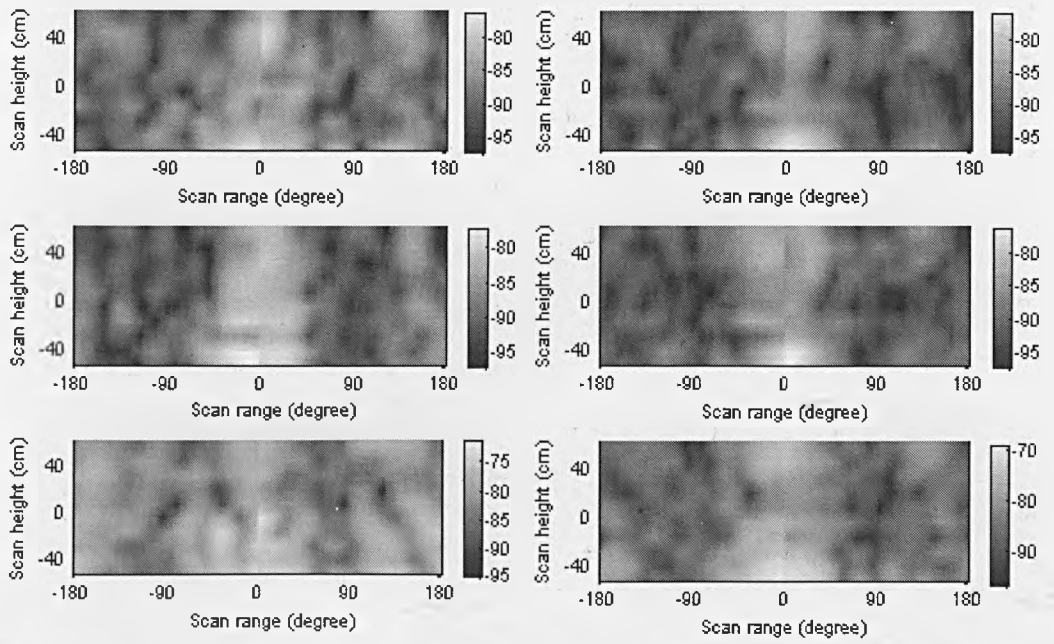

Fig. B.8. Radiation patterns of the dummy EUT with the front panel shown in Fig. 2.1(b). Frequency: 1 GHz.

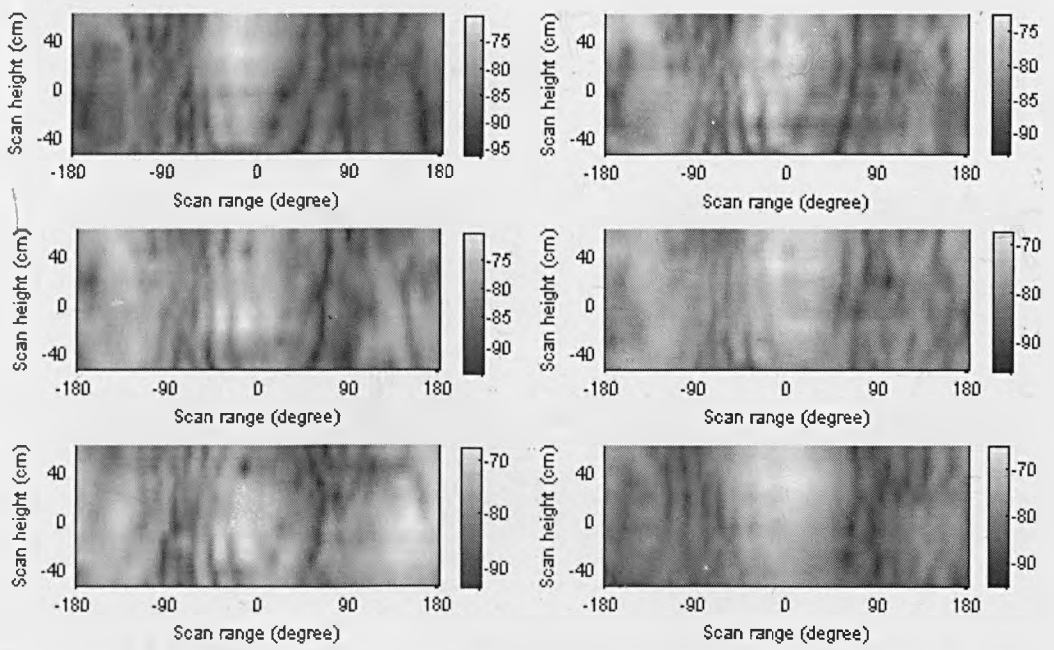

Fig. B.9. Radiation patterns of the dummy EUT with the front panel shown in Fig. 2.1(b). Frequency: 2 GHz.

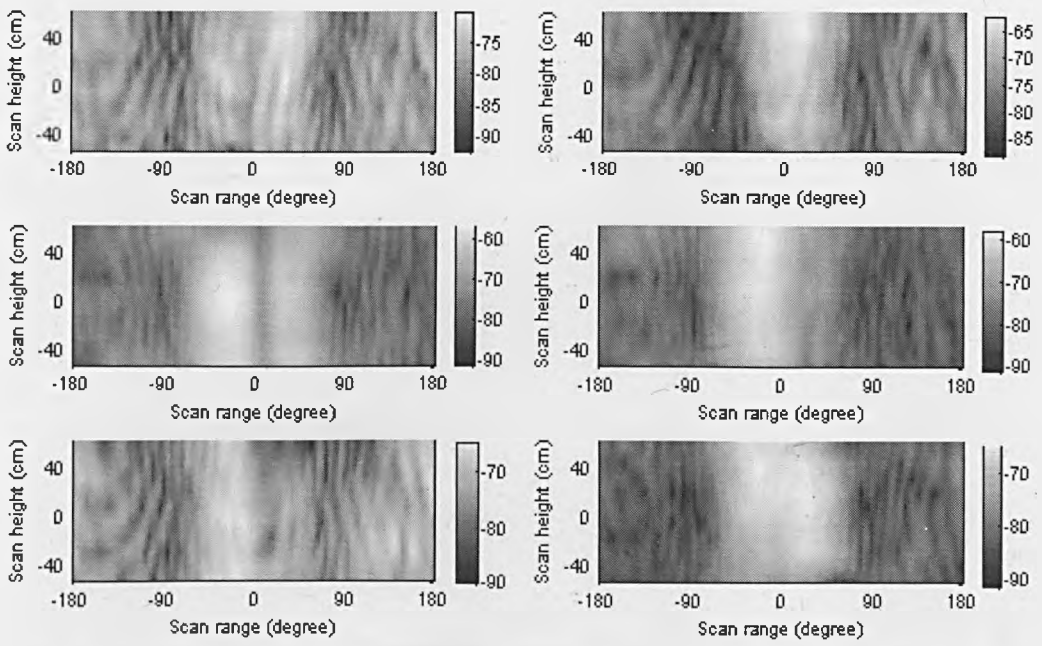

Fig. B.10. Radiation patterns of the dummy EUT with the front panel shown in Fig. 2.1(b).

Frequency: 3 GHz.

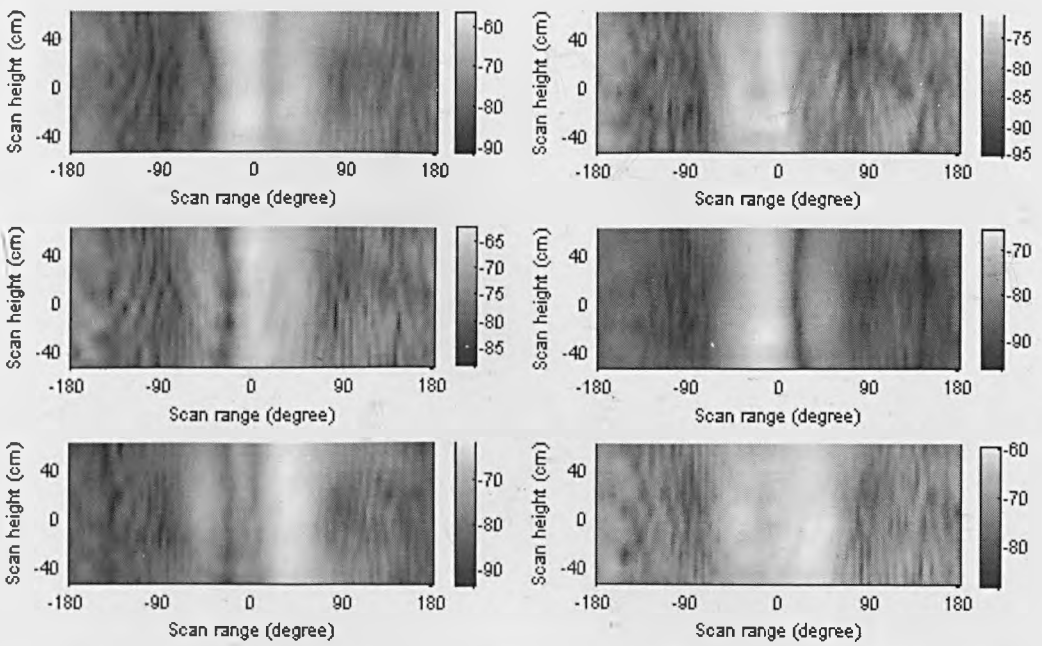

Fig. B.11. Radiation patterns of the dummy EUT with the front panel shown in Fig. 2.1(b).

Frequency: 4 GHz.

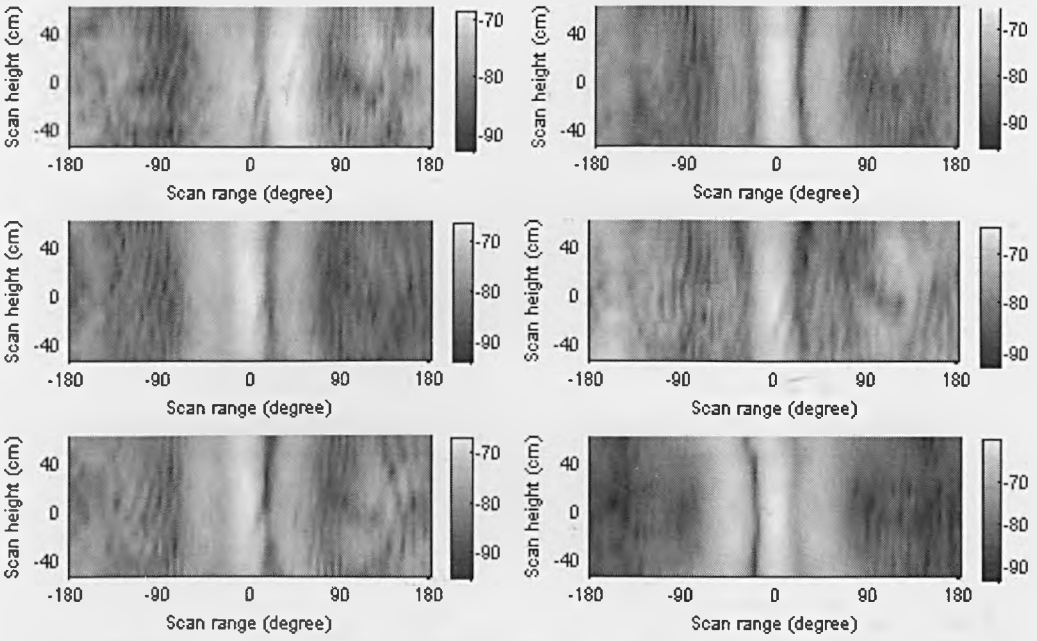

Fig. B.12. Radiation patterns of the dummy EUT with the front panel shown in Fig. 2.1(b). Frequency: 5 GHz.

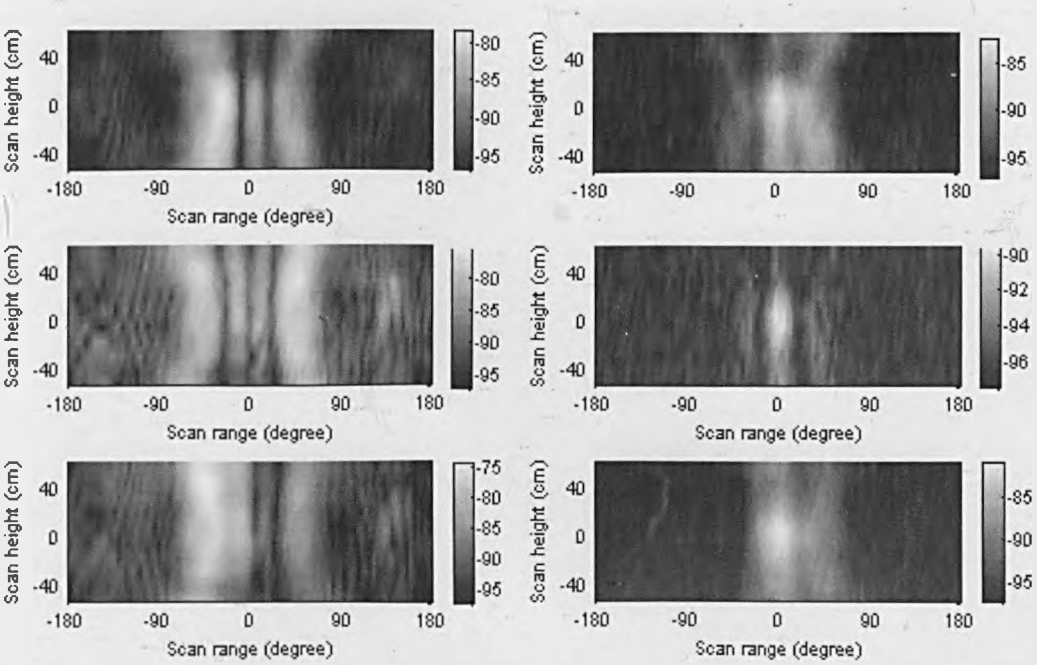

Fig. B.13. Radiation patterns of the dummy EUT with the front panel shown in Fig. 2.1(b). Frequency: 6 GHz.

B.3 Radiation Patterns of the Dummy EUT with the Front Panel Shown in Fig. 2.1 (c)

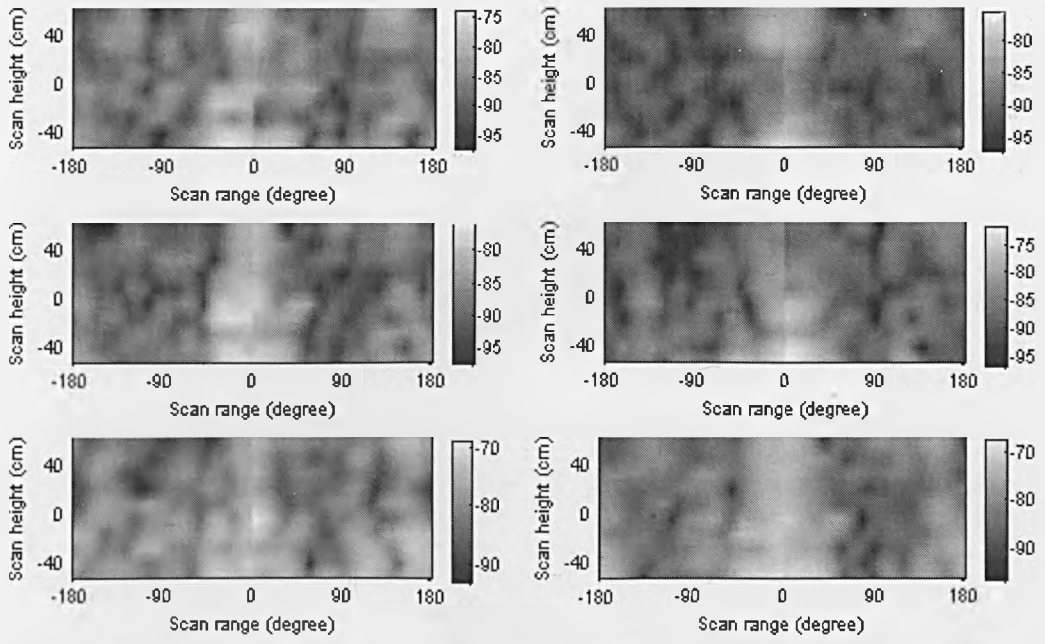

Fig. B.14. Radiation patterns of the dummy EUT with the front panel shown in Fig. 2.1(c). Frequency: 1 GHz.

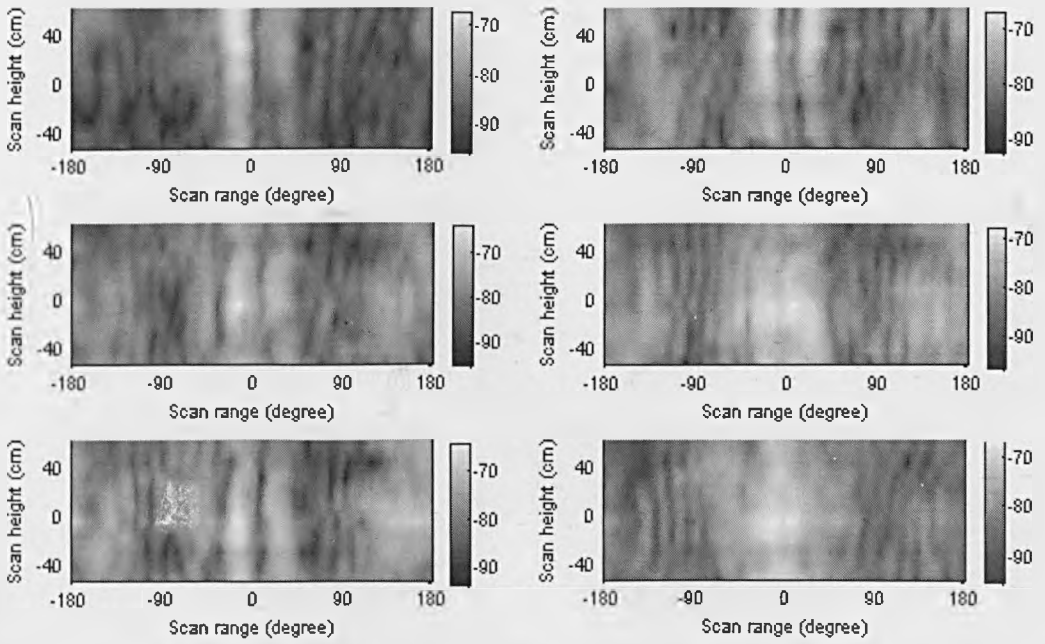

Fig. B.15. Radiation patterns of the dummy EUT with the front panel shown in Fig. 2.1(c). Frequency: 2 GHz.

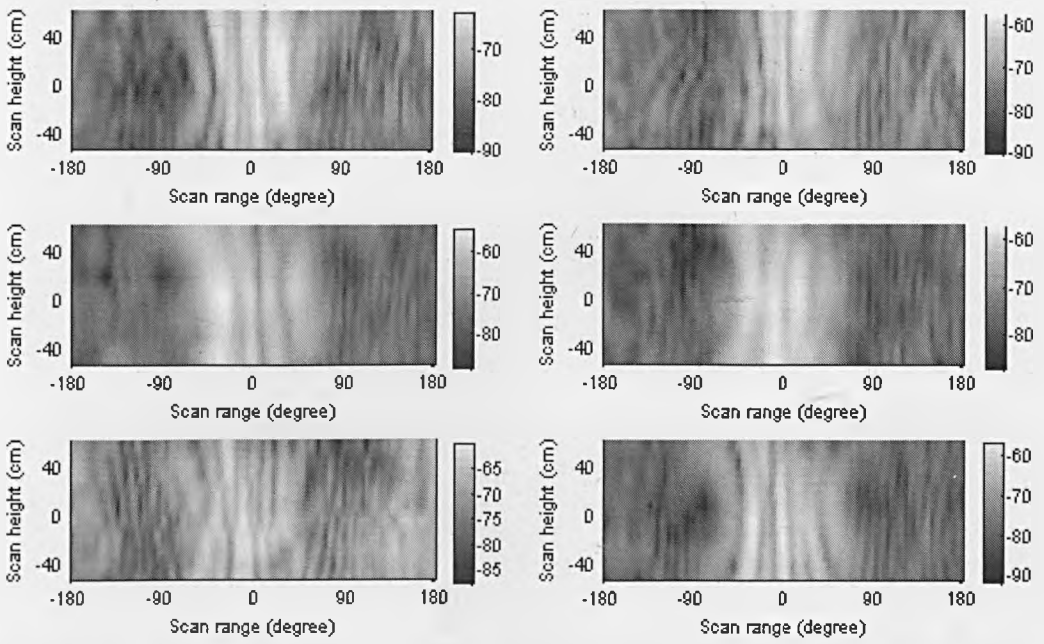

Fig. B.16. Radiation patterns of the dummy EUT with the front panel shown in Fig. 2.1(c). Frequency: 3 GHz.

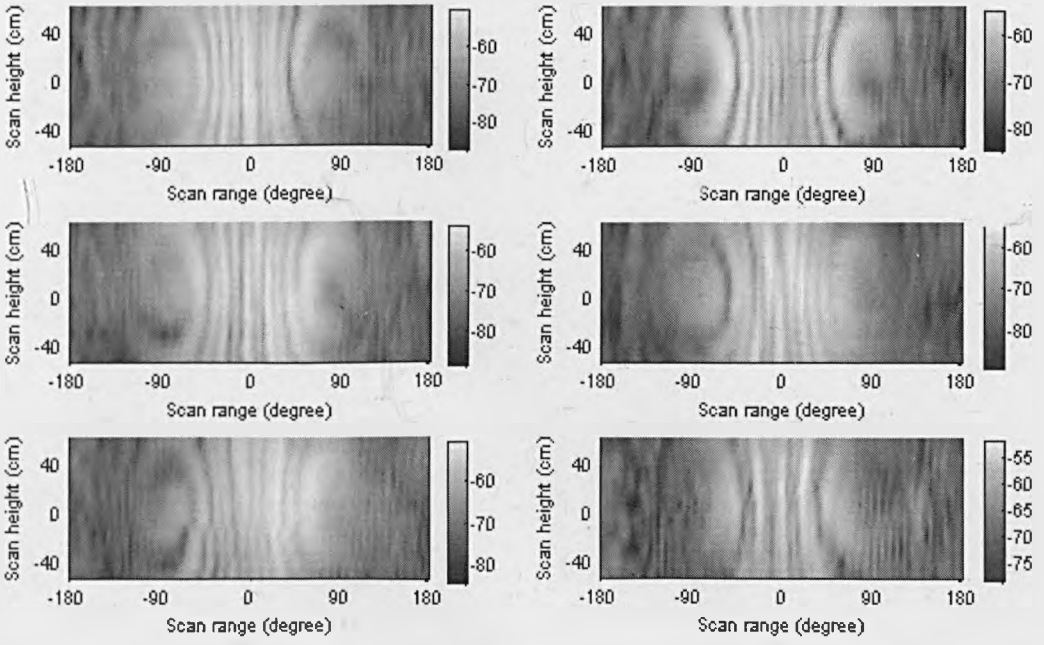

Fig. B.17. Radiation patterns of the dummy EUT with the front panel shown in Fig. 2.1(c). Frequency: 4 GHz.

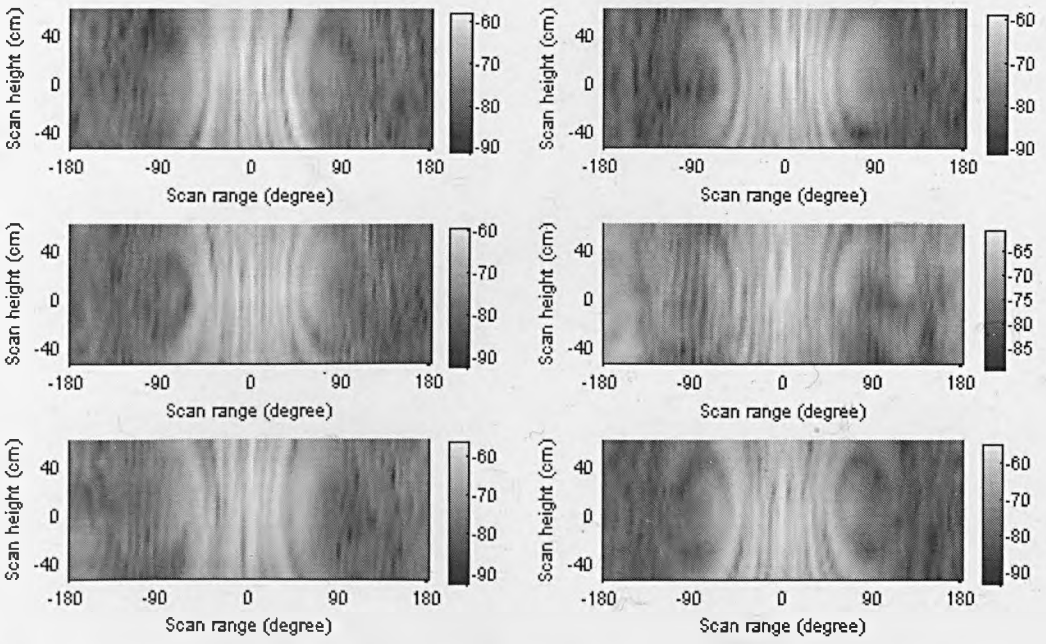

Fig. B.18. Radiation patterns of the dummy EUT with the front panel shown in Fig. 2.1(c). Frequency: 5 GHz.

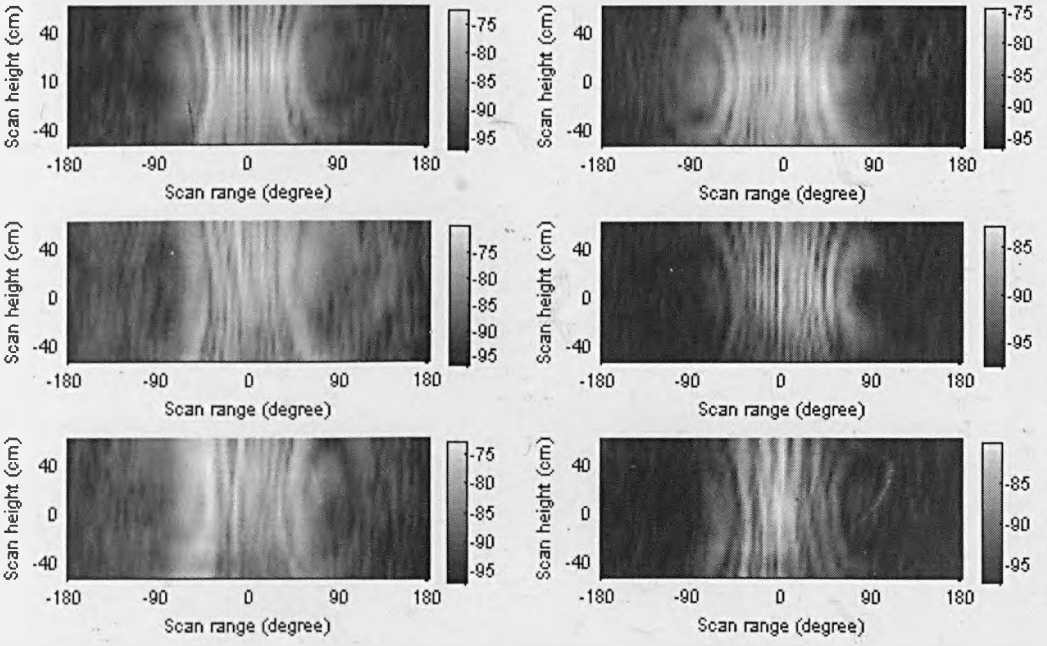

Fig. B.19. Radiation patterns of the dummy EUT with the front panel shown in Fig. 2.1(c). Frequency: 6 GHz.

B.4 Radiation Patterns of the RC

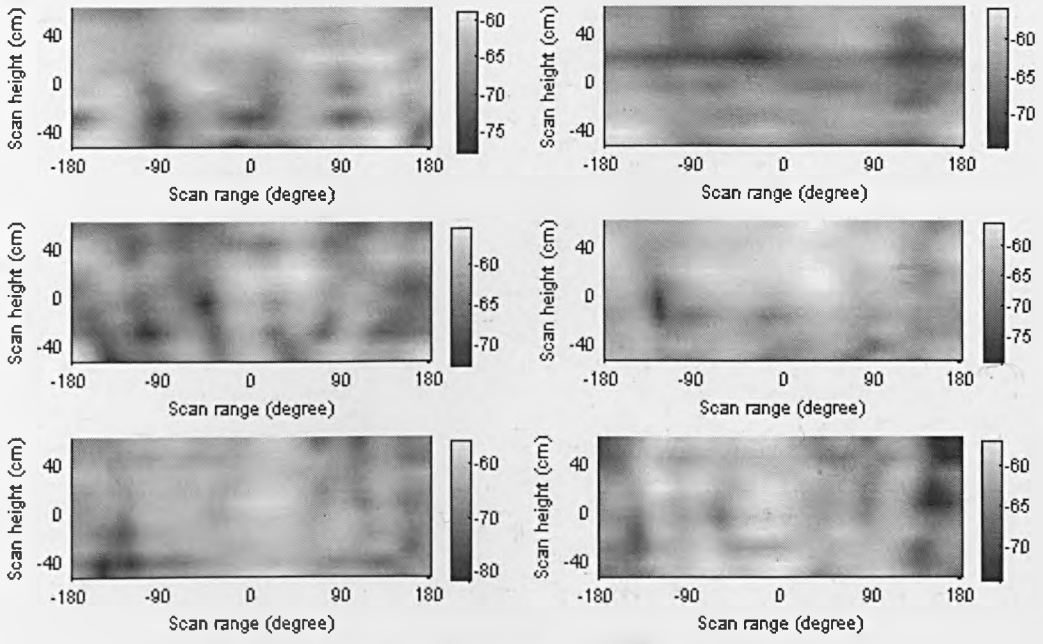

Fig. B.20. Radiation patterns of the RC. Frequency: 1 GHz.

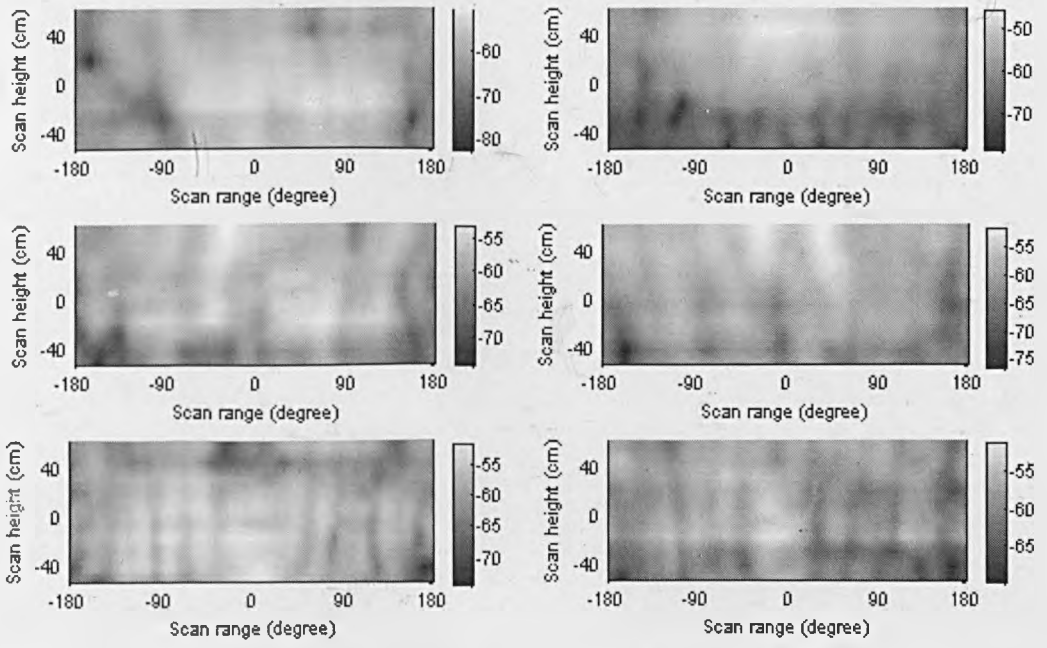

Fig. B.21. Radiation patterns of the RC. Frequency: 2 GHz.

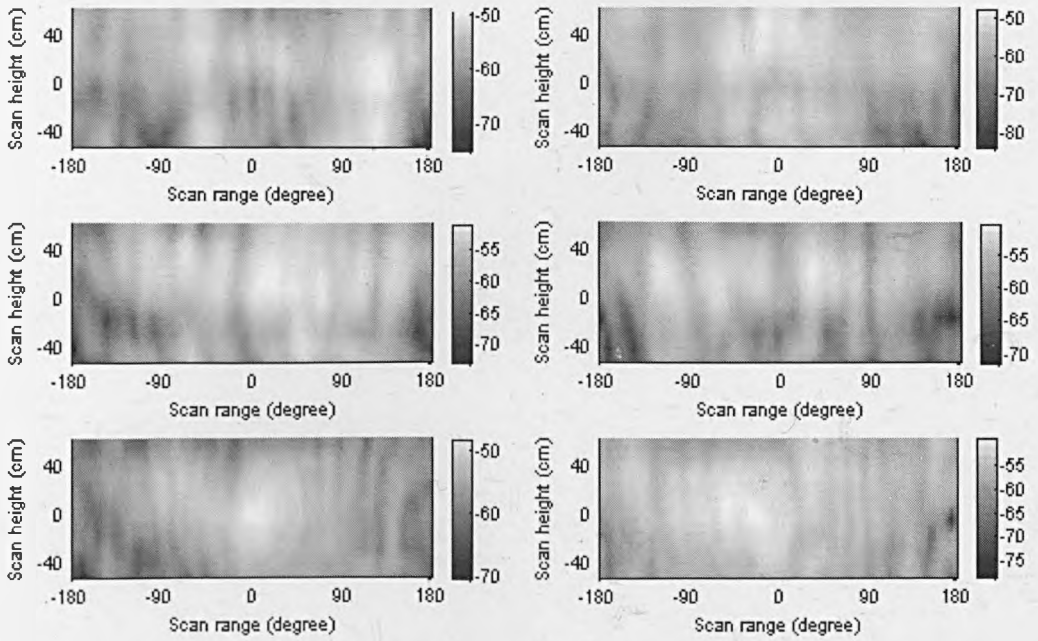

Fig. B.22. Radiation patterns of the RC. Frequency: 3 GHz.

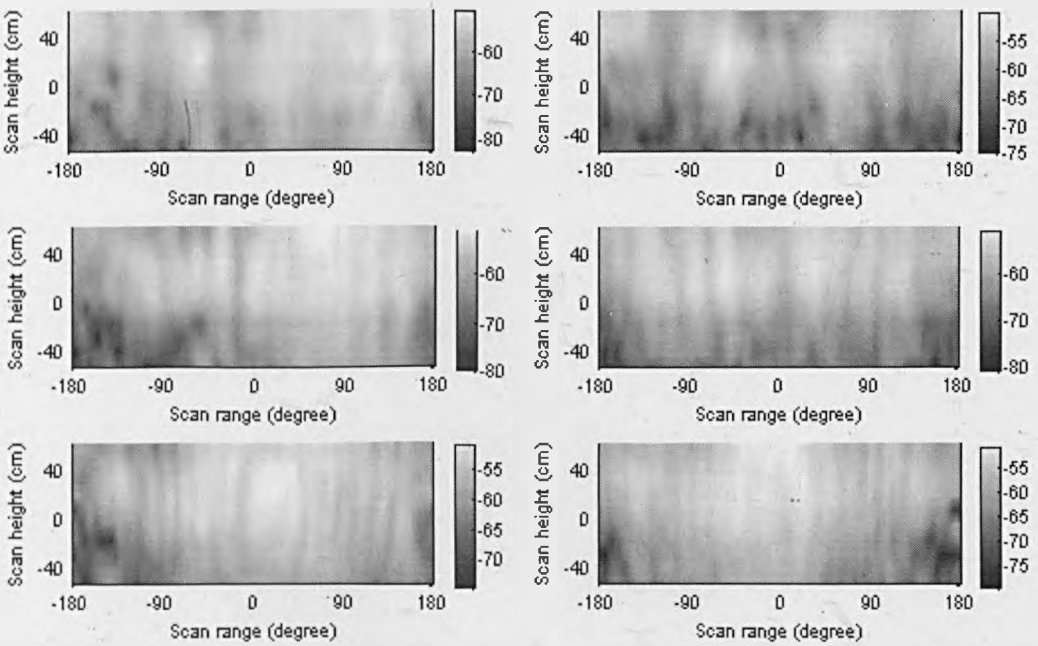

Fig. B.23. Radiation patterns of the RC. Frequency: 4 GHz.

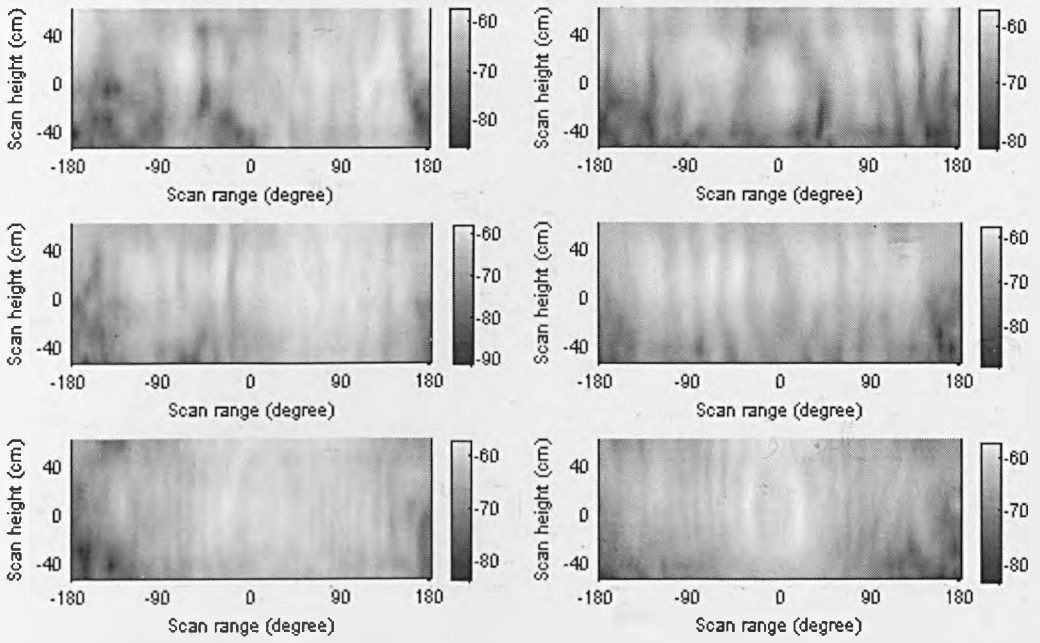

Fig. B.24. Radiation patterns of the RC. Frequency: 5 GHz.

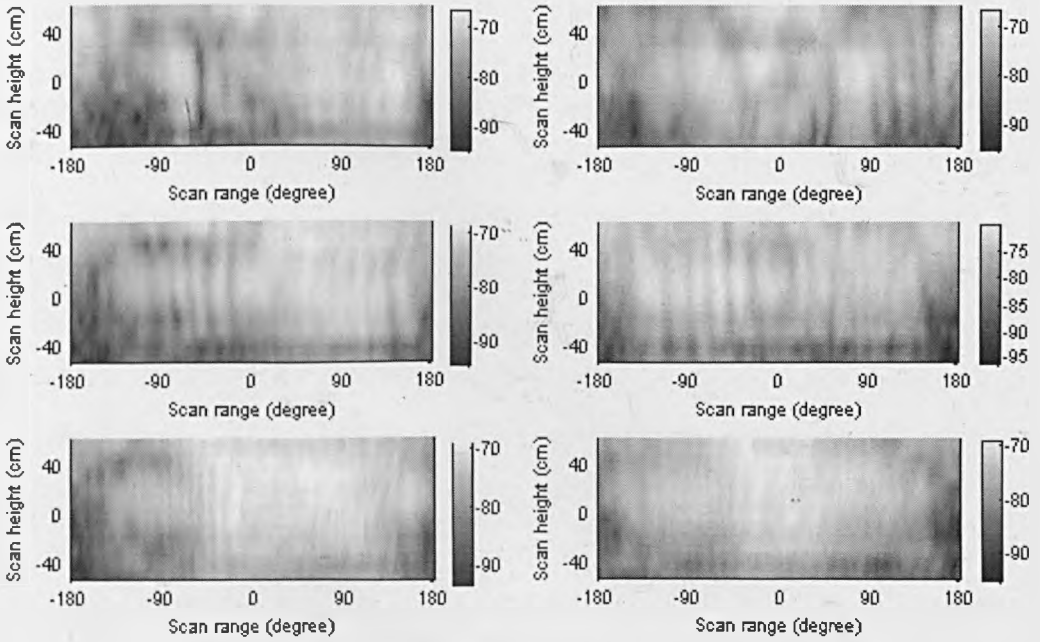

Fig. B.25. Radiation patterns of the RC. Frequency: 6 GHz.

Appendix C

A New Method for Determining the Maximum Emission of Equipment at Frequencies above 1 GHz in Anechoic Chambers

C.1 Introduction

In 2005, a measurement method for the emission measurement at frequencies above 1 GHz was proposed for inclusion in CISPR publication 16-2-3 [31], where the fully anechoic chamber (FAC) is the assumed test environment. According to this method, if the EUT is encompassed by the 3 dB beam width of the measuring antenna, only one azimuth scan around the EUT is required. This method assumes the polarization of the emissions is known and so may be aligned with that of the measurement antenna.

A typical equipment is electrically large at frequencies above 1 GHz and has many apertures on its enclosure for ventilation, display and disk insertion. These apertures act as a randomized array of slot antennas. It has been illustrated in Chapter 3 that due to the interferences of the radiations of the slots, the radiations from the enclosure may express fast spatial variation and have various polarizations. However, an antenna in the receiving mode is expected to not respond to the fields outside of its effective area and the field components vertical to its polarization. Thus, in order to test the maximum emission accurately, no matter whether the beam width of the receive antenna is larger than the EUT, it is necessary to perform the measurement by scanning the receive antenna on an area encompassing the EUT with enough scan resolution and two orthogonal polarizations of the measurement antenna at each test

point are required. The magnitude of the electric field at each test point may be estimated by Equation (3.5) and the scan resolution may be determined by Equation (A.5), which gives the possible minimum distance between a constructive interference and an instructive interference. Consequently, the maximum emission should be determined by the maximum one of all the field magnitudes from every test point. The measurement technique originally proposed in Chapter 3 for the radiations of an equipment enclosure is instinctively used here to determine its maximum radiation. Such measurement technique requires a number of measurements, being time consuming and so unwanted. However, promising results have been obtained here by statistic analyses on the maximum emissions derived from reduced test points, indicating a modest number of measurements may ensure an accurate estimate of the maximum emission of an equipment.

The contents of this appendix are organized as follows. In Section C.2 the deficiencies of one azimuth scan and a single polarization of the measurement antenna are illustrated respectively by the measurement results presented. Then in Section C.3 the measurement technique for radiations proposed in Chapter 3 is suggested to determine the maximum radiation. To achieve data reduction, the possible measurement results from reduced scan resolutions are simulated and statistic analyses on the maximum emissions derived from the reduced scan resolutions are performed, indicating dozens of test points spread evenly on a cylindrical surface centred an EUT may enable a relative accurate estimation of the maximum radiation of this EUT. Conclusions are given in Section C.4.

C.2 Deficiencies of the Measurement Method Proposed by CISPR 16-2-3

To illustrate the deficiency of the measurements performed by one azimuth scan, examples of the radiation patterns measured by an antenna with a fixed polarization on two azimuth cuts are given in Fig. C.1. For convenience, the measurement set-up is same as that given in Chapter3 and the EUT is the dummy EUT used for the shielding measurement. So the measurement results presented here are actually part

of those obtained during the radiating shielding measurements in the anechoic chamber.

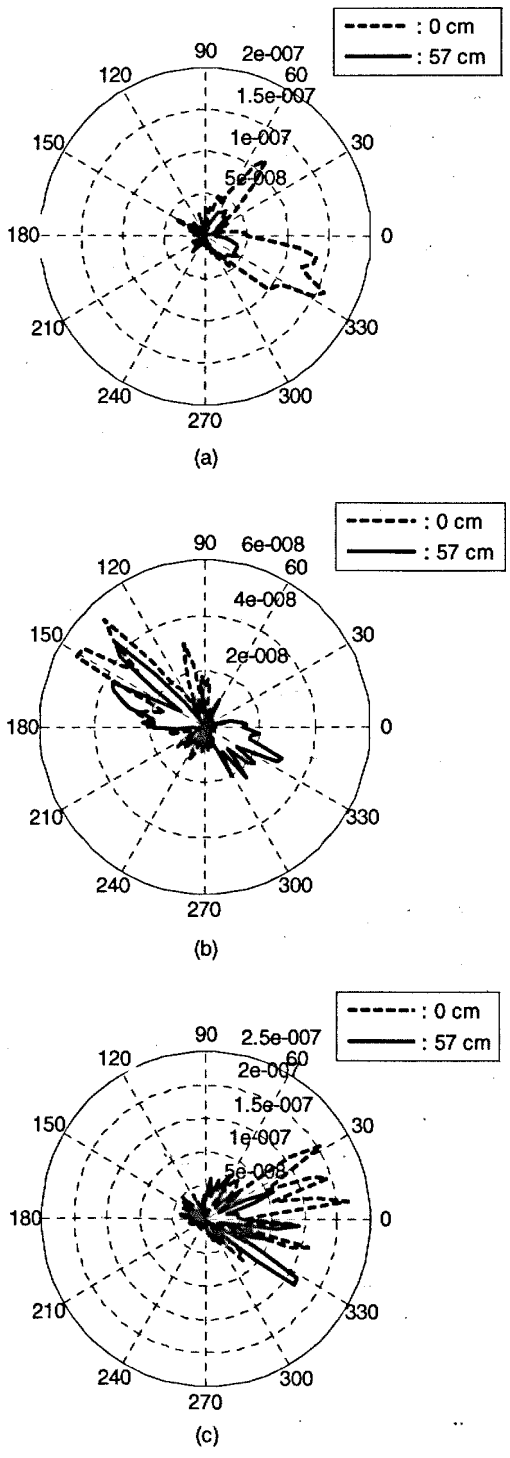

Fig. C.1 Azimuth patterns measured at two scan heights 0 cm (dashed line) and 57 cm (solid line). Configuration of the slots in the front panel: (a) two rectangular slots, (b) one CD slot and (c) one CD slot and sixteen short slots. Frequency: 3GHz. Polarization of the measurement antenna: horizontal.

It can be seen in Fig. C1 the radiation patterns measured at different heights of the azimuth cut are quite different, and so are the maximum fields. For example, the difference between the maximum fields at the two azimuth patterns shown in Fig. C.1(b) is 5.4 dB. Obviously, one azimuth scan cannot ensure an accurate estimation of the maximum radiation and thus additional azimuth scans are required. Considering the interference characteristics of the radiations of an equipment, to ensure the maximum radiation can be captured by the measurement antenna, both the scan step at each azimuth cut and the height difference between two closest azimuth cuts should be determined by Equation (A.5).

Moreover, because of the interferences of the radiations, the polarizations of the radiated fields at different test points are various and unpredictable. This means even if the measurement antenna can meet the maximum emission, one fixed orientation of the measurement antenna cannot ensure the magnitude of the emission is estimated. Thus, it has been suggested in Chapter 3 that at each test point, the measurement antenna should be oriented vertically and horizontally, and the magnitude of the electric field may be estimated by Equation (3.5). To illustrate the deficiency of the measurements performed by the measurement antenna with one fixed polarization, examples of $E_{max,\theta}$, $E_{max,h}$ and E_{max} of the dummy EUT with different configurations of slots are plotted in Fig. C.2. Here $E_{max,\theta}$ is the maximum electric field derived from the radiation pattern measured by an antenna horizontally polarized, $E_{max,h}$ is the maximum electric field derived from the radiation pattern measured by the antenna vertically polarized and E_{max} is the maximum one of the field strength estimated by Equation (3.5) from every test point. The radiation patterns analyzed here are those obtained during the shielding measurement in the anechoic chamber.

It can be seen in Fig. C.2 that $E_{max,\theta}$ is usually different from $E_{max,h}$, and both of them are less than the E_{max}. Either the difference between $E_{max,\theta}$ and E_{max} or the difference between $E_{max,h}$ and E_{max} may be more than 5 dB, indicating one fixed polarization of the measurement antenna is not sufficient to determine the maximum emission of an equipment enclosure.

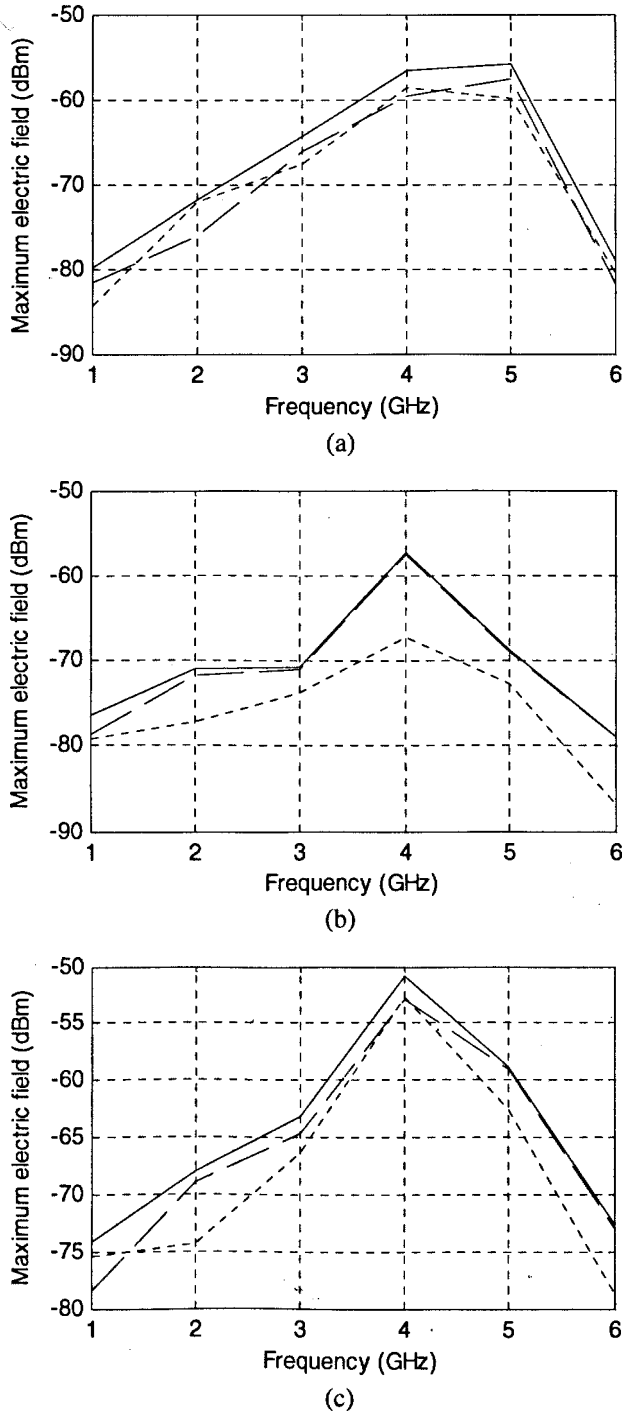

Fig. C.2 Comparisons of $E_{max,\theta}$ (dotted line), $E_{max,h}$ (dashed line) and E_{max} (solid line). Configuration of the slots in the front panel: (a) two rectangular slots, (b) one CD slot and (c) one CD slot and sixteen short slots.Frequency: 3 GHz. Source position: 1.

The agreement between $E_{max,h}$ and E_{max} shown in Fig. C.2(b) indicates if there is only one slot on the enclosure which acts as a dipole according to the Babinet's principle [26], the polarizations of the emissions from this slot are perpendicular to the slot.

So the maximum radiation may be determined by the antenna with one fixed polarization perpendicular to the slot. However, this is not a common case because a typical equipment enclosure generally has a number of slots with various orientations.

C.3 Data Reduction

As discussed above, to obtain an accurate estimate of the maximum radiation of equipment, one azimuth scan of the measurement antenna with a fixed polarization is not enough and the measurement technique propose in Chapter 3 for radiations should be employed. However the measurements required by such measurement technique are time consuming and so unwanted. It is expected here that lager scan resolution will not significantly affect the measurement accuracy of the maximum emission. The measurement effort may be saved if the effect of the scan resolution on the uncertainty of the maximum emission can be quantified.

To simulate the measurement results with reduced scan resolution, the original measurement data matrix is reduced in size step by step. In detail, at the 'N'th reduction pass, in every N+1 successive columns of the original measurement date matrix, only one column is remained and the remained columns should have the same spacing. Such reduction is also applied to the rows of the original measurement data matrix. Thus, $(N+1)^2$ reduced data matrices can be obtained. Each of these reduced data matrices, including $1/(N+1)^2$ of the original test points, is the possible measurement result from the scan resolution equal to $1/N+1$ of the original one.

Consider one measured radiation pattern of the dummy EUT, i.e. an original measurement data matrix consists of 40 rows and 200 columns. Fig. C.3(a) gives all the possible differences between the E_{max} of the original data matrix and that of the reduced data matrix, and Fig. C.3(b) gives all the possible differences between the 95th percentile field E_{95th} of the original data matrix and that of the reduced data matrix. At each reduced scan resolution, the maximum one of the absolute differences may be expressed as a measurement of uncertainty. It can be seen in Fig. C.3 as the scan resolution, i.e. the number of sampling points decreases, the

uncertainty increases. Comparisons between Fig. C.3(a) and Fig. C.3(b) indicate that for a given scan resolution, the uncertainty of the E_{95th} is always less than that of the E_{max}. The reason has been illustrated in Chapter 4. The results shown in Fig. C.3 also indicate that even when there are only 80 test points spread evenly on the original cylindrical surface, i.e., the reduced data matrix consists of 4 rows and 20 columns, the derived E_{max} values remain within –4 dB of the E_{max} of the original data matrix and the derived E_{95th} values remain within $\pm$3 dB of the E_{95th} of the original data matrix.

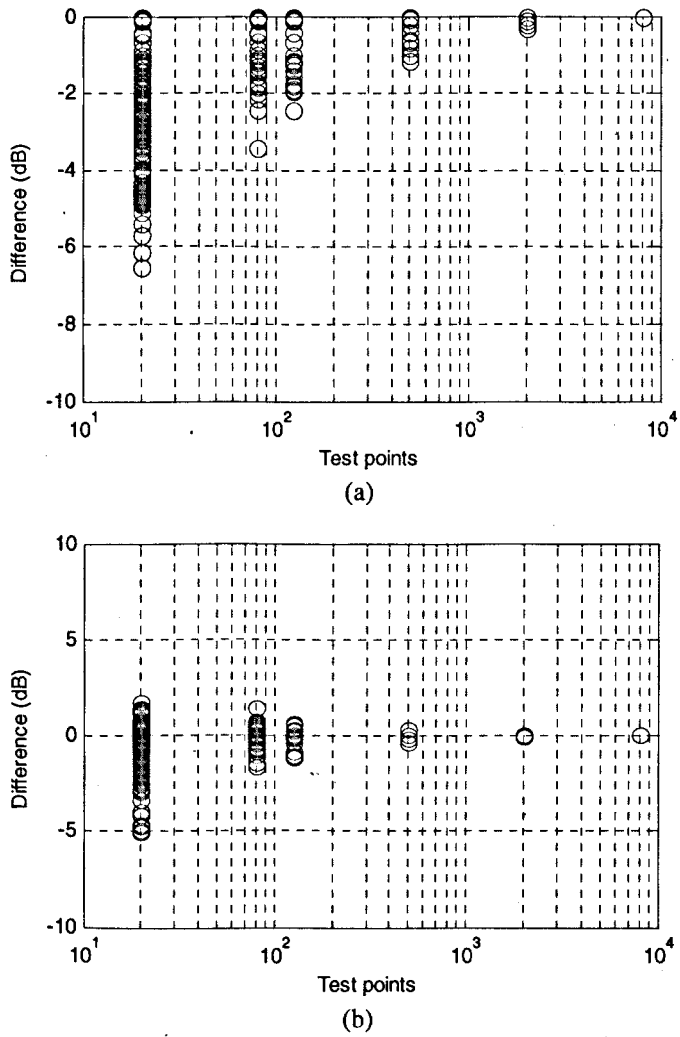

Fig. C.3(a) All the possible differences between the E_{max} of the original data matrix and that of the reduced data matrix versus the number of test points; (b) all the possible differences between the E_{95th} of the original data matrix and that of the reduced data matrix versus the number of test points. Configuration of the slots in the front panel: one CD slot and sixteen short slots. Frequency: 3GHz. Source position: 1.

It seems 4 × 20 test points on the cylindrical surface can ensure a relatively accurate estimate of the E_{max} of the dummy EUT. During our radiating shielding measurements, 108 radiation patterns of the dummy EUT were obtained. For each of these radiation patterns, all the possible reduced matrices with 4 × 20 sampling points were simulated and the uncertainty of the E_{max} was derived from these reduced data matrices. The obtained 108 uncertainties are given in Fig. C.4.

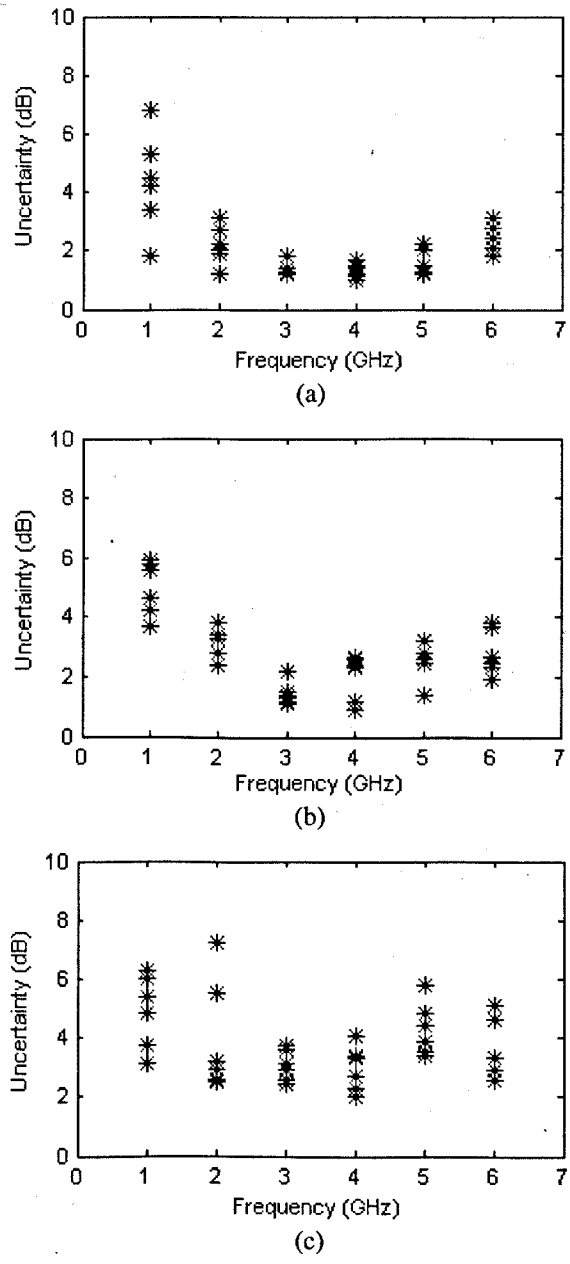

Fig. C.4 The uncertainty of the E_{max} results from the reduced data matrices with 4×20 test points. Configuration of the slots in the front panel: (a) two rectangular slots, (b) one CD slot and (c) one CD slot and sixteen short slots.

Similarly, the 108 uncertainties of the E_{95th} results from the reduced data matrices with 4×20 sampling points are plotted in Fig. C.5.

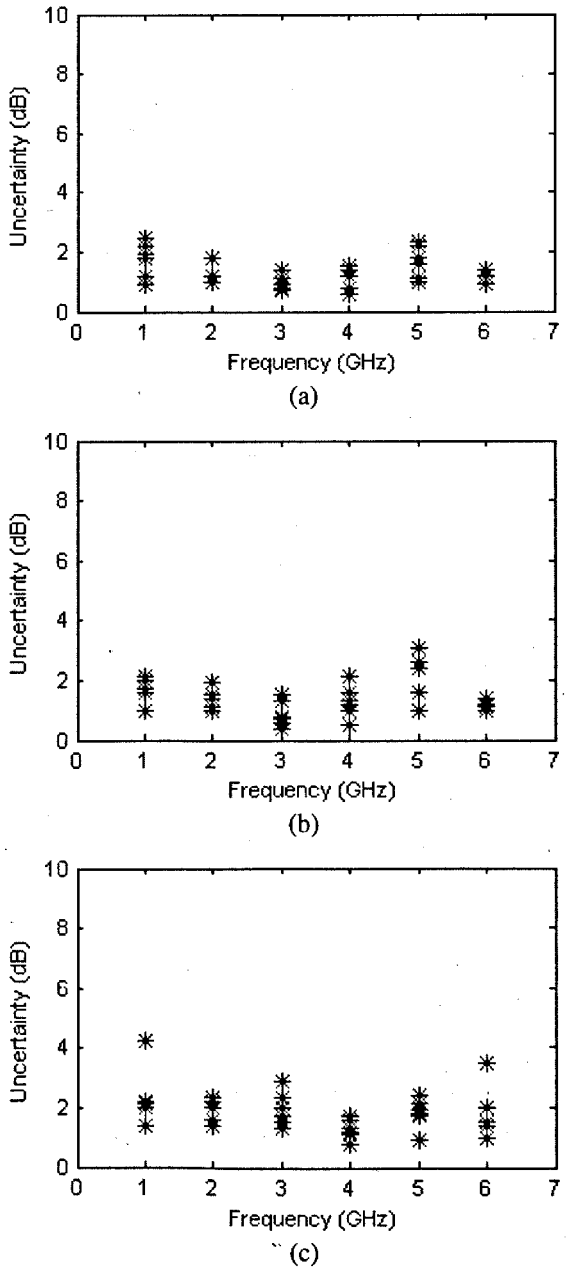

Fig. C.5 The uncertainty of the E_{95th} results from the reduced data matrices with 4 × 20 test points. Configuration of the slots in the front panel: (a) two rectangular slots, (b) one CD slot and (c) one CD slot and sixteen short slots.

In Fig. C.4, about 95% and 60% of the uncertainty values are respectively, less than 6 dB and 3 dB. However, in Fig. C.5, about 97% of the uncertainty values are less than 3 dB.

C.4 Discussion

At frequencies above 1 GHz, an equipment enclosure is generally electrically large. The magnitudes of its radiations express fast spatial variation and the polarizations of the radiations are various and unpredictable. These are mainly due to the interferences of the radiations from the slots with various orientations. It has been shown here that the measurement method for the maximum emission proposed in CISPR 12-2-3 is technically wrong because it does not consider the field variation on the elevation direction and the different polarizations of the emissions. Theoretically, to ensure an accurate estimate of the maximum radiation, an antenna scan on a surface encompassing the EUT with a sufficient scan resolution should be performed and at each test point two orthogonal polarizations of the measurement antenna are required. Such measurement is time consuming.

However, statistic results indicate effective estimates of the maximum radiated field can be obtained from a modest number of measurements made on a surface surrounding the EUT. It has been shown that at frequencies from 1 GHz to 6 GHz, measurements on a grid with 4 rows and 20 columns on a cylindrical surface with radius of 1 m centred by the EUT can ensure the uncertainty of the E_{max} less than 6 dB and the uncertainty of the E_{95th} less than 3 dB.

Appendix D

Photographs of Measurements

D.1 Determination of the RC

Fig. D.1. The 480 mm × 480 mm × 120 mm cavity used for determining the RC.

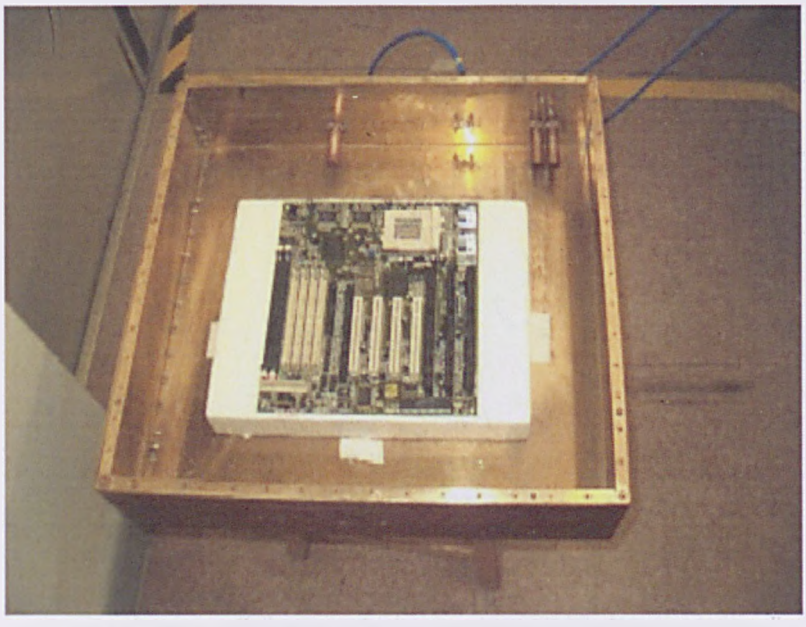

Fig. D.2. A 260 mm × 240 mm PC mainboard placed inside the cavity.

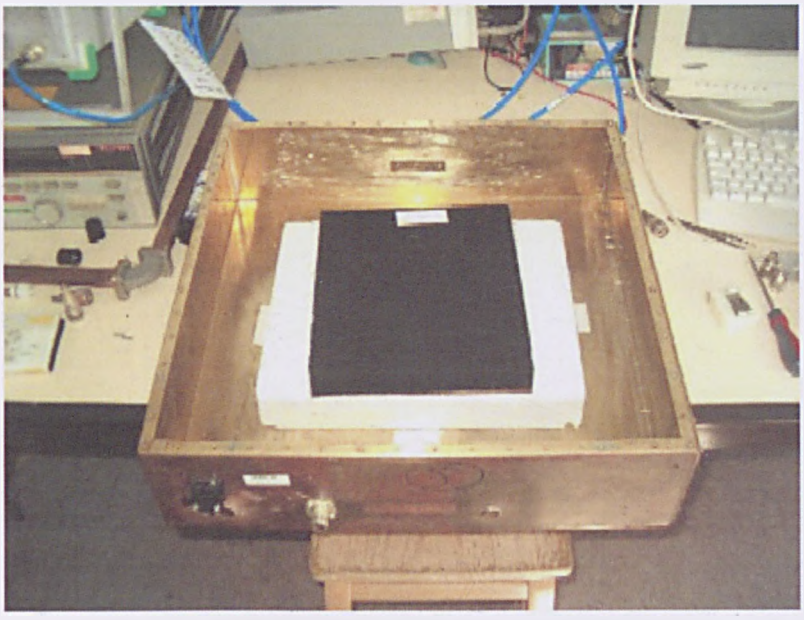

Fig. D.3. A 300 mm × 240 mm RC placed inside the cavity.

D.2 Radiating Shielding Measurements in the Medium Sized Anechoic Chamber

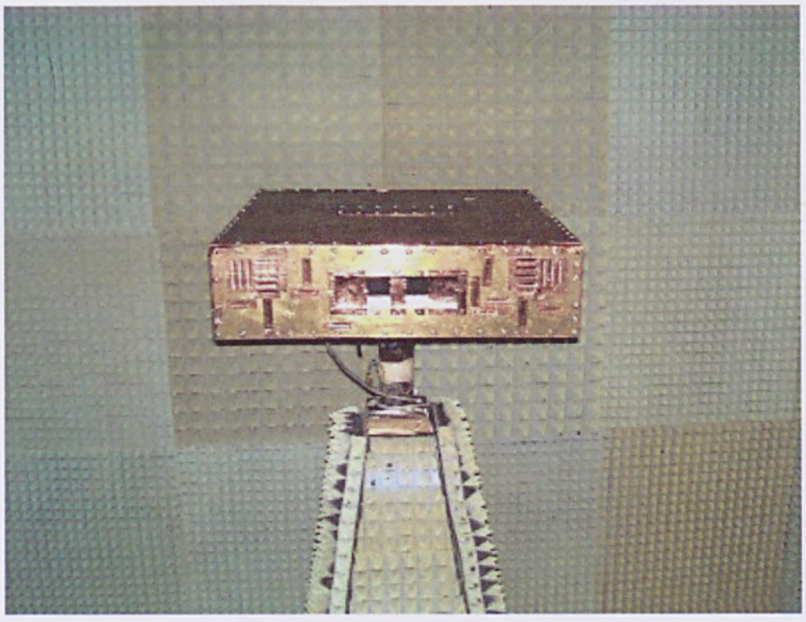

Fig. D.4. The 480 mm × 480 mm × 120 mm dummy EUT on the turntable in the medium sized anechoic chamber.

Fig. D.5. The 40 mm balanced dipole on the mast in the medium sized anechoic chamber.

D.3 Radiating Shielding Measurements in the Medium Sized Reverberation Chamber

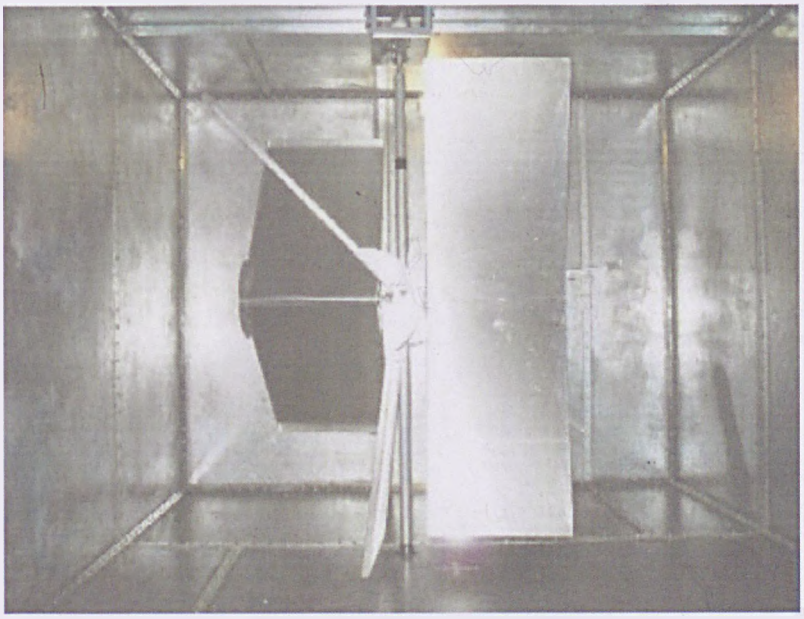

Fig. D.6. The mode stirrer paddle in the medium sized reverberation chamber.

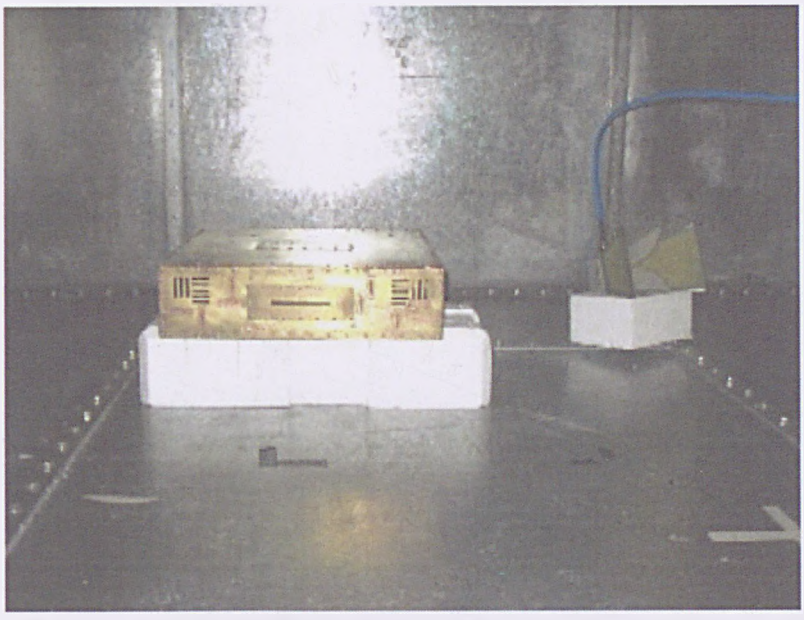

Fig. D.7. The dummy EUT and the reference antenna (horn) in the medium sized reverberation chamber.

D.4 Immunity Shielding Measurements in the Small Sized Reverberation Chamber

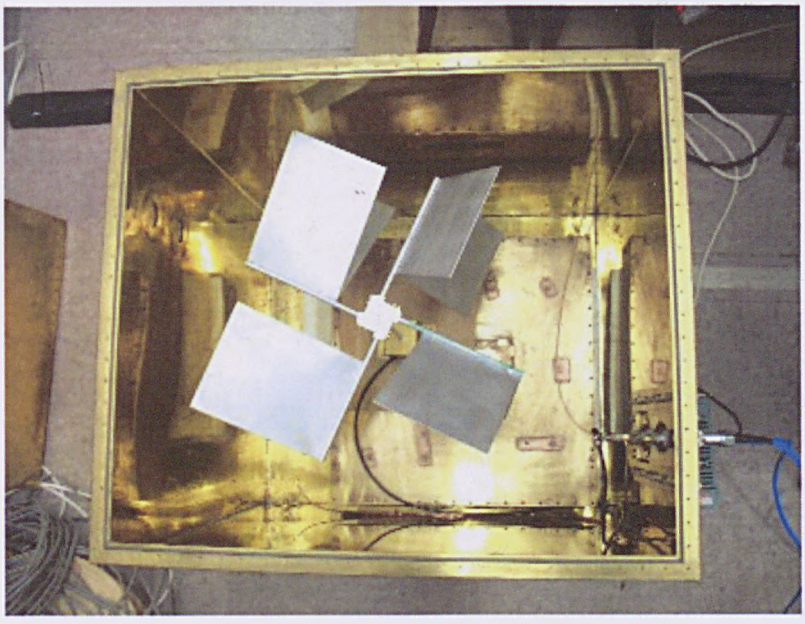

Fig. D.8. Top view of the opened small sized reverberation chamber containing the mode stirrer paddle and the dummy EUT placed on the bottom.

Appendix E

Matlab Program of the Point Source Modelling

```
% Use the point source modeling to predict the emission pattern on a half cylindrical
% surface centered the EUT with holes on one face, and calculate E.F.95th or
% E.F.max on the whole cylindrical surface. In this case, two small holes are
% considered.

a=1;                    % test distance (m)
z0=377;                 % impedance of free space, 377 ohm
ef95=[];
efmax=[];

for f=1:6               % frequency (GHz)
lamda=0.3/f;            % wavelength (m)
ef95row=[];
efmaxrow=[];

for i=1:6               % to compare the emission patterns measured at 6 different
                        % source positions, at each frequency, this program runs 6
                        % times
x1=-0.025;
y1=0.24;
z1=0;                   % position of the first hole, i.e., the point source 1 (x1,y1,z1)
hdegree=[pi/180+asin(0.24/a):pi/90:pi-asin(0.24/a)];  % horizontal scan region in
                        % front of the panel with holes, 90 steps
zdh=[-0.6:0.02:0.6];    % verticacl scan height, from -0.6 m to 0.6 m
```

```
xdphi=-a*cos(hdegree); % the x coordination of the scan grids
ydphi=a*sin(hdegree);  % the y coordination of the scan grids

% To calculate distance between each test point and the source point
sqra=(xdphi-x1).^2;
sqrb=(ydphi-y1).^2;
d1=[];
r1=[];
for zdh=-0.6:0.02:0.6;
   d=sqrt(sqra+sqrb+(zdh-z1)^2);
   r=acos((zdh-z1)./d);
   d1=[d1
      d];              % matrix of the distances between the point source 1 and
                       % each test point
   r1=[r1
      r];              % at each test point, the angle between the incident wave and
                       % z axis
end
a1=rand;               % the amplitude of the emission is range
                       % from 0 ~ 1
theta1=rand*2*pi;      % the phase of the emission is range from 0 ~ 2*pi
realv1=sin(r1).*(a1./d1).*cos(2*pi*d1/lamda+theta1);  % the real part of the 'z'
                       % component of the electric field at each test point
imagv1=sin(r1).*(a1./d1).*sin(2*pi*d1/lamda+theta1);  % the imagine part of the 'z'
                       % component of the electric field at each test point

x2=0.025;
y1=0.24;
z2=0;                  % position of the first hole, i.e., the point source 2 (x1,y1,z1)

% To calculate distance between each test point and the source point
sqra=(xdphi-x2).^2;
```

```
sqrb=(ydphi-0.24).^2;
d2=[];
r2=[];
for zdh=-0.6:0.02:0.6;
   d=sqrt(sqra+sqrb+(zdh-z2)^2);
   r=acos((zdh-z2)./d);
   d2=[d2
      d];                  % matrix of the distances between the point source 2 and
                           % each test point
   r2=[r2
      r];                  % at each test point, the angle between the incident wave
                           % and z axis
end
a2=rand;                   % the amplitude of the emission is range from 0 ~ 1
theta2=rand*2*pi;          % the phase of the emission is range from 0 ~ 2*pi
realv2=sin(r2).*(a2./d2).*cos(2*pi*d2/lamda+theta2);
imagv2=sin(r2).*(a2./d2).*sin(2*pi*d2/lamda+theta2);

Power=(realv1+realv2).^2+(imagv1+imagv2).^2;  % the power tested at each test
                           % point

% To plot emission pattern
figure
imagesc (Power); figure(gcf)
xlabel('Scan range (degree)')
ylabel('Scan height (cm)')
set(gca,'xticklabel',{'-56';'-36';'-16';'4';'24';'44';'64'})
set(gca,'yticklabel',{'40';'20';'0';'-20';'-40';'-60'})

%To calculate ef95 and efmax
[m,n]=size(Power);
Power=Power(:);
```

```
Power=sort(Power);
Power=flipud(Power);
totalpwr=sum(Power);
factor=(pi-2*asin(0.24/a))/(2*pi);  % the ratio between the simulated scan area to the
                                    % area of the 360 degree scan area
avgpwr=factor*totalpwr/(m*n);
p95=Power(round(0.05*m*n/factor),:);
r95=p95/avgpwr;
ef95row=[ef95row r95];
pmax=max(Power);
rmax=pmax/avgpwr;
efmaxrow=[efmaxrow rmax];
end
ef95=[ef95
  ef95row];          % results of ef95 at 6 frequencies, at each frequency 6 ef95
                     % values are obtained.
efmax=[efmax
  efmaxrow];         % results of ef95 at 6 frequencies, at each % frequency 6 ef95
                     % values are obtained.
end
```

References

[1] P. F. Wilson and M.T.Ma, "Techniques for measuring the electromagnetic shielding effectiveness of materials: Part I," *IEEE Trans. Electromagn. Compat.*, vol. 30, no.3, pp. 239-250, Aug. 1988.

[2] P. F. Wilson and M.T.Ma, "Techniques for measuring the electromagnetic shielding effectiveness of materials: Part II," *IEEE Trans. Electromagn. Compat.*, vol. 30, no.3, pp. 251-259, Aug. 1988.

[3] "Standard Test Method for Measuring the Electromagnetic Shielding Effectiveness of Planar Materials," ASTM D4935, Sep. 1989.

[4] "International Electrotechnical Commission, 61000-4-21 ELECTROMAGNETIC COMPATIBILITY (EMC), Part 4: Testing and Measurement Techniques, Section 21: Reverberation Chamber Test Methods."

[5] "Method of Attenuation Measurement for Enclosures, Electromagnetic Shielding, for Electronic Test Purposes," MIL Standard 285, 1956.

[6] "Standard Method for Measuring the Effectiveness of Electromagnetic Shielding Enclosures," IEEE STD 299, 1997.

[7] C. L. Holloway, D. A. Hill, J. Ladbury, G. Koepke, and R. Garcia, "Shielding effectiveness measurements of materials using nested reverberation chambers," *IEEE Trans. Electromagn. Compat.*, vol. 45, no.2, pp. 350-356, May 2003.

[8] S. A. Schelkunoff, "The Impedance Concept and its Application to Problems of Reflection, Refraction, Shielding and Power Absorption," *Bell System Technical Journal 17*, pp. 17-49, 1938.

[9] C. R. Paul, *Introduction to electromagnetic compatibility*: Wiley, 1992.

[10] "Gasketing Material, Conductive, Shielding Gasket, Electronic, Elastomer, EMI/RFI, General Specifications For," MIL-G-83528, Jul. 1992.

[11] Y. K. Hong, C. Y. Lee, C. K. Jeong, D. E. Lee, K. Kim, and J. Joo, "Method and apparatus to measure electromagnetic interference shielding efficiency and its shielding characteristics in the broadband frequency ranges," *Rev. Sci. Instrum.*, vol. 74, no.2, pp. 1098-1102, Feb. 2003.

[12] M. S. Sarto and A. Tamburrano, "Innovative test method for the shielding effectiveness measurement of conductive thin films in a wide frequency range," *IEEE Trans. Electromagn. Compat.*, vol. 48, no.2, pp. 331-341, May 2006.

[13] J. Catrysse, " A new measuring cell for the characterisation of flat samples of shielding materials, in the frequency range from 1-18 GHz," in *Proc. of Int. Symp. on Electromagnetic Compatibility, EMC Europe 2002*, Sorrento, Italy, Sep. 2002.

[14] J. C. G. Field, "An introduction to electromagnetic screening theory," *Inst. Elect. Eng. Colloq. Screening Shielding, U.K*, pp. 1/1-1/15, Nov. 1983.

[15] D. Hill, "Electromagnetic theory of reverberation chambers." NIST. Boulder, CO: NIST Tech. Note 1506, Dec. 1998.

[16] C. F. Bunting and S.-P. Yu, "Field penetration in a rectangular box using numerical techniques: an effort to obtain statistical shielding effectiveness," *IEEE Trans. Electromagn. Compat.*, vol. 46, no. 2, pp. 160-168, May 2004.

[17] D. W. P. Thomas, A. C. Denton, T. Konefal, T. Benson, C. Christopoulos, J. F. Dawson, A. C. Marvin, S. J. Porter, and P. Sewell, "Model of the electromagnetic fields inside a cuboidal enclosure populated with conducting planes or printed circuit boards," *IEEE Trans. Electromagn. Compat.*, vol. 43, no. 2, pp. 161-169, May 2001.

[18] A. C. Marvin, J. F. Dawson, S. Ward, L. Dawson, J. Clegg, and A. Weissenfeld, "A proposed new definition and measurement of the shielding effect of equipment enclosures," *IEEE Trans. Electromagn. Compat.*, vol. 46, no. 3, pp. 459-468, Aug. 2004.

[19] A. C. Marvin and Y. Cui, "Anechoic and reverberation chamber shielding measurement at frequencies above 1 GHz," in *Proc. of IEEE Int. Symp. on EMC*, Portland, USA, Aug. 2006.

[20] F. Ustuner, A. Akses, I. Araz, and B. Colak, "A method for evaluating the shielding effectiveness of small enclosures," in *Proc. of IEEE Int. Symp. on EMC*, Montreal, Canada, Aug. 2001.

[21] D. W. P. Thomas, A. C. Denton, T. Konefal, T. Benson, C. Christopoulos, J. F. Dawson, A. C. Marvin, and S. J. Porter, "Characterisation of the shielding effectiveness of loaded equipment enclosures," *EMC York 99, IEE Conference Publication 464*, pp. 89-94, 1999.

[22] D. A. Hill, M. T. Ma, A. R. Ondrejka, B. F. Riddle, M. L. Crawford, and R. T. Johnk, "Aperture excitation of electrically large, lossy cavities," *IEEE Trans. Electromagn. Compat.*, vol. 36, no. 3, pp. 169-178, Aug. 1994.

[23] M. P. Robinson, J. D. Turner, D. W. P. Thomas, J. F. Dawson, M. D. Ganley, A. C. Marvin, S. J. Porter, T. M. Benson, and C. Christopoulos, "Shielding effectiveness of a rectangular enclosure with a rectangular aperture," *Electronics Letters*, vol. 32, no. 17, pp. 1559-1560, Aug. 1996.

[24] J. D. Turner, M. P. Robinson, T. M. Benson, C. Christopoulos, J. F. Dawson, M. D. Ganley, A. C. Marvin, S. J. Porter, and D. W. P. Thomas, "An evaluation of the shielding effectiveness of cabinets," in *Proc. of the 12th Int. Zurich Symp. on EMC*, Zurich, Switzerland, Feb. 1997, pp. 229-234.

[25] S. Criel, R. De Smedt, E. Laermans, F. Olyslager, D. De Zutter, N. Lietaert, and A. De Clercq, "Theoretical and experimental determination of the shielding effectiveness of test enclosures," in *Proc. of the 12th Int. Zurich Symp. on EMC*, Zurich, Switzerland, Feb. 1997, pp. 223-228.

[26] C. A. Balanis, *Antenna theory: analysis and design*, 2nd ed: John Wiley and Sons, New York, 1997.

[27] H. A. Mendez, "Shielding theory of enclosures with apertures," *IEEE Trans. Electromagn. Compat.*, vol. EMC-20, pp. 296-305, May 1978.

[28] M. P. Robinson, S. J. Porter, and P. O. g. Oorth, "Reflection and transmission coefficients of printed circuit boards," in *Proc. of Int. Symp. on Electromagnetic Compatibility, EMC Europe 2000*, Brugge, Belgium, Sep. 2000, pp. 209-213.

[29] *York EMC Products " CGE02: Comb Generator Emittor," Data Sheet. Available: http://www.yorkemc.co.uk/instrumentation/cge02/.*

[30] M. P. Robinson, J. Clegg, and A. C. Marvin, "Radio Frequency Electromagnetic Fiel s in Large Conducting Enclosures: Effects of Apertures and Human Bodies on Propagation and Field-Statistics," *IEEE Trans. Electromagn. Compat.*, vol. 48, no.2, pp. 304-310, May 2006.

[31] "*Specification for Radio Disturbance and Immunity Measuring Apparatus and Methods – Part 2-3: Methods of Measurement of Disturbances and Immunity – Radiated Disturbance Measurements,* CISPR Publication 16-2-3-Amd.1, Ed. 1.0, 2005".

[32] P. F. Wilson, D. A. Hill, and C. L. Holloway, "On determining the maximum emissions from electrically large sources," *IEEE Trans. Electromagn. Compat.*, vol. 44, no.1, pp. 79-86, Feb. 2002.

[33] T. H. Loh and M. J. Alexander, "A method to minimize emission measurement uncertainty of electrically large EUTs in GTEM cells and FARs above 1 GHz," *IEEE Trans. Electromagn. Compat.*, vol. 48, no.4, pp. 434-440, Nov. 2006.

[34] D. W. Welsh, D. Bozec, and M. R. Tyndall, "Feasibility Study into the Application of Numerical Modelling in EMC Standardisation Radio Emission Measurement Methods." Final report (AY4607) for the radio communications agency, York EMC Services Ltd., Univ. of York. [Online]. Available: http://www.ofcom.org.uk/research/technology/ctc/emc/feasibility_ap_num_mod.pdf

[35] M. L. Crawford and G. H. Koepke, "Design, evaluation, and use of a reverberation chamber for performing electromagnetic susceptibility/vulnerability measurements," NBS Tech. Note 1092, 1986.

[36] T. A. Loughry, "Frequency stirring: an alternate approach to mechanical mode-stirring for the conduct of electromagnetic susceptibility testing," Phillips Laboratory, Kirtland Air Force Base, NM, Technical Report 91-1036, 1991.

[37] M. Born and E. Wolf, *Principles of optics*, 7th ed: Cambridge U.P., New York, 1999.

[38] C. L. Holloway, J. Ladbury, J. Coder, G. Koepke, and D. A. Hill, "Measuring Shielding Effectiveness of Small Enclosures/Cavities with a Reverberation Chamber," in *Proc. of IEEE Int. Symp. on EMC*, Honolulu, USA, Jul. 2007.